Strathclyde Institute of Pharmacy and Biomedical Sciences

High pressure as a tool for polymorph screening in small organic molecules

A thesis presented for the degree of

Doctor of Philosophy

in the Faculty of Science of the

University of Strathclyde

Ian Blackwood Hutchison

May 2017

This thesis is the result of the author's original research. It has been composed by the author and has not been previously submitted for examination which has led to the award of a degree.

Signed:

Date:

Abstract

Application of high pressure is a well-known tool used to induce. Presented in this thesis are the studies of three small organic molecules under high pressure, investigating the importance of particle size, the choice of pressure-transmitting medium (PTM) and the solvent from which the material is recrystallised on the high-pressure behaviour of the material.

Chapters 3 describes the characterisation of a metastable polymorph of glycolide, formed at high pressure and recovered to ambient conditions. Chapter 4 describes a neutron diffraction study of glycolide under high pressure, characterising the behaviour of each of the two known forms as well as seeking to characterise a third polymorph which had been observed during earlier work.

Chapter 5 presents a neutron diffraction study of acrylamide under high pressure in three different pressure-transmitting media – a 1:1 (v/v) mixture of pentane and iso-pentane, a 4:1 (v/v) mixture of methanol and ethanol, and iso-propyl alcohol (IPA). A different high pressure phase was identified in each of the three media, with the crystal structures of those in the pentanes and methanol/ethanol environments being fully solved.

Chapter 6 describes a study of caprolactam under high pressure, through a combination of single crystal X-ray diffraction and powder neutron diffraction. In this study, it was observed that a caprolactam sample recrystallised from ethyl acetate underwent a polymorph transition to one high pressure phase, while a sample recrystallised from alcohol (either ethanol or 1-butanol) underwent a polymorph transition to a different high pressure form despite the fact that both samples were in the same polymorphic form at the beginning of the experiment. The high pressure form observed from the sample recrystallised from ethanol (or 1-butanol) was fully structurally solved. Recent progress made by the group beyond the scope of this PhD have permitted unit cell parameters to be fitted to the neutron

diffraction data, although associated discussion of this form is limited due to time constraints.

Acknowledgements

First and foremost, I would like to thank my supervisor, Dr Iain Oswald. His support and guidance has been invaluable, his sense of humour appreciated and his encouragement throughout the write-up process gratefully received.

I am greatly indebted to colleagues at the STFC's Rutherford Appleton Laboratory for their irreplaceable help, expertise and company during the long hours on the PEARL beamline. Thanks go to Dr Craig Bull and Dr Nick Funnell, with special thanks to the late Dr Bill Marshall.

For their endless help and advice in the lab, as well as their general company, my thanks go to the other members of Dr Oswald's research group – Dr Amit Delori, Dr Syed Atif Raza, and Lauren Connor – and to everyone in room 501R and the founding members of Cake Thursdays.

Thanks also go to my second supervisor, Dr Andrew Urquhart, whose enthusiasm for the project was especially valued when the early stages of the research seemed to bring no progress.

I would like to thank my two supervisors from my undergraduate industrial placement with Technologie Servier, Dr Philippe Letellier and Dr Michael Lynch, for sparking my interest in solid state chemistry.

Financial support from the EPSRC is gratefully acknowledged.

I would also like to thank everyone at Carnall Farrar, particularly Dame Ruth Carnall, Colin Carnall, Hannah Farrar, Ben Richardson and Bev Evans for their support and encouragement over the last year while I have struggled to balance working with completing this thesis.

I would like to thank to my parents, brother, and wider family for all their support, and to all my friends for constantly asking "Have you finished yet?".

Finally, I would like to express my deepest thanks to Becca for her endless support and encouragement over the last four years. I am very much looking forward to being able to spend weekends together again.

Table of Contents

List of Figures

List of Tables

Chapter 1 – Introduction

1.1 The Crystalline State

1.1.1 The Crystal Lattice and the Unit Cell

A crystal lattice is a highly ordered structure. Taking any one point in the three-dimensional lattice, this point is periodically repeated throughout the structure. Joining these repeating points by imaginary straight lines, the lattice can be split into three-dimensional boxes called the unit cell. The unit cell is the smallest block from which the entire lattice can be built through three-dimensional repetition. Depending on the symmetry present within the crystal structure, the unit cell may be further broken down into an asymmetric unit, which is the unique symmetry-independent portion of the structure and may consist of a single molecule, more than one molecule, or a fraction of a molecule if an inversion centre is present. The asymmetric unit relates atoms and molecules within and between unit cell to one another. Figure 1.1 shows an example of a unit cell, where the axial lengths are described by *a*, *b*, and *c* (measured in Ångstroms, Å) and the interaxial angles are described by α, β and γ (measured in degrees, °).

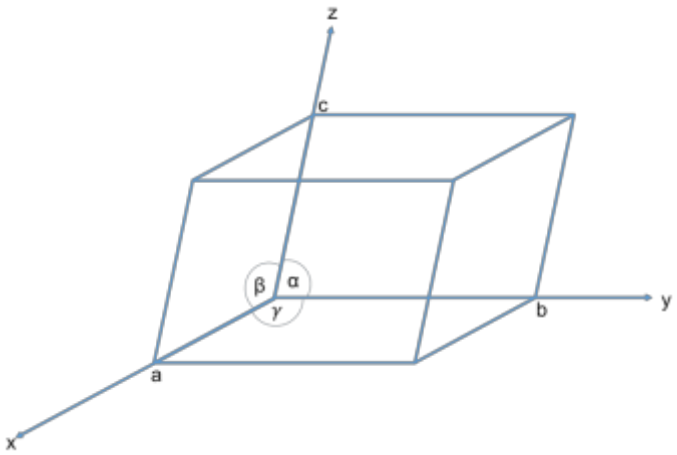

Figure 1.1 - A crystallographic unit cell

Crystals can be categorised as one of seven crystal systems depending on its unit cell parameters, as summarised in Table 1.1. The seven crystal systems encompass the 32 point groups of non-translational symmetry, and can be split into 230 space

groups depending upon the presence or absence of certain non-translational symmetry. These symmetry elements can be glide planes, in which a point is reflected through a mirror plane and then translated along the direction of that mirror plane, or screw axes, in which a point is rotated around an axis and then translated along the direction of the that axis.

Table 1.1 - Crystal systems and their unit cell restrictions

Crystal System	**Unit Cell Restrictions**
Triclinic	None
Monoclinic	$\alpha = \beta = 90°$
Orthorhombic	$\alpha = \beta = \gamma = 90°$
Tetragonal	$a = b$; $\alpha = \beta = \gamma = 90°$
Trigonal	$a = b$; $\alpha = \beta = 90°$; $\gamma = 120°$
Hexagonal	$a = b$; $\alpha = \beta = 90°$; $\gamma = 120°$
Cubic	$a = b = c$; $\alpha = \beta = \gamma = 90°$

1.1.2 Polymorphism

Polymorphism is the ability of a substance to exist in more than one distinct crystalline state. In their liquid or gaseous states, these different polymorphs are identical, but the different packing arrangements in their solid state can give rise to marked differences in their physico-chemical properties such as melting point, stability, solubility, electrical conductivity, heat capacity, and solid-state reactions. A common example of polymorphism (or allotropism, as it is referred to in the case of chemical elements) is that of elemental carbon, which can exist as diamond, graphite, fullerenes, carbon nanotubes or lonsdaleite. These allotropes highlight the vast differences possible in properties. Diamond is the hardest known material, optically transparent, chemically inert and electrically insulating; graphite is soft, black, chemically reactive and electrically conducting. Polymorphism is common in organic molecules, with McCrone stating that "*in general, the number of forms*

known for a given compound is proportional to the time and money spent in research on that compound" (McCrone, 1965).

Polymorphism can be induced in a number of different ways, as summarised in Table 1.2 (Lee, 2014).

Table 1.2 - Methods of obtaining polymorphs

1	Crystallisation from a single of mixed solvents/HTS
2	Thermal activation of the solid substrates
3	Crystallisation from the melt
4	Desolvation/dehydration of solvates/hydrates by heat or by re-slurry
5	Crystallisation in nano-confined structures
6	Seeding/pseudo-seeding
7	Solution mediated polymorphic transformation/slurry
8	Solid-state polymorphic transformation
9	Mechanical activation of the solid substance
10	Crystallisation in a capillary tube
11	Exposure to vapour at high or low humidity
12	Exposure to organic vapour
13	Directed crystallisation on molecular substrates
14	Crystallisation in the presence of tailor-made additives
15	Laser induced crystallisation
16	Crystallisation from a supercritical fluid
17	Structure prediction

1.2 Crystal Structure Determination

A number of techniques can be used to determine the crystal structure of a substance. Often, spectroscopic techniques such as Raman spectroscopy and Infrared spectroscopy are used as a means to assess when a sample may have undergone a polymorph transition, with the crystal structures then to be determined via techniques such as X-ray diffraction (XRD), which can be carried out on a single crystal sample or a powdered sample, or neutron diffraction.

1.2.1 Raman Spectroscopy

Raman spectroscopy is used to provide a "fingerprint" in order to identify molecules or functional groups within them. It is based on the principle that, when a sample is subjected to a beam of monochromatic light, this light interacts with the molecular vibrations, exciting them to virtual states before relaxation results in the emission of a photon. This scattering can be either elastic (Rayleigh scattering), in which the incident and emitted photons are of the same frequency, or inelastic, in which the frequency of the emitted photon differs to that of the incident photon. Raman spectroscopy concerns inelastic scattering, which in turn can be described as either Stokes or anti-Stokes, as depicted in Figure 1.2.

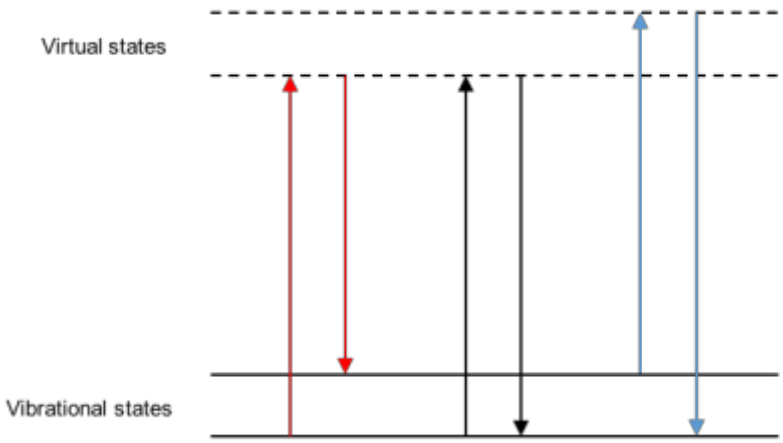

Figure 1.2 - A representation of the electron transitions in Raman spectroscopy. The red arrows represent Stokes scattering, in which the molecule relaxes to a vibrational energy level higher than its initial state. The black arrows represent Rayleigh scattering, in which the incident and emitted photons are of equal frequency. The blue arrows represent Anti-Stokes scattering, in which the emitted photon has a higher frequency than the incident photon, with the molecule relaxing to a vibrational state lower than its initial state.

Polymorph transitions can be monitored using a number of techniques, of which Raman spectroscopy is just one. Alterations in the environment of functional groups can influence the wavelength at which characteristic Raman signals are observed, or can result in the broadening or splitting of a characteristic peak, for example. Thanks in part to the very small sample volume requirement and the rapid collection time, Raman spectroscopy is commonly used to identify polymorphs, including in high

throughput polymorph screening (Dračínský et al., 2013; Morissette et al., 2004; Porter, Elie, & Matzger, 2008; Price, Grzesiak, & Matzger, 2005).

1.2.2 X-ray diffraction

X-ray diffraction (XRD) is one of the most important techniques in crystal structure determination. Exposure of a crystal sample to X-rays results in constructive interference with the sample's electrons when Bragg's law (Equation 1.1) is fulfilled:

Eq. 1.1: $$n\lambda = 2d\ sin\theta$$

where *n* is an integer, λ is the wavelength of the incident radiation (nm), *d* is the interplanar distance (Å) and θ is the scattering angle of the diffracted X-ray beam. Where the incident radiation occurs at another angle, such that Bragg's Law is not fulfilled, destructive interference will occur giving rise to the scattered X-rays being partially or completely out of phase.

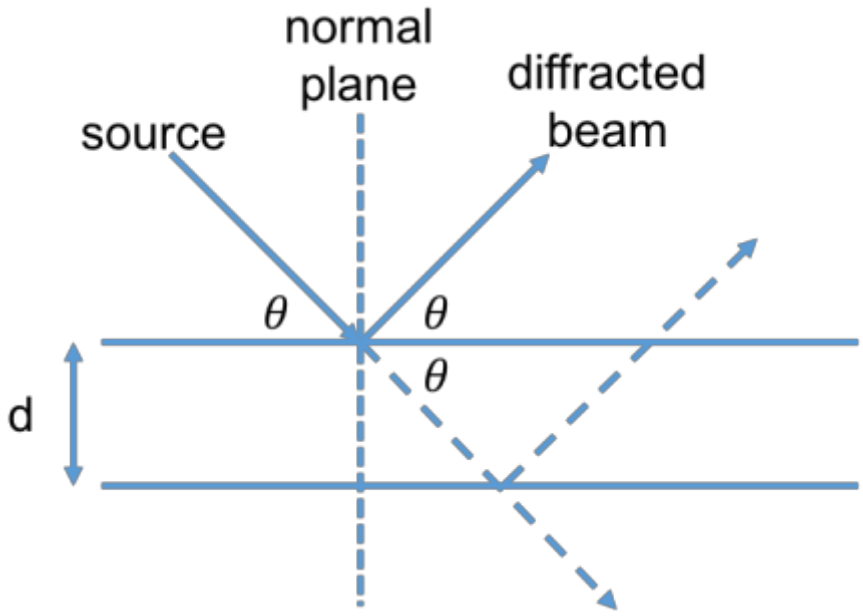

Figure 1.3 - A two-dimensional representation of Bragg's Law in which the planes (separated by distance, d) are denoted by the horizontal lines.

X-rays diffracted by the electrons within the sample are recorded by a detector to produce a characteristic diffraction pattern, in which the positions of the reflections relate to the dimensions of the unit cell (see Equations 1.6 – 1.12), while the atomic positions within the unit cell can be derived from reflection intensities. The diffraction pattern, displaying symmetry both in terms of the reflection positions and intensities, can be viewed as a unit cell in reciprocal space – the reciprocal lattice.

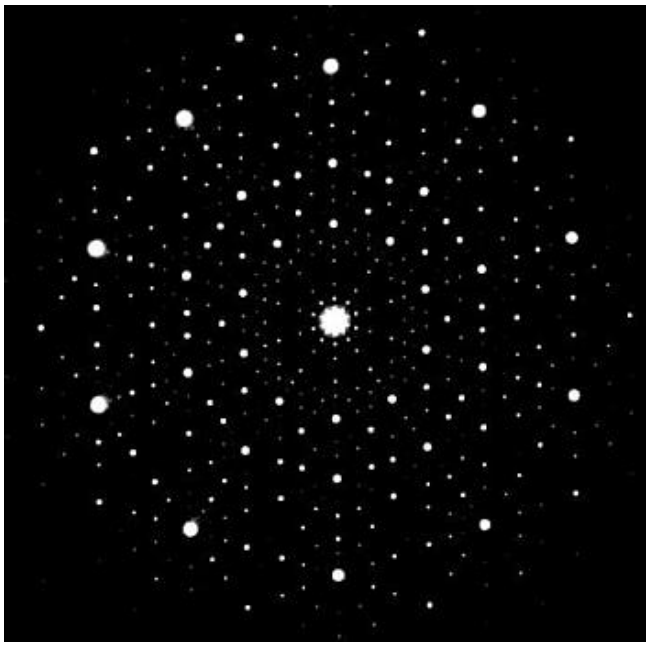

Figure 1.4 - Single crystal diffraction pattern of an aluminium-manganese alloy (Shechtman, Blech, Gratias, & Cahn, 1984).

The intensity of each of the the *hkl* indices can be converted (using Fourier transformation) to an observed structural amplitude, $|F_o|$, which can then be assigned to a structure factor, *F*. The structure factor represents both amplitude and phase:

Eq. 1.2 $$F(hkl) = |F(hkl)| \,.\, exp[i\emptyset(hkl)]$$

The reverse Fourier transformation allows the calculation of electron density, ρ, within the direct lattice at coordinates *x,y,z*:

Eq. 1.3 $$\rho(xyz) = \frac{1}{V}\sum_{h,k,l}|F(hkl)|\, exp\,[i\emptyset(hkl)]\, exp[-2\pi i(hx + ky + lz)]$$

In this way, it can be seen that every part of a crystal structure contributes towards every reflection present in a diffraction pattern. This means that, unlike in spectroscopic techniques where a part of the spectrum can be used to deduce information about a portion of the molecular structure, the entire diffraction pattern must be observed to permit successful structural solution.

As the structural model is refined to reflect the observed diffraction intensities, the accuracy of the model can be expressed in two way, both of which compare the calculated diffraction intensities based upon the model, $|F_C|$, with the observed diffraction intensities, $|F_O|$. The R-factor and the weighted R^2, in which each reflection is assigned its own weighted, *w*, are shown in Equations 1.4 and 1.5, respectively. As the accuracy of the model improves, the R-factor decreases towards zero.

Eq. 1.4 $$R = \frac{\sum||F_o|-|F_c||}{\sum|F_o|}$$

Eq. 1.5 $$wR^2 = \frac{\sqrt{\sum w\left(F_o^2 - F_c^2\right)^2}}{\sum w\left(F_o^2\right)^2}$$

As previously described, the position of peaks in a diffraction pattern relate to the unit cell dimensions. The distance, *d*, and the incident or scattering angle, θ, are directly proportional, with the relationship between *d* and the unit cell parameters for each crystal setting described in Equations 1.6 (triclinic), 1.7 (monoclinic), 1.8 (rhombohedrally-centred trigonal), 1.9 (hexagonal and primitive trigonal), 1.10 (orthorhombic), 1.11 (tetragonal) and 1.12 (cubic).

Eq. 1.6
$$\frac{1}{d_{hkl}^2} = \left[\frac{h^2}{a^2}sin^2\alpha + \frac{k^2}{b^2}sin^2\beta + \frac{l^2}{c^2}sin^2\gamma + \frac{2kl}{bc}(\cos\beta\cos\gamma - \cos\alpha) + \frac{2hl}{ac}(\cos\alpha\cos\gamma - \cos\beta) + \frac{2hk}{ab}(\cos\alpha\cos\beta - \cos\gamma)\right][(1 - cos^2\alpha - cos^2\beta - cos^2\gamma + 2\cos\alpha\cos\beta\cos\gamma)^{-1}]$$

Eq. 1.7
$$\frac{1}{d_{hkl}^2} = \frac{h^2}{a^2 sin^2\beta} + \frac{k^2}{b^2} + \frac{l^2}{c^2\ sin^2\beta} - \frac{2hl\cos\beta}{ac\ sin^2\ \beta}$$

Eq. 1.8
$$\frac{1}{d_{hkl}^2} = \frac{1}{a^2}\left(\frac{(h^2 + k^2 + l^2)sin^2\alpha + 2(hk + kl + hl)(cos^2\alpha - \cos\alpha)}{1 + cos^3\alpha - 3\ cos^2\alpha}\right)$$

Eq. 1.9
$$\frac{1}{d_{hkl}^2} = \frac{4}{3a^2}(h^2 + k^2 + hk) + \frac{l^2}{c^2}$$

Eq. 1.10
$$\frac{1}{d_{hkl}^2} = \frac{h^2}{a^2} + \frac{k^2}{b^2} + \frac{l^2}{c^2}$$

Eq. 1.11
$$\frac{1}{d_{hkl}^2} = \frac{h^2 + k^2}{a^2} + \frac{l^2}{c^2}$$

Eq. 1.12
$$\frac{1}{d_{hkl}^2} = \frac{h^2 + k^2 + l^2}{a^2}$$

1.2.3 Neutron Diffraction

Neutron diffraction is a complementary technique to X-ray diffraction. While X-rays are diffracted by the electrons in a sample, incident neutrons are diffracted by the atomic nuclei. Scattering only occurs when the neutrons pass within very close

proximity of the nucleus, and so intensities in neutron diffraction are lower in comparison to X-ray diffraction. As a result, a larger sample volume is used for neutron diffraction experiments in order to obtain similar intensities. Since neutron diffraction permits the positions of atomic nuclei to be determined, it is more accurate in than X-ray diffraction when determining atomic positions, since the electron densities detected in X-ray diffraction may be distorted due bonding effects.

In X-ray diffraction, the scattering factor of an atom, f, is directly proportional to the atomic number, Z, and the diffraction intensity depends upon the scattering angle of the radiation, θ. Contrastingly in neutron diffraction, the scattering power of an atom is independent of the atomic number, and remains constant for all scattering angles. Even different isotopes can exhibit very different behaviour in neutron diffraction. Samples are usually deuterated to avoid the incoherent scattering observed with ^{1}H atoms. This is illustrated in Figure 1.4.

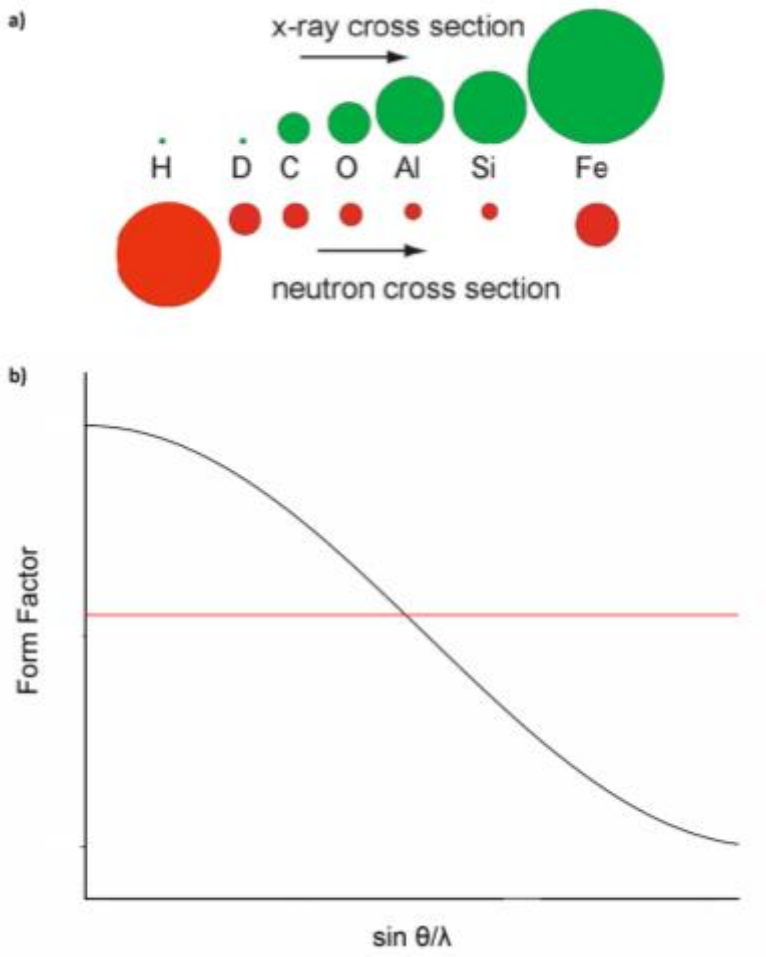

Figure 1.5 - a) the X-ray and neutron scattering cross sections for a selection of atoms, and b) form factor of X-rays and neutrons with respect to the angle of incidence. In a), it can be seen that whilst cross section increases with Z for X-rays, there is no such direct relationship for neutrons. In b), the black line represents form factor for X-ray diffraction whilst the red line represents that for neutron diffraction. Figure a) reproduced from (Copley, 2007).

The vast differences observed in scattering power between atoms can be exploited in neutron diffraction. Sample environments are typically constructed of materials exhibiting null-scattering or very weak scattering, such as the TiZr alloy used in the Paris-Edinburgh cell or vanadium cans used in ambient-condition experiments.

Neutron Facilities

Neutron diffraction is carried out at specialist facilities, such as the ISIS neutron spallation source at the Rutherford Appleton Laboratory (Oxfordshire, UK), or the

neutron source reactors at the Institut Laue-Langevin (Grenoble, France) and the Argonne National Laboratory (Illinois, USA).

At ISIS, hydride ions (H^-) are accelerated through two accelerators, up to 35% of the speed of light before entering a third accelerator which takes the form of a circular synchrotron. Upon entering the synchrotron, the H^- ions are stripped of their electrons, leaving the protons (H^+) to accelerate around the synchrotron. The protons are separated into two bunches as they are accelerated during their 12,000 revolutions of the synchrotron, before being diverted to one of the two target stations. Here, the protons bombard a tungsten targets at 84% of the speed of light, emitting neutrons which are then slowed by passing through hydrogenous materials. The neutrons are directed towards an array of beamline instruments, each catering to specific types of sample or study.

The diffraction pattern is collected as a function of the time-of-flight (ToF) of the neutrons, with each having travelled a specified distance, *L*, from the source to the sample and finally to the detector. Equation 1.13 shows the relationship between time of flight (*t*), flight path distance (*L*), d-spacing (*d*) and the scattering angle (θ).

Eq. 1.13 $$t = \frac{2m_n L}{h} d \sin\theta$$

where m_n is the mass of a neutron, and *h* is Planck's constant. From this equation the relationship between the crystal structure (d) and the ToF measurement is apparent.

1.3 High Pressure Crystallography

Much research has previously been conducted into structural changes at high pressures, with polymorphism and polymerisation both among the common observations. Research into the behaviour of materials under high pressure stemmed partially from interest in geochemical and planetary processes, as well as

the aim of synthesising ultra-hard materials such as diamond (McMillan, 2006), and research in this area has been ongoing for over 100 years. Some of the early work carried out by P. W. Bridgman in the early part of the 20th century. Bridgman's high pressure research included the coagulation of egg albumin at pressures of 0.5 – 0.7 GPa (Bridgman, 1914a) and high pressure phase changes in various materials including sodium, potassium, carbon dioxide, carbon tetrachloride and diphenylamine (Bridgman, 1914b).

The interest in high pressure behaviour of materials has not weaned over the years, with high pressure research conducted on a wide range of materials. Metals such as iron (Takahashi & Bassett, 1964), salts including sodium chloride (Bassett, Takahashi, Mao, & Weaver, 1968), and other inorganic materials such as phosphorous nitride imide (Marchuk, Pucher, Karau, & Schnick, 2014) have all been reported to exhibit high pressure polymorphism. Small organic materials such as pentaerythritol (Katrusiak, 1995), , glycine (Dawson et al., 2005), isopropyl alcohol (Ridout & Probert, 2014) and as well as pharmaceutical materials such as piroxicam (Childs & Hardcastle, 2007), paracetamol (Boldyreva, Shakhtshneider, Ahsbahs, Sowa, & Uchtmann, 2002; Fabbiani et al., 2004; Oswald et al., 2009), piracetam (Fabbiani, Allan, Parsons, & Pulham, 2005). The literature shows that polymorphism, or formation of solvates, can commonly be induced by simple application of pressure to a sample, or be recrystallisation from a solution at elevated pressures (Fabbiani et al., 2004).

As well as being a common route to the production of polymorphs, pressure is also commonly used as a tool to achieve polymerisation. Polymerisation at high pressure has been observed in materials ranging from small organics such as benzene (Gauthier, Chervin, & Pruzan, 1991; Pruzan et al., 1990), acrylic and methacrylic acids (Oswald & Urquhart, 2011), and diacetylenes (Jin, Plonka, Parise, & Goroff, 2013) to C_{60} and C_{70} fullerenes (Sundar et al., 1996) and carbon-metal network composites such as $Li_3Fe(CN)_6$ (Li et al., 2015).

1.4 Importance of Polymorphism

Polymorphism is of great importance in a number of industries. In the pharmaceutical industry, the stability, solubility and efficacy of an active pharmaceutical ingredient (API) all depend upon its solid form. In addition to this, the solid form of an API can often have important consequences on intellectual property and patent law. The detonation potentials of energetic materials can vary greatly between polymorphic forms of the same material, while the polymorphism of materials such as L-glutamic acid (a pre-cursor to monosodium glutamate) is important in the food industry.

The application of high pressure has been shown to be a powerful tool for inducing polymorphism, and the importance of thorough polymorph screening in industries such as pharmaceuticals has been well documented. The failure of pharmaceutical industries to rigorously screen for polymorphs can be extremely costly, as illustrated by a number of case examples.

Ritonavir

Ritonavir, the API in Abbott Laboratories' retroviral drug Norvir, was first introduced to the market in the mid-1990s. After some 240 lots of the capsules had been successfully produced, a previously unknown polymorph appeared during the production process. The new form was much less soluble than the original, reducing the drug's bioavailability to below 5% (Bauer, 2008).

This appearance of this new form meant the product had to be temporarily withdrawn from the market in 1998, costing manufacturer Abbott Laboratories an estimated $250m in sales as well as hundreds of millions of dollars in research and development costs in solve the issue (Morissette, Soukasene, Levinson, Cima, & Almarsson, 2003).

Ranitidine Hydrochloride

Hundreds of patents are based on the crystal form of a pharmaceutical product, with these being granted on the basis of improved stability, stability, bioavailability, or

processing properties such as ease of filtration. One such example is that of ranitidine hydrochloride, the active pharmaceutical ingredient in the anti-ulcer drug Zantac (GlaxoSmithKline). The original patent covered a number of related molecules, but only one polymorph of ranitidine hydrochloride. After a new polymorph was discovered, GlaxoSmithKline patented this new form, designated Form 2. This meant that upon expiry of the Form 1 patent, generic manufacturers were permitted to market only the original Form 1, as Form 2 was still under patent.

1.5 General Aims

The importance of polymorphism in the pharmaceutical industry, amongst a number of other sectors, has been well documented. Whilst it has been shown that the application of high pressure is one possible route to obtaining novel polymorphs of a wide variety of molecules, including small organics such as pharmaceuticals, the precise ways in which factors such as sample particle size, the choice of pressure-transmitting medium, or the solvent of recrystallisation used influence the high-pressure behaviour of such materials has not been extensively studied.

A greater understanding of the ways in which polymorph screening can be conducted using high pressure could be an invaluable development with direct applications in the pharmaceutical industry. Before the potential of high pressure as a tool for polymorph screening can be fully exploited, further appreciation of the process conditions and experimental factors which may influence the transformation from one polymorph to another must first be achieved.

The aim of the research in this thesis was to explore the use of high pressure as a tool for screening for polymorphs of small organic molecules, and specifically focuses on how specific experimental parameters can alter the behaviour of a substance under high pressure.

The study of glycolide (Chapters 3 – 4) includes the investigation into the impact particle size can have on the observation of a polymorph transition, as well as the examination of fully hydrogenous materials (rather than deuterated materials) on the PEARL beamline at the ISIS Neutron and Muon source. The study of acrylamide

(Chapter 5) stresses the importance of the pressure-transmitting medium used during the screening process, while the study of caprolactam (Chapter 6) shows that the solvent used in the recrystallisation process during the production of the crystalline sample can determine the high-pressure behaviour observed.

Each of these studies highlights aims to show the importance of using pressure as a tool for polymorph screening in the pharmaceutical industry, in order to ensure an exhaustive knowledge of the polymorphs during the development of new products. As McCrone suggested (McCrone, 1965), more comprehensive range of potential routes to obtaining polymorphs increases potential number of polymorphs that may be discovered. An ability to form a wider range of polymorphs may in turn allow for the careful selection of experimental conditions and to tailor properties such as stability and solubility to best suit the desired application. An example of this may be the formulation of pharmaceutical material with a higher dissolution rate, allowing a fast-acting product to be brought to the market.

1.5 References

Bassett, W. A., Takahashi, T., Mao, H.-K., & Weaver, J. S. (1968). Pressure-Induced Phase Transformation in NaCl. *J. Appl. Phys.*, *39*(1), 319–325. http://doi.org/10.1063/1.1655752

Bauer, J. F. (2008). Polymorphism - A Critical Consideration in Pharmaceutical Development, Manufacturing, and Stability. *Journal of Validation Technology*, 15–23.

Boldyreva, E. V., Shakhtshneider, T. P., Ahsbahs, H., Sowa, H., & Uchtmann, H. (2002). Effect of high pressure on the polymorphs of paracetamol. In *Journal of Thermal Analysis and Calorimetry* (Vol. 68, pp. 437–452). http://doi.org/10.1023/A:1016079400592

Bridgman, P. W. (1914a). Article : the Coagulation of Albumen By Pressure, 511–512.

Bridgman, P. W. (1914b). Change of phase under pressure. I. the phase diagram of eleven substances with especial reference to the melting curve. *Physical Review*, *3*(3), 153–203. http://doi.org/10.1103/PhysRev.3.153

Childs, S. L., & Hardcastle, K. I. (2007). Cocrystals of piroxicam with carboxylic acids. *Crystal Growth and Design*, *7*(7), 1291–1304.

http://doi.org/10.1021/cg060742p

Copley, J. R. D. (2007). NIST Center for Neutron Research Summer School on Methods and Applications of Neutron Spectroscopy. In *Dynamics and Neutron Scattering*.

Dawson, A., Allan, D. R., Belmonte, S. A., Clark, S. J., David, W. I. F., McGregor, P. A., … Sawyer, L. (2005). Effect of high pressure on the crystal structures of polymorphs of glycine. *Crystal Growth and Design*, *5*(4), 1415–1427. http://doi.org/10.1021/cg049716m

Dračínský, M., Procházková, E., Kessler, J., Šebestík, J., Matějka, P., & Bouř, P. (2013). Resolution of organic polymorphic crystals by raman spectroscopy. *Journal of Physical Chemistry B*, *117*(24), 7297–7307. http://doi.org/10.1021/jp404382f

Fabbiani, F. P. A., Allan, D. R., David, W. I. F., Moggach, S. A., Parsons, S., & Pulham, C. R. (2004). High-pressure recrystallisation—a route to new polymorphs and solvates. *CrystEngComm*, *6*(82), 504–511. http://doi.org/10.1039/B406631F

Fabbiani, F. P. A., Allan, D. R., Parsons, S., & Pulham, C. R. (2005). An exploration of the polymorphism of piracetam using high pressure. *CrystEngComm*, *7*(29), 179. http://doi.org/10.1039/b418976k

Gauthier, M., Chervin, J. C., & Pruzan, P. (1991). Pressure-Induced Polymerization of Cyclic Molecules: A Study of Benzene and Thiophene (pp. 87–95). Springer US. http://doi.org/10.1007/978-1-4899-2480-3_8

Jin, H., Plonka, A. M., Parise, J. B., & Goroff, N. S. (2013). Pressure induced topochemical polymerization of diiodobutadiyne: a single-crystal-to-single-crystal transformation. *CrystEngComm*, *15*(16), 3106. http://doi.org/10.1039/c3ce26851a

Katrusiak, A. (1995). High-pressure X-ray diffraction study of pentaerythritol. *Acta Crystallographica Section B*, *51*(5), 873–879. http://doi.org/10.1107/S010876819500098X

Lee, E. H. (2014). A practical guide to pharmaceutical polymorph screening & selection. *Asian Journal of Pharmaceutical Sciences*, *9*(4), 163–175. http://doi.org/10.1016/j.ajps.2014.05.002

Li, K., Zheng, H., Hattori, T., Sano-Furukawa, A., Tulk, C. A., Molaison, J., … Mao, H. K. (2015). Synthesis, Structure, and Pressure-Induced Polymerization of Li3Fe(CN)6 Accompanied with Enhanced Conductivity. *Inorganic Chemistry*, *54*(23), 11276–11282. http://doi.org/10.1021/acs.inorgchem.5b01851

Marchuk, A., Pucher, F. J., Karau, F. W., & Schnick, W. (2014). A High-Pressure Polymorph of Phosphorus Nitride Imide Angewandte. *Angewandte Chemie International Edition*, *53*(9), 2469–2472. http://doi.org/10.1002/anie.201309020

McCrone, W. C. (1965). Physics and Chemistry of the Organic Solid-State. In D. Fox

(Ed.), *Physics and Chemistry of the Organic Solid-State* (pp. 726–767). New York: Wiley Interscience.

McMillan, P. F. (2006). Chemistry at high pressure. *Chem. Soc. Rev.*, *35*(10), 855–857. http://doi.org/10.1039/b610410j

Morissette, S. L., Almarsson, Ö., Peterson, M. L., Remenar, J. F., Read, M. J., Lemmo, A. V., … Gardner, C. R. (2004). High-throughput crystallization: Polymorphs, salts, co-crystals and solvates of pharmaceutical solids. *Advanced Drug Delivery Reviews*. http://doi.org/10.1016/j.addr.2003.10.020

Morissette, S. L., Soukasene, S., Levinson, D., Cima, M. J., & Almarsson, O. (2003). Elucidation of crystal form diversity of the HIV protease inhibitor ritonavir by high-throughput crystallization. *Proceedings of the National Academy of Sciences of the United States of America*, *100*(5), 2180–2184. http://doi.org/10.1073/pnas.0437744100

Oswald, I. D. H., Chataigner, I., Elphick, S., Fabbiani, F. P. A., Lennie, A. R., Maddaluno, J., … Smith, R. I. (2009). Putting pressure on elusive polymorphs and solvates. *CrystEngComm*, *11*(2), 359–366. http://doi.org/10.1039/B814471K

Oswald, I. D. H., & Urquhart, A. J. (2011). Polymorphism and Polymerisation of Acrylic and Methacrylic Acid at High Pressure. *Crystengcomm*, *13*(14), 4503–4507. http://doi.org/10.1039/c1ce05295k

Porter, W. W., Elie, S. C., & Matzger, A. J. (2008). Polymorphism in carbamazepine cocrystals. *Crystal Growth and Design*, *8*(1), 14–16. http://doi.org/10.1021/cg701022e

Price, C. P., Grzesiak, A. L., & Matzger, A. J. (2005). Crystalline polymorph selection and discovery with polymer heteronuclei. *Journal of the American Chemical Society*, *127*(15), 5512–5517. http://doi.org/10.1021/ja042561m

Pruzan, P., Chervin, J. C., Thiéry, M. M., Itié, J. P., Besson, J. M., Forgerit, J. P., & Revault, M. (1990). Transformation of benzene to a polymer after static pressurization to 30 GPa. *The Journal of Chemical Physics*, *92*(1990), 6910. http://doi.org/10.1063/1.458278

Ridout, J., & Probert, M. R. (2014). Low-temperature and high-pressure polymorphs of isopropyl alcohol. *CrystEngComm*, *16*(32), 7397. http://doi.org/10.1039/C4CE01012D

Shechtman, D., Blech, I., Gratias, D., & Cahn, J. W. (1984). Metallic phase with long-range orientational order and no translational symmetry. *Physical Review Letters*, *53*(20), 1951–1953. http://doi.org/10.1103/PhysRevLett.53.1951

Sundar, C. S., Sahu, P. C., Sastry, V. S., Rao, G. V. N., Sridharan, V., Premila, M., … Sood, A. K. (1996). Pressure-induced polymerization of fullerenes: A comparative study of C60 and C70. *Physical Review B*, *53*(13), 8180–8183. http://doi.org/10.1103/PhysRevB.53.8180

Takahashi, T., & Bassett, W. A. (1964). High-Pressure Polymorph of Iron. *Science*, *145*(3631), 483–486. Retrieved from http://www.jstor.org/stable/1714581

Chapter 2 – Materials and Methods

2.1 Materials Used

All materials and solvents used in this research were commercially available and were purchased from from Sigma Aldrich or Fluka (UK). Materials were used as received or recrystallised as specified in the body of this thesis.

2.2 Diamond-Anvil Cell

Merrill-Bassett diamond-anvil cells, DACs, (Merrill & Bassett, 1974) were used to apply high pressure to the samples during X-ray and Raman studies within this research. DACs allow *in-situ* measurements to be made using analytical techniques such as Raman spectroscopy and X-ray diffraction (XRD). In a DAC the sample is placed between two opposing diamond faces and subjected to high pressure when these diamond faces are pushed together (see Figure 2.1). A pressure-transmitting medium (PTM) is added into the sample chamber before it is sealed. The PTM ensures the hydrostatic application of pressure, whilst also ensuring the sample chamber does not collapse in on itself as force is applied. In the DACs used, each of the two diamonds are embedded into a tungsten carbide (WC) backing disc. Once the sample chamber has been sealed, pressure is applied by tightening screws between the two backing discs.

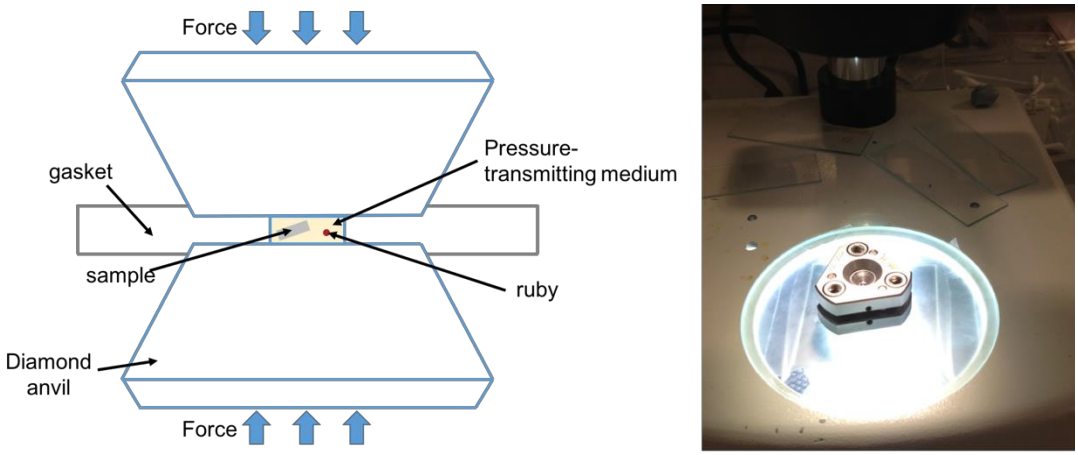

Figure 2.1 - Schematic representation of a diamond-anvil cell (left) and a photograph of a DAC on a microscope.

A small ruby sphere is also added into the sample chamber. The laser-induced fluorescence of ruby varies with pressure, allowing *in-situ* pressure measurement using a Raman spectrometer using Equation 2.1 (Forman, Piermarini, Barnett, & Block, 1972):

Equation 2.1: $$P = \left[\frac{1905}{4}\left(\frac{\lambda}{\lambda_0}\right)^B - 1\right]$$

where *P* is the pressure (measured in GigaPascals, GPa), λ and λ_0 are the wavelength (measured in nanometres, nm) of the ruby R_1 line at elevated and ambient pressures, respectively, and 1905 and 4 are both least-squares fit parameters.

2.3 Large Volume Press

A large volume press, designed and built by the group of Professor Konstantin Kamenev (Centre for Science at Extreme Conditions, University of Edinburgh) was employed during the research on glycolide. The design and use of this press is described in detail within Chapter 3.

2.4 Raman Spectroscopy

Raman spectra were collected on a ThermoScientific DXR Raman microscope with a 532 nm laser and an extended range grating. This grating in this instrument is in a fixed geometry hence another specialised grating was employed so that both the Raman spectrum and ruby fluorescence could be measured without changing over the parts and recalibrating. Spectra were analysed using OMNIC 8.0 software.

2.5 X-Ray Diffraction

Single crystal X-ray diffraction intensities were collected using a Bruker APEX II diffractometer with an Incotec IμS microsource (λ = 0.71073 Å). The data were reduced using SAINT within Bruker's APEX II software and absorption corrections applied using SADABS. In general, crystal structures were solved by direct methods

(SIR92), and refined against F^2 using Crystals, but the specific details of each refinement can be found in each of the experimental chapters.

High pressure powder X-ray diffraction data were collected on the same instrument, with the diffraction rings integrated using Bruker's Pilot plug-in (Bruker, 2014). Details of the experiment can be found in Chapter 3.

Powder X-ray diffraction data were collected on a Bruker AXS D8-Advance transmission diffractometer equipped with θ/θ geometry, primary monochromated radiation (Cu-Kα_1 λ = 1.54056 Å), a Bruker Vantec 1D position sensitive detector (PSD) and an automated multi-position *x-y* sample stage. Samples were ground lightly before being mounted on a 28 position sample plate supported on a polyimide (Kapton, 7.5 µm thickness) film. Data were collected from each sample in the range 4 – 35 ° 2θ with a 0.015 ° 2θ step size and 1 sec. step^{-1} count time.

2.6 Neutron Diffraction and the Paris-Edinburgh Press

Neutron diffraction data were collected on the PEARL beamline at the STFC's ISIS Neutron and Muon source (Oxfordshire, UK). Unless otherwise stated, samples and pressure-transmitting media were deuterated in order to avoid the high levels of background associated with the large incoherent scattering cross-section of hydrogen. Sample loading and data collection and refinement details are included in each of the relevant chapters.

In all neutron studies, samples were loaded into a Paris-Edinburgh cell (Figure 2.2), with data being collected in the transverse scattering geometry in which the main detector bank covers the range 81.2° < 2θ < 98.8°. Data collected at each pressure point were electronically summed across the detector banks. Pawley and Rietveld refinements were conducted using TOPAS Academic (Bruker, 2009).

Figure 2.2 - The loaded and sealed Paris-Edinburgh cell (left), and the complete cell assembly being lowered into position at the PEARL beamline (right).

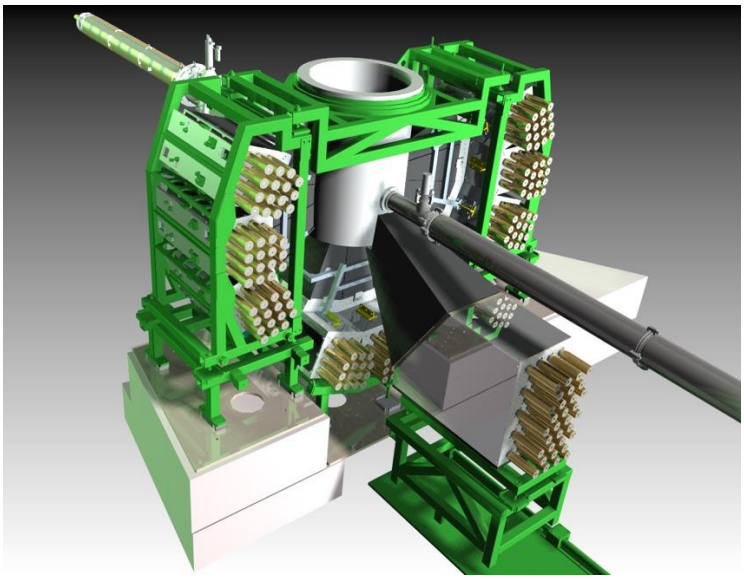

Figure 2.3 - The PEARL beamline set-up, in which the Paris-Edinburgh cell is loaded into the silver cylinder. The neutron beam passes through the instrument (from back to front in this diagram), with scattered neutrons intensities being measured by the detector banks around the P-E cell (ISIS, 2015).

2.7 The PIXEL Method

The PIXEL Method (Gavezzotti, 2003) was employed throughout this research to assess the relative stabilities of crystal lattices with changing pressure, allowing observed phase transitions to be explained in energetic terms. This method uses the electron densities of isolated molecules to calculate the intermolecular forces between molecules in a crystal lattice. It allows the intermolecular energies to be assigned to specific pairs of molecules, with such energies being broken down into their Coulombic, dispersion, polarisation and repulsion terms (Equation 2.2):

Equation 2.1: $$E_{tot} = E_c + E_p + E_d + E_r$$

where E_{tot} is the total energy, E_c is the Coulombic energy, E_p is the polarisation energy, E_d is the dispersion energy and E_r is the repulsion energy.

The molecular volume is broken into pixels before a condensation factor of *n* is applied to reduce the number of such pixels (producing so-called superpixels of *n* x *n* x *n*). At each superpixel of molecule B, the electrostatic potential generated by molecule A and the associated Coulombic potential is calculated. Similarly, the linear polarisation energies at each pixel or superpixel of molecule B due to the electric fields exerted by surrounding molecules is calculated. The dispersion energy is calculated as the sum of the pixel-pixel terms in a London-type expression. Finally, the repulsion energies (which are independent of the condensation levels) are calculated across all pairs of overlapping charge density elements. This procedure is sensitive to stepsize (typically 0.8 Å) and the symmetry operations present. For example, pairs of symmetry operations such as a translation ± *x* may have slightly different overlap integrals. In this case, the average of the two is taken as the best approximation.

The PIXEL method has been used for a wide range of studies, with Gavezzotti's 2003 publication having 170 citations to date (as of 22/1/2017, Scopus). Although the

PIXEL method is not verified for high-pressure systems, there have been numerous examples of these calculations being applied to such systems without any reported issues. Acrylic acid (Johnston, Marshall, Parsons, Urquhart, & Oswald, 2014), glycine (Moggach, Marshall, Rogers, & Parsons, 2015) and piperidine (Budd, Ibberson, Marshall, & Parsons, 2015) are just a few such examples.

2.8 References

Bruker, A. X. S. (2009). *General profile and structure analysis software for powder diffraction data*. *Scientific American* (Version 5, Vol. 302). http://doi.org/10.1038/scientificamerican0610-4

Bruker, A. X. S. (2014). APEX2.

Budd, L. E., Ibberson, R. M., Marshall, W. G., & Parsons, S. (2015). The effect of temperature and pressure on the crystal structure of piperidine. *Chemistry Central Journal*, *9*(1). http://doi.org/10.1186/s13065-015-0086-3

Forman, R. A., Piermarini, G. J., Barnett, J. D., & Block, S. (1972). Pressure measurement made by the utilization of ruby sharp-line luminescence. *Science (New York, N.Y.)*, *176*, 284–285. http://doi.org/10.1126/science.176.4032.284

Gavezzotti, A. (2003). Calculation of intermolecular interaction energies by direct numerical integration over electron densities. 2. An improved polarization model and the evaluation of dispersion and repulsion energies. *Journal of Physical Chemistry B*, *107*(10), 2344–2353. http://doi.org/10.1021/jp022288f

ISIS. (2015). Science and Technology Research Agencies. Retrieved July 4, 2016, from http://www.isis.stfc.ac.uk/instruments/pearl/pearl2122.html

Johnston, B. F., Marshall, W. G., Parsons, S., Urquhart, A. J., & Oswald, I. D. H. (2014). Investigation of acrylic acid at high pressure using neutron diffraction. *Journal of Physical Chemistry B*, *118*(14), 4044–4051. http://doi.org/10.1021/jp502095n

Merrill, L., & Bassett, W. A. (1974). Miniature Diamond Anvil Pressure Cell for Single-Crystal X-Ray-Diffraction Studies. *Rev. Sci. Instrum.*, *45*(2), 290–294. http://doi.org/Doi 10.1063/1.1686607

Moggach, S. A., Marshall, W. G., Rogers, D. M., & Parsons, S. (2015). How focussing on hydrogen bonding interactions in amino acids can miss the bigger picture: a high-pressure neutron powder diffraction study of glycine. *CrystEngComm*, *17*(28), 5315–5328. http://doi.org/10.1039/C5CE00327J

Chapter 3 – Polymorphism of a polymer pre-cursor: Metastable glycolide polymorph recovered via large scale high-pressure experiments

This chapter was accepted to CrystEngComm 2015,**17**, 1778-1782:

DOI: 10.1039/C5CE00119F

Part of the chapter relating to the design of the Large volume press was written by K. Kamenev (University of Edinburgh) but is present in this chapter to ensure the complete story is portrayed.

I would like to thank Angelo Gavezzotti for his useful discussions around the PIXEL calculations and Professor Alastair Florence for his helpful comments and to the EPSRC Centre for Innovative Manufacturing in Continuous Manufacturing and Crystallography for the use of their X-ray powder diffractometer.

3.1 Introduction

Glycolide (1,4 Dioxane-2,5-dione) is an important molecule as it is the precursor to the biodegradable polymers polyglycolic acid (PGA) and one of the monomers involved in poly(lactic-co-glycolic) acid (PLGA). Both of these polymers are of great interest in the areas of controlled drug delivery and other biomedical applications (Bala, Hariharan, & Kumar, 2004; Jain, 2000), PGA has commonly been used in bio-absorbable sutures, such as Dexon® for several decades (Pillai & Sharma, 2010; Solhaug & Heimann, 1975), and has also found applications as tissue engineering scaffolds (Day et al., 2004), and food packaging materials (Miller, 2013) (Krehalon®). There are several examples of PLGA-based drug delivery systems, such as Lupron Depot®, Risperidal® Consta™ and Arestin®) already on the market (Mundargi, Babu, Rangaswamy, Patel, & Aminabhavi, 2008). Polymerisation of these materials usually occurs through the use of catalysts and solvothermal routes which provides a consistent product that has defined physical properties that are beneficial to their applications.

Another route by which polymerisation can occur is through the use of pressure. Many studies have investigated the use of pressure to induce the polymerisation of small molecule systems (Ceppatelli, Santoro, Bini, & Schettino, 2000; Chelazzi, Ceppatelli, Santoro, Bini, & Schettino, 2005; Murli & Song, 2010). Recently our group has been investigating the polymerisation process of small organic molecules using high pressure techniques with a view that the solid-state structure, i.e. polymorph, may alter the resulting polymeric structure and/or inhibit the reaction (Johnston, Marshall, Parsons, Urquhart, & Oswald, 2014)(Oswald & Urquhart, 2011). In expansion of this work, we started to investigate the possibility of inducing ring-opening polymerisation under high pressure, as seen in carnosine (Murli, Mishra, Thomas, & Sharma, 2012a).

Glycolide (Figure 3.1) is a 6-membered ring structure formed via dehydration of glycolic acid, and has shown only one polymorphic form under ambient conditions (Belenkaya, B. G., Belsky, V. K., Dementev, A. I., Sakharova, V. I., Chernikova, 1997).

It is well-known that small molecules exhibit polymorphism under high pressure conditions (Millar et al., 2010),(Satthaphut, Sutcliffe, & Oswald, 2014),(F. P. A. Fabbiani et al., 2007),(Patyk, Skumiel, Podsiadło, & Katrusiak, 2012),(Seryotkin, Drebushchak, & Boldyreva, 2013) and that ring opening can occur (Murli, Mishra, Thomas, & Sharma, 2012b). As such we chose to explore whether glycolide would exhibit polymorphism at high pressure with subsequent ring opening polymerisation to form a novel polymer structure as observed in other systems (Chelazzi et al., 2005; Johnston et al., 2014).

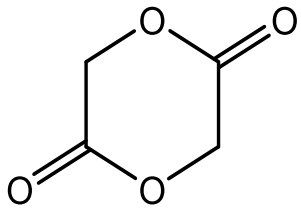

Figure 3.1 - Chemical structure of glycolide.

3.2 Experimental, Results and Discussion

3.2.1 Initial Experiments

Using a Merrill-Bassett diamond-anvil cell (DAC) (Leo Merrill & Bassett, 1974; Moggach, Allan, Parsons, & Warren, 2008a), the behaviour of glycolide under hydrostatic conditions was studied up to 8 GPa, using *in-situ* Raman spectroscopy. During this experiment part of the crystal was crushed into a polycrystalline sample which gave a different spectrum to the single crystal when a pressure of 0.58 GPa was applied. At 0.40 GPa, the low pressure form was successfully refined, whilst at 0.58 GPa the data were of too poor quality to solve the structure, illustrating that the crystal had undergone a reconstructive phase transition in this pressure range. Some of the key differences that were observed were in the CH stretch (3100-2900 cm^{-1}) and the ester linkage region (1900-1600 cm^{-1}) (Figure 3.2) suggesting that a conformational change to a higher molecular symmetry had occurred or that the

new form possesses fewer independent molecules to describe the crystal structure. A separate study of glycolide powder under non-hydrostatic conditions up to 8 GPa displayed no further significant changes in the Raman spectra obtained showing that polymerisation did not occur under either hydrostatic or non-hydrostatic conditions. In all experiments, the Raman spectrum of the high-pressure form did not change upon decompression to ambient pressure and appeared stable for at least 2 days. Only a few cases have been reported of the recovery of high-pressure forms of organic species compared with the inorganic solid state, the most notable examples being those of GABA monohydrate (seeding) (Fabbiani, Buth, Levendis, & Cruz-Cabeza, 2014), and paracetamol (DAC and large-volume press recovery) (Boldyreva, Shakhtshneider, Ahsbahs, Sowa, & Uchtmann, 2002)(Oswald et al., 2009).

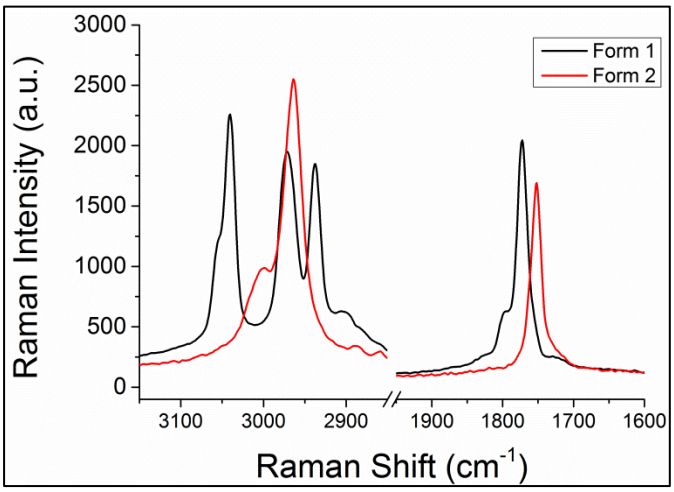

Figure 3.2 - Raman spectra of Forms I and II of glycolide, focussing on the C-H stretch region and the ester-linkage region.

The persistence of the high-pressure form of glycolide to ambient pressure and the low pressure of transformation highlighted the possibility of conducting large-scale high-pressure production of this polymorph. With this in mind, large volume (LV) experiments were conducted using a hydraulic press designed and built by the Kamenev group at the University of Edinburgh (for a detailed description of the press, see Figure 3.3).

3.2.2 Large Volume Experiments and Structure Solution

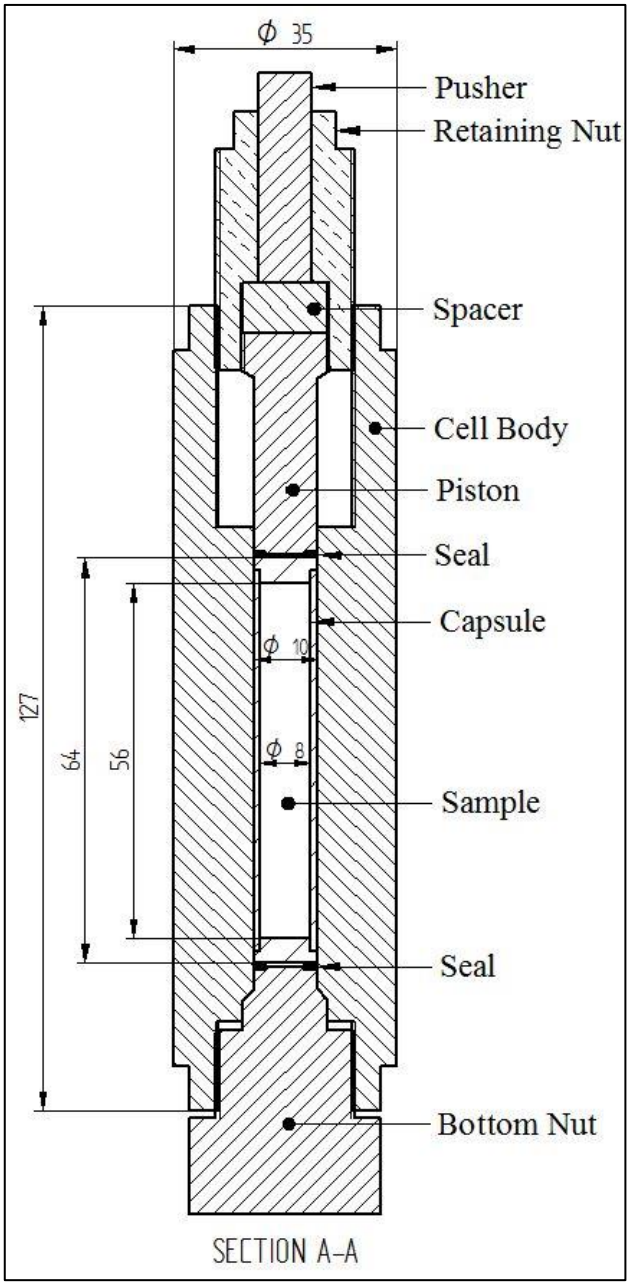

Figure 3.3 - Design of the large volume press. Measurements are given in millimetres. For further details on the large volume press, see Appendix 3.1.

At the heart of this cell is a PTFE capsule (i.d. 8 mm; length 60 mm), that can hold up to ~3 cm^3 of liquid which can be compressed to ~0.8 GPa. For our experiment, a 1.5 g sample of glycolide was placed into a PTFE capsule, with the remaining volume

being filled with petroleum ether as the pressure-transmitting medium (PTM). The capsule was sealed at both ends using a PTFE cap and wrapped in PTFE tape to ensure a proper seal. After the assembly of the pressure cell was complete, it was placed in a hydraulic press and a load of 5 tons was applied, which is equivalent to 0.6 GPa. The sample was left at high pressure for approximately 24 hours. After this time, the load was decreased and the sample recovered to ambient pressure and filtered over a Buchner funnel before analysis using Raman spectroscopy which showed that it was Form II. The recovered material was subsequently used to seed crystal growth from a saturated solution in acetone, and the resulting crystals were analysed via spectroscopic and X-ray diffraction techniques. These were stable for up to 12 days.

Single crystals of diffraction quality were obtained from the seeding experiments and analysed. The data, collected at 293 K, confirmed that a new polymorph had been formed, herein designated Form II. Form II is observed in orthorhombic *Pbca* with unit cell dimensions *a* = 5.2400(2) Å, *b* = 7.4389(3) Å and *c* = 11.7763(4) Å (*cf*. Form I, in monoclinic $P2_1/n$, with unit cell parameters a = 6.710 Å, b = 14.959 Å, c = 9.621 Å, and β = 98.93°) (Belenkaya, B. G., Belsky, V. K., Dementev, A. I., Sakharova, V. I., Chernikova, 1997); the refinement details can be found in the Section 3.5. Form II crystallises with one molecule sitting on an inversion centre as opposed to the two molecules observed in Form I. The increase in the crystal and molecular symmetry that was alluded to via the Raman spectra is confirmed with the diffraction experiment. The molecule undergoes a significant conformational change during the phase transition from a twist-boat conformation to a near-planar ring structure. In fact, due to the position of the molecule with respect to the inversion centre the initial model was planar and gave a suitable model with an R-factor ~4%. The thermal parameters for the oxygen atoms were observed to be larger than their neighbours when refined in the planar model indicating that there was disorder present in the crystal structure. The disordered model was created by splitting the oxygen atoms into two and refining them with distance (taken from Form I), thermal and vibrational similarity restraints. The inversion centre dictates that the molecule is

centrosymmetric however it is our belief that whilst the data suggest centrosymmetry the actual model possesses one molecule containing O10, O30, O31' and O10', while the other molecule contains O11, O31, O10' and O30'; the carbon and hydrogen atoms are the same in both molecules. Our reasoning for this is that we only required modest pressures to change the conformation and so it is unlikely that the molecule has moved over the planar transition state (70 kJ mol^{-1} higher in energy than Form I) into the chair conformation. For comparison, P. A. Wood *et al.* observed high pressure polymorphism in L-serine in which a conformational change of 40 kJ mol^{-1} required a pressure of between 4.5 GPa and 5.2 GPa to be applied (Wood et al., 2008). However, the molecular rearrangement in serine required a change in hydrogen bonding which may account for the greater pressure required. The crystallographic data can be found in Appendix 3.2.

Projection of the Form I molecules along the methylene groups conveys a V-configuration that distorts considerably over the phase transition (Figures 3.4c & 3.4d). The least-squares planes (1: O4, C3, O8, C5 and C2; and 2: C2, C5, C6, O1 and O7) are observed to be at an angle of ~144° to each other in both molecules, whereas this angle is decreased to ~173° in Form II. The change in relative energies of this conformational change has been calculated using Gaussian 09 to be -30 & -40 kJ mol^{-1} from each molecule in Form I (Frisch et al., 2009). The model and ring puckering analysis portrays a pseudo-chair conformation due to the inversion centre, but it is unlikely that this is the true conformation of the molecule. Calculation of the energy of a planar structure gave an energy barrier of ~70 and ~60 kJ mol^{-1} (using the molecules in the Form I as a reference). Due to the modest pressures that glycolide was subjected to, the likely structure remains the twist-boat conformation albeit being less puckered. Figure 3.4d is a representation of the hypothesised conformation (that violates the crystal symmetry) however the disorder present within the model provides the necessary symmetry equivalent atoms.

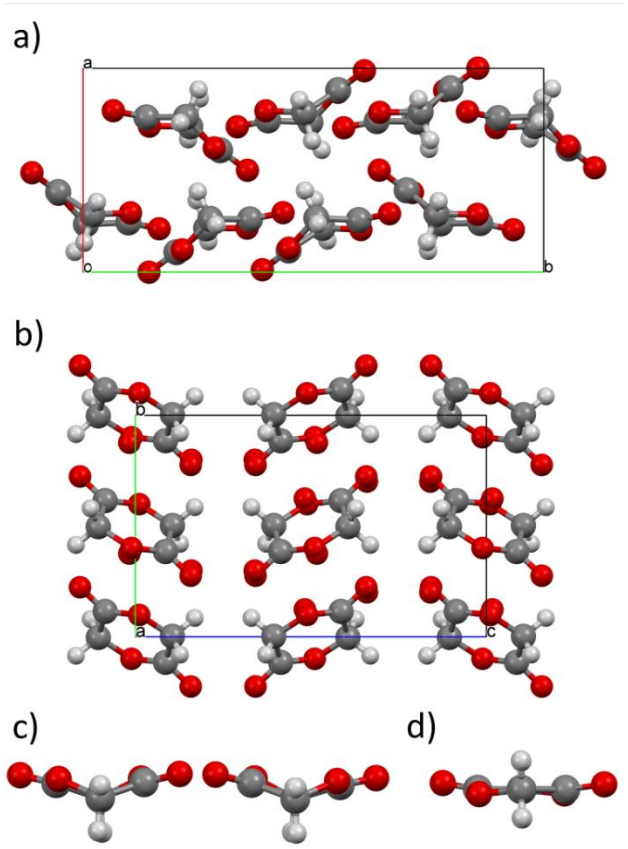

Figure 3.4 - Packing diagrams of a) Form I and b) Form II of glycolide. c) The two molecules in Form I exhibit a highly puckered twist-boat conformation whilst d) the molecule in Form II is almost planar.

To ensure that the recrystallised form was the same as that obtained at pressure a sample of glycolide powder, crushed between two glass slides to ensure small and uniform particle size, was analysed via Raman spectroscopy. This softer method of sample preparation was used to ensure the sample remained crystalline and was of the same polymorph. After confirming that this was the case, the powder was loaded into a DAC along with petroleum ether and the pressure increased to 0.20 GPa. The sample was left at this pressure for approximately 54 hours, and re-analysed via Raman spectroscopy. The Raman spectrum matched the previously-observed patterns of Form II while the pressure had dropped to 0.12 GPa. The DAC was aligned using normal high pressure single crystal diffraction procedures. The data were collected with a single exposure of 600 seconds covering a scan width of 20° and the data analysed in the Phase ID module found in the APEX2 software

package. Pawley refinement was performed using TOPAS academic (Bruker, 2009), showing the powder pattern to match that of of Form II (Figure 3.5).

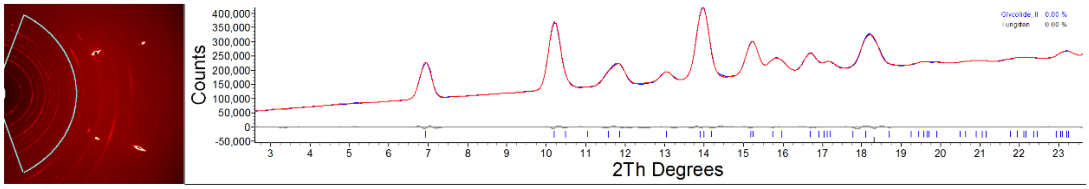

Figure 3.5 - Diffraction image (left) and powder diffraction pattern (right) of glycolide Form II. The bright spots in the diffraction image are caused by the diamonds of the DAC. The diffraction rings at high 2-theta angle are caused by the tungsten gasket. The Pawley fit of the data fits very well with the calculated pattern from the single crystal (R_{wp} = 0.79%).

3.2.3 PIXEL Calculations

To quantify the energy difference between the two polymorphs, PIXEL calculations were performed using Form I and a modified model of Form II (Gavezzotti, 2003)·(J D Dunitz & Gavezzotti, 2012). PIXEL requires a full molecule to be present to perform the calculation, and so the symmetry of the crystal was reduced to meet this criterion. This requirement aids us in our interpretation of the crystal structure. For these calculations, we were able to choose the atoms that best represented the assumed boat conformation rather that the symmetry-imposed chair conformation. Using this model, the total energies for Forms I and II were -79.1 and -89.0 kJ mol^{-1}, respectively.

Figures 3.9 and 3.10 show the most significant interactions in Form I and Form II, respectively, where Interaction 1 is the strongest observed in the crystal structure. Table 3.2 details the breakdown of energies with respect to coulombic, polarisation, dispersion and repulsion forces as calculated using PIXELC module of the CLP suite of programs (Gavezzotti, 2003). In the construction of Figure 3.10 the disorder model was used due to the imposition of the inversion symmetry. We stress that the boat conformation was used in the calculation of the energies. The diagrams are the best approximation.

The most notable interaction from Form I is the molecular interaction that encompasses an anti-parallel C=O dimer (Int. 1). Although PIXEL gives molecule-

molecule energies an important contribution to this energy is the dispersion component which is known to contribute to carbonyl-carbonyl interactions. These interactions have been shown by Allen *et al.* to be comparable with medium strength hydrogen bonds (Allen, Baalham, Lommerse, & Raithby, 1998). Interestingly, despite the strength of these interactions Form II does not possess any such interactions. Previous work by our group on acrylic acid showed that both low pressure and high pressure phases possessed these interactions (Johnston et al., 2014).

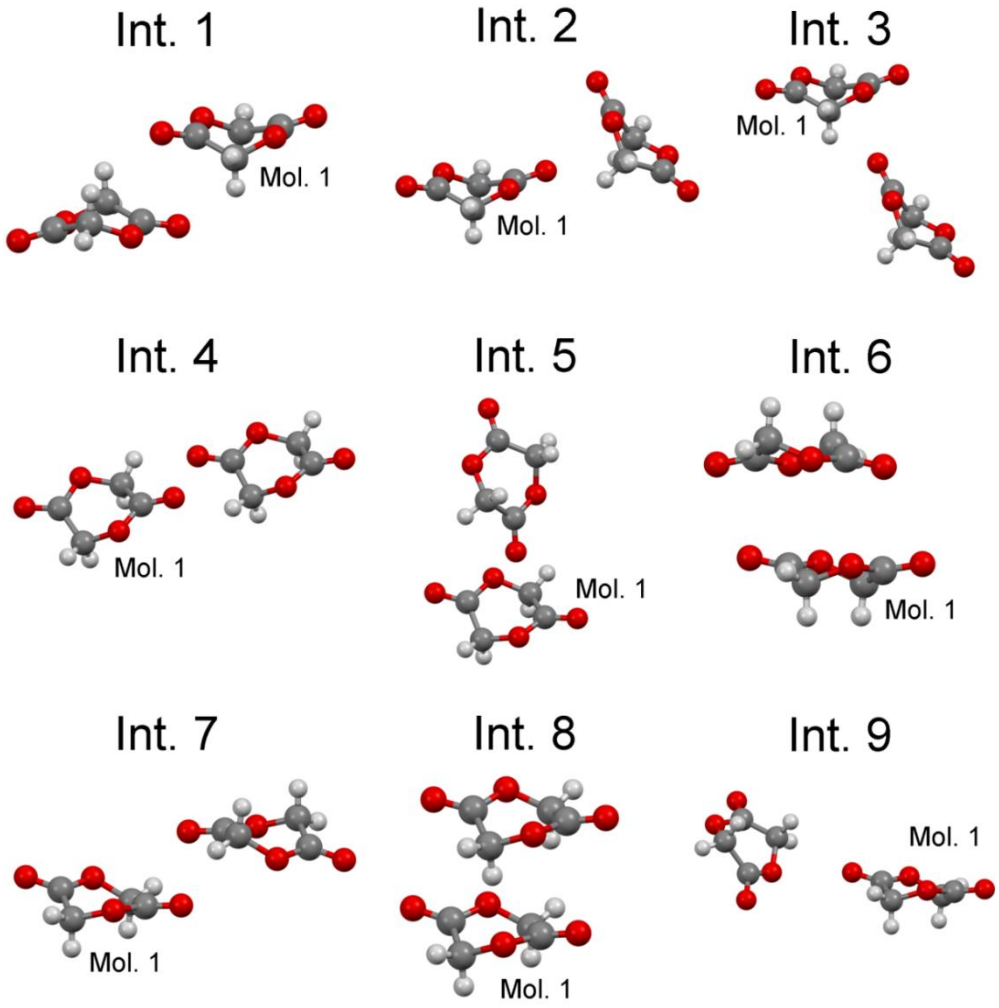

Figure 3.6 - The nine most prominent interactions in Form I of glycolide ranging from -10.5 to -34.9 kJ mol^{-1}. Table 3.2 shows the interaction energies.

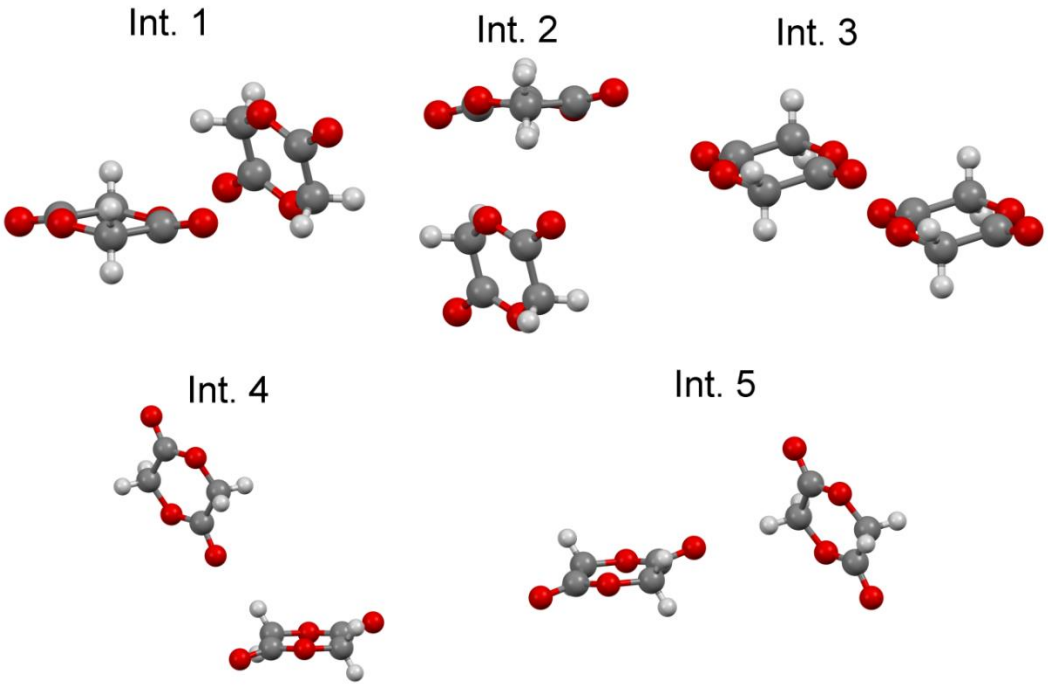

Figure 3.7 - The five most prominent interactions in Form II of glycolide ranging from -9.0 to -25.0 kJ mol^{-1}. Table 3.2 shows the interaction energies.

Table 3.1 - The interactions energies in kJ mol^{-1} for Forms I and II of glycolide as calculated by PIXELC.

Interaction	C_m-C_m dist. [a] (Å)	E_{coul} (kJ mol^{-1})	E_{pol} (kJ mol^{-1})	E_{disp} (kJ mol^{-1})	E_{rep} (kJ mol^{-1})	E_{tot} (kJ mol^{-1})
Form I						
1	5.219	-27.5	-5.9	-15.4	13.9	-34.9
2	5.725	-18.7	-4.6	-10.2	12.4	-21.1
3	5.613	-19.0	-5.1	-11.0	15.9	-19.2
4	6.415	-11.1	-2.4	-7.2	5.3	-15.4
5	5.897	-9.3	-1.9	-7.8	3.8	-15.2
6	3.800	-5.2	-2.6	-16.2	9.6	-14.3
7	5.935	-10.0	-4.9	-11.6	14.4	-12.1
8	5.596	-7.8	-2.0	-8.2	6.3	-11.7
9	6.616	-9.1	-1.9	-5.1	5.6	-10.5

Form II						
1	4.546	-19.0	-5.9	-17.3	17.3	-25.0
2	4.553	-15.1	-4.8	-16.0	12.6	-23.3
3	5.240	-8.0	-1.4	-7.0	1.9	-14.5
4	6.976	-6.9	-1.2	-3.2	2.0	-9.3
5	6.953	-7.3	-1.5	-3.8	3.5	-9.0

[a]C_m denotes the centre of mass.

It should be noted that the total energies of -79.1 and -89.0 kJ mol^{-1} for Forms I and II, respectively, represent the intermolecular energy only and do not consider the conformational energy change between forms. As one can observe, for this conformation, Form II is more stable with respect to intermolecular energies. The change in Z' does pose a small problem with regard to the calculation of the conformational energy changes. The molecules in Form I are 30 and 40 kJ mol^{-1} more stable than the conformation of Form II, as calculated using Gaussian (Gavezzotti, 2003). To the best approximation we have halved each value and summed them to give an approximate change in conformational energy to be +35 kJ mol^{-1}. Therefore, the energy change is 25 kJ mol^{-1} in favour of Form I, hence Form II is the metastable form. Dunitz and Gavezzotti provided evidence that higher density polymorphs are not necessarily the most stable form and glycolide seems to be another example of this (J D Dunitz & Gavezzotti, 2012). The calculated densities of Forms I and II are 1.619 g cm^{-3} and 1.680 g cm^{-3}, respectively, as summarised in Appendix 3.2.

3.2.4 Disappearing polymorphism

A further three LV experiments (herein labelled LVP2, LVP3 and LVP 4) were conducted to ensure the tractable nature of the high-pressure form as well as its stability at ambient pressure. Our initial experiment had shown that the Form II was stable for two days however we wished to confirm the rate of conversion with PXRD

measurements. The first of these runs showed that the powder produced from the pressure experiment was a mixture of Forms I and II within an hour of decompression (Figure 3.6).

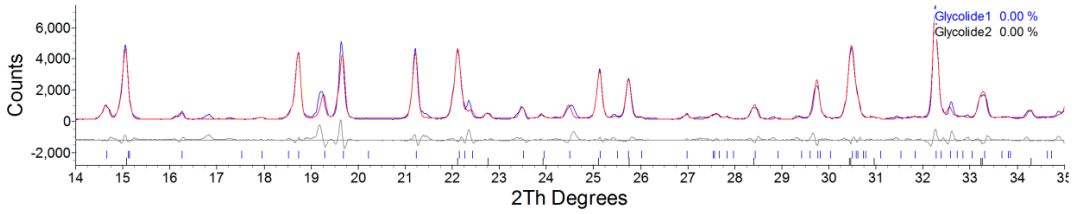

Figure 3.8 - Pawley fit of the recovered material from LVP2 with Forms I and II of glycolide.

In LVP2, the conversion to Form II was not complete but we were able to Pawley fit both unit cells of Form I and II to the pattern confirming that the recrystallised sample that we observed was indeed the form produced at high pressure (Bruker, 2009). There are other peaks which cannot be attributed to either polymorph of glycolide, or to glycolic acid, suggesting the possible low-level presence of some impurities.

However, two subsequent attempts (during one of which, the sample particle size was reduced by grinding prior to loading into the LV press at 0.54 GPa for approximately 54 hours) yielded pure Form I (Figures 3.7 and 3.8). The final large volume press experiment, LVP4, was carried out in order to determine if particle size was an important factor in the extent of conversion from Form I to Form II. Glycolide was gently ground to ensure small particle size before being loaded into the large volume press. Having previously obtained Form II at 0.12 GPa in a DAC experiment, this sample was prepared in the same way and then taken to 0.54 GPa. The sample was left at high pressure for 54 hours before decompression, drying over a Buchner funnel and analysis by PXRD. The observed pattern, shown in Figure 3.8, shows that the resulting powder was pure Form I.

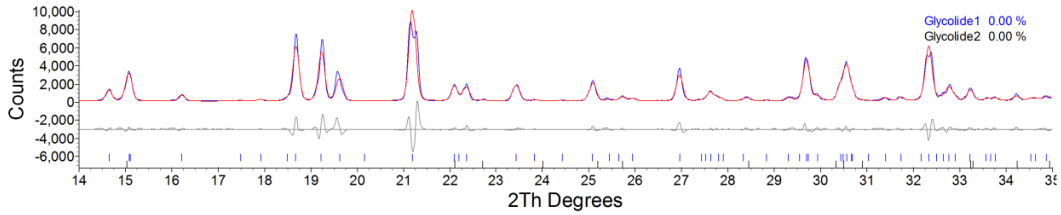

Figure 3.9 - Pawley fit of the recovered material from LVP3 with Forms I and II of glycolide.

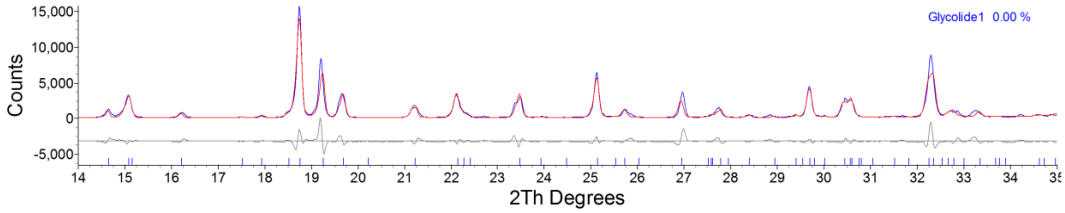

Figure 3.10 - Pawley fit of the powder recovered from experiment LVP4 against the unit cell parameters of Form I.

The failure to recover Form II to ambient pressure is very surprising given the fact that we were able to recrystallise Form II from acetone and that these crystals were stable for 12 days. There are two explanations for this behaviour; firstly, the conversion from Form I to Form II was not complete in the cases of the latter large volume experiments. Secondly, the environment and equipment had been contaminated with seeds of Form I and so any sort of manipulation of the solid after the initial experiments results in the conversion to the more stable form.

The first explanation can be rationalised from the previous DAC experiment where the polycrystalline part of the sample converted whilst the large crystal remained in Form I. This provides evidence that the crystallite size is critical for the conversion to the new form, with smaller particle sizes providing more nucleation sites for the phase transition to occur. However, in the last LV experiment we ensured that the crystals were lightly ground before loading but this did not yield a positive result.

It appears, then, that this may be another case of disappearing polymorphism where our lab environment, including diffractometer and large volume press, has been

contaminated with seeds of Form I leading to rapid conversion to the more stable form (Jack D. Dunitz & Bernstein, 1995). To confirm this disappearing polymorph effect, further experiments in other "uncontaminated" laboratories and environments would need to be conducted (Bombicz, Czugler, Tellgren, & Kálmán, 2003; Webb & Anderson, 1978).

3.3 Conclusions

In this chapter, we have shown the ability to isolate a new polymorph of glycolide at high pressure, recover this to ambient pressure in large scale, and we have been able to seed crystallisation experiments under ambient pressure. Glycolide has shown a large conformational change at relatively low pressures but there was no observation of polymerisation through the application of pressure. The change in behaviour of this form with successive experiments shows that this may be another example of disappearing polymorphism.

3.4 Appendices

Appendix 3.1 – Design and Manufacture of the Large Volume Hydraulic Press

The cross-sectional view of the pressure cell with some key dimensions is shown in Figure 3.5. The key component of the cell is its body made from BERYLCO-25 alloy with the yield strength of 1.4 GPa and machined as a cylinder opened from both ends. The inner diameter of the bore made inside the body of the cell is 10 mm. This is produced with the view to accommodate standard sample PTFE capsule to prevent potential contamination issue if the sample is expected to react with the cell material. The outer diameter of the body of the cell is 35 mm. Calculations conducted by using finite element analysis and experimental testing show that the cell can safely reach the pressure of 0.8 GPa.

The second most important part of the pressure cell is the piston which slides in the bore of the cell and is used for applying pressure to the sample. The piston is also made of BERYLCO-25, and has a copper seal which prevents the capsule from being extruded and prevents the liquid sample from leaking out. In Figure 3.5 the piston is shown in its initial position. At the beginning of the experiment, the cell can accommodate approximately 2.8 mL of the sample in the capsule (10 mm diameter, 64 mm long).

The pressure in the cell is generated in a hydraulic press. It is transmitted to the piston through a tungsten carbide (WC) pusher and measured by the pressure gauge of the press. The attainable pressure inside the cell was calibrated by comparing the pressure on the gauge of the hydraulic press during loading and comparing it with the results generated by finite-element method. Once the required pressure is achieved the retaining nut is rotated to lock the pressure inside the cell. The spacer between the pusher and the piston acts to prevent the twisting torque on the piston from the retaining nut. The spacer and the retaining nut are made from BERYLCO-25 alloy. Once the pressure inside the cell is locked the load in the hydraulic press can be released and the pressure can be retained for the reaction to take place.

Appendix 3.2 - Crystallographic data for Forms I and II of glycolide collected at ambient temperature and pressure

Crystal data Form I at ambient pressure, CCDC deposition number 1043574: $C_4H_4O_4$, M = 116.07, a = 6.7039 (2), b = 14.9481 (4), c = 9.6177 (2) Å, β = 98.9365(18)°, V = 952.10(4) Å^3, T = 296(2) K, space group $P2_1/n$, Z = 8, calculated density = 1.619 g cm^{-3}, 9333 reflections measured, 2092 independent reflections (R_{int} = 0.027). The final R_1 value was 0.045 (I > 2σ(I)). The final wR(F^2) value was 0.123 (all data). Crystal data Form II at ambient pressure, CCDC deposition number 1043575: $C_4H_4O_4$, M = 116.07, a= 5.2400 (2), b = 7.4389 (3), c = 11.7763 (4), V = 459.04(3) Å^3, T = 293(2) K, space group *Pbca*, Z = 4, calculated density = 1.679 g cm^{-3}, 7121 reflections measured, 470 independent reflections (R_{int} = 0.036). The final R_1 value was 0.042 (I > 2σ(I)). The final wR(F^2) value was 0.093 (all data).

Table 3.2 - The interactions energies in kJ mol^{-1} for Forms I and II of glycolide as calculated by PIXELC

	Form I	Form II
Crystal data		
Crystal system, space group	Monoclinic, $P2_1/n$	Orthorhombic, *Pbca*
Temperature (K)	296	293
a, *b*, *c* (Å)	6.7039 (2), 14.9481 (4), 9.6177 (2)	5.2399 (2), 7.4388 (3), 11.7763 (4)
α, β, γ (°)	90, 98.9365 (18), 90	90, 90, 90
V (Å^3)	952.10 (2)	459.02 (2)
Z	8	4
μ (mm^{-1})	0.15	0.16
Density (Mg/m^3)	1.619	1.680
Crystal size (mm)	0.50 × 0.20 × 0.20	0.42 × 0.35 × 0.21
Data collection		
T_{min}, T_{max}	0.85, 0.97	0.69, 0.97

No. of measured, independent and observed [$I > 2.0\sigma(I)$] reflections	9333, 2092, 1879	7121, 470, 456
R_{int}	0.027	0.036
$(\sin\theta/\lambda)_{max}$ (Å^{-1})	0.641	0.625
Refinement		
$R[F^2 > 2\sigma(F^2)]$, $wR(F^2)$, S	0.035, 0.085, 1.06	0.042, 0.093, 0.96
No. of reflections	2075	470
No. of parameters	146	55
No. of restraints	0	38
Δ_{max}, Δ_{min} (e Å^{-3})	0.19, -0.16	0.14, -0.19

CheckCIF statements

Form I

912_ALERT_4_C Missing # of FCF Reflections Above STh/L= 0.600 9

The data are 99.9% to ACTA minimum resolution.

Resolution & Completeness Statistics (Cumulative and Friedel Pairs Averaged)

Theta sin(th)/Lambda Complete Expected Measured Missing

20.82 0.500 0.999 1003 1002 1

23.01 0.550 0.998 1333 1331 2

25.24 0.600 0.999 1712 1711 1

---------- ACTA Min. Res. ---

27.11 0.641 0.995 2102 2092 10

128_ALERT_4_G Alternate Setting of Space-group P21/c P21/n

152_ALERT_1_G The Supplied and Calc. Volume s.u. Differ by ... 2 Units

432_ALERT_2_G Short Inter X...Y Contact O4 .. C7 .. 2.94 Ang.

760_ALERT_1_G CIF Contains no Torsion Angles ..... ?

808_ALERT_5_G No Parseable SHELXL Style Weighting Scheme Found !

929_ALERT_5_G No Weight Pars,Obs and Calc R1,wR2,S not checked !

960_ALERT_3_G Number of Intensities with I .LT. - 2*sig(I) .. 7

Noted, no action taken

Form II

088_ALERT_3_C Poor Data / Parameter Ratio 8.55

910_ALERT_3_C Missing # of FCF Reflections Below Th(Min) 1

912_ALERT_4_C Missing # of FCF Reflections Above STh/L= 0.600 2

313_ALERT_2_C Oxygen with three covalent bonds (rare) O30

313_ALERT_2_C Oxygen with three covalent bonds (rare) O31

301_ALERT_3_G Note: Main Residue Disorder ..... 50 Perc.

432_ALERT_2_G Short Inter X...Y Contact O30 .. C2 .. 2.96 Ang.

432_ALERT_2_G Short Inter X...Y Contact O31 .. C2 .. 3.01 Ang.

811_ALERT_5_G No ADDSYM Analysis: Too Many Excluded Atoms .... !

860_ALERT_3_G Note: Number of Least-Squares Restraints 38

The model is disordered and therefore parameters for both components are required. The data are 99.8 % complete to the ACTA min. resolution. The contacts may be a little close but these will be artefacts of the disorder.

Resolution & Completeness Statistics (Cumulative and Friedel Pairs Averaged)

Theta	sin(th)/Lambda	Complete	Expected	Measured	Missing
20.82	0.500	0.996	236	235	1
23.01	0.550	0.994	317	315	2
25.24	0.600	0.998	415	414	1
----------	----------	----------	----------	----------	ACTA Min. Res. ---
26.39	0.625	0.994	473	470	3

199_ALERT_1_G Check the Reported _cell_measurement_temperature 293 K

200_ALERT_1_G Check the Reported _diffrn_ambient_temperature 293 K

The temperature of data collection was 293K

152_ALERT_1_C The Supplied and Calc. Volume s.u. Differ by ... 14 Units

760_ALERT_1_G CIF Contains no Torsion Angles ..... ?

808_ALERT_5_G No Parseable SHELXL Style Weighting Scheme Found !

929_ALERT_5_G No Weight Pars,Obs and Calc R1,wR2,S not checked !

Noted, no action taken.

3.5 References

Allen, F. H., Baalham, C. A., Lommerse, J. P. M., & Raithby, P. R. (1998). Carbonyl-Carbonyl Interactions can be Competitive with Hydrogen Bonds. *Acta Cryst*, *54*, 320–329. http://doi.org/10.1107/S0108768198001463

Altomare, A., Cascarano, G., Giacovazzo, C., Guagliardi, A., Burla, M. C., Polidori, G., & Camalli, M. (1994). SIRPOW .92 – a program for automatic solution of crystal structures by direct methods optimized for powder data. *Journal of Applied Crystallography*, *27*(3), 435–436. http://doi.org/10.1107/S0021889894000221

Bala, I., Hariharan, S., & Kumar, M. N. V. R. (2004). PLGA nanoparticles in drug delivery: the state of the art. *Critical Reviews in Therapeutic Drug Carrier Systems*, *21*, 387–422. http://doi.org/10.1615/CritRevTherDrugCarrierSyst.v21.i5.20

Belenkaya, B. G., Belsky, V. K., Dementev, A. I., Sakharova, V. I., Chernikova, N. Y. (1997). No Title. *Crystallogr. Rep.*, *42*, 449.

Betteridge, P. W., Carruthers, J. R., Cooper, R. I., Prout, K., & Watkin, D. J. (2003). CRYSTALS version 12: software for guided crystal structure analysis. *Journal of Applied Crystallography*, *36*(6), 1487–1487. http://doi.org/10.1107/S0021889803021800

Boldyreva, E. V., Shakhtshneider, T. P., Ahsbahs, H., Sowa, H., & Uchtmann, H. (2002). Effect of high pressure on the polymorphs of paracetamol. In *Journal of Thermal Analysis and Calorimetry* (Vol. 68, pp. 437–452). http://doi.org/10.1023/A:1016079400592

Bombicz, P., Czugler, M., Tellgren, R., & Kálmán, A. (2003). A Classical Example of a Disappearing Polymorph and the Shortest Intermolecular H · · · H Separation Ever Found in an Organic Crystal Structure. *Angewandte Chemie International Edition*, *42*(17), 1957–1960. http://doi.org/10.1002/anie.200219504

Bruker, A. X. S. (2009). *General profile and structure analysis software for powder diffraction data*. *Scientific American* (Version 5, Vol. 302). http://doi.org/10.1038/scientificamerican0610-4

Ceppatelli, M., Santoro, M., Bini, R., & Schettino, V. (2000). Fourier Transform Infrared Study of the Pressure and Laser Induced Polymerization of Solid Acetylene. *Journal of Chemical Physics*, *113*(14), 5991–6000. http://doi.org/Pii [S0021-9606(00)50735-1]\nDoi 10.1063/1.1288800

Chelazzi, D., Ceppatelli, M., Santoro, M., Bini, R., & Schettino, V. (2005). Pressure-induced polymerization in solid ethylene. *Journal of Physical Chemistry B*, *109*(46), 21658–21663. http://doi.org/10.1021/jp0536495

Day, R. M., Boccaccini, A. R., Shurey, S., Roether, J. A., Forbes, A., Hench, L. L., & Gabe, S. M. (2004). Assessment of polyglycolic acid mesh and bioactive glass for soft-tissue engineering scaffolds. *Biomaterials*, *25*, 5857–5866. http://doi.org/10.1016/j.biomaterials.2004.01.043

Dunitz, J. D., & Bernstein, J. (1995). Disappearing Polymorphs. *Accounts of Chemical Research*, *28*(4), 193–200. http://doi.org/10.1021/ar00052a005

Dunitz, J. D., & Gavezzotti, A. (2012). Proteogenic Amino Acids: Chiral and Racemic Crystal Packings and Stabilities. *The Journal of Physical Chemistry B*, *116*(23), 6740–6750. http://doi.org/10.1021/jp212094d

Fabbiani, F. P. A., Allan, D. R., David, W. I. F., Davidson, A. J., Lennie, A. R., Parsons, S., … Warren, J. E. (2007). High-pressure studies of pharmaceuticals: An exploration of the behavior of piracetam. *Crystal Growth and Design*, *7*(6), 1115–1124. http://doi.org/10.1021/cg0607710

Fabbiani, F. P. a, Buth, G., Levendis, D. C., & Cruz-Cabeza, A. J. (2014). Pharmaceutical hydrates under ambient conditions from high-pressure seeds: a case study of GABA monohydrate. *Chemical Communications (Cambridge, England)*, *50*, 1817–9. http://doi.org/10.1039/c3cc48466a

Florence, A. J., Baumgartner, B., Weston, C., Shankland, N., Kennedy, A. R., Shankland, K., & David, W. I. F. (2003). Indexing powder patterns in physical form screening: Instrumentation and data quality. *Journal of Pharmaceutical Sciences*, *92*(9), 1930–1938. http://doi.org/10.1002/jps.10459

Frisch, M. J., Trucks, G. W., Schlegel, H. B., Scuseria, G. E., Robb, M. A., Cheeseman, J. R., … Fox, D. J. (2009). Gaussian 09, Revision A.01. *Gaussian Inc Wallingford CT*. Wallingford CT. http://doi.org/citeulike-article-id:9096580

Gavezzotti, A. (2003). Calculation of intermolecular interaction energies by direct numerical integration over electron densities. 2. An improved polarization model and the evaluation of dispersion and repulsion energies. *Journal of Physical Chemistry B*, *107*(10), 2344–2353. http://doi.org/10.1021/jp022288f

Jain, R. a. (2000). The manufacturing techniques of various drug loaded biodegradable poly(lactide-co-glycolide) (PLGA) devices. *Biomaterials*, *21*(23), 2475–2490. http://doi.org/10.1016/S0142-9612(00)00115-0

Johnston, B. F., Marshall, W. G., Parsons, S., Urquhart, A. J., & Oswald, I. D. H. (2014). Investigation of acrylic acid at high pressure using neutron diffraction.

Journal of Physical Chemistry B, *118*(14), 4044–4051. http://doi.org/10.1021/jp502095n

Merrill, L., & Bassett, W. A. (1974). Miniature Diamond Anvil Pressure Cell for Single-Crystal X-Ray-Diffraction Studies. *Rev. Sci. Instrum.*, *45*(2), 290–294. http://doi.org/Doi 10.1063/1.1686607

Merrill, L., & Bassett, W. A. (1974). Miniature diamond anvil pressure cell for single crystal x-ray diffraction studies. *Review of Scientific Instruments*, *45*, 290–294. http://doi.org/10.1063/1.1686607

Millar, D. I. A., Oswald, I. D. H., Barry, C., Francis, D. J., Marshall, W. G., Pulham, C. R., & Cumming, A. S. (2010). Pressure-cooking of explosives--the crystal structure of epsilon-RDX as determined by X-ray and neutron diffraction. *Chemical Communications (Cambridge, England)*, *46*(31), 5662–4. http://doi.org/10.1039/c0cc00368a

Miller, S. A. (2013). Sustainable polymers: Opportunities for the next decade. *ACS Macro Letters*, *2*, 550–554. http://doi.org/10.1021/mz400207g

Moggach, S. A., Allan, D. R., Parsons, S., & Warren, J. E. (2008a). Incorporation of a new design of backing seat and anvil in a Merrill-Bassett diamond anvil cell. *Journal of Applied Crystallography*, *41*, 249–251. http://doi.org/10.1107/S0021889808000514

Moggach, S. A., Allan, D. R., Parsons, S., & Warren, J. E. (2008b). Incorporation of a new design of backing seat and anvil in a Merrill-Bassett diamond anvil cell. *Journal of Applied Crystallography*, *41*(2), 249–251. http://doi.org/10.1107/S0021889808000514

Mundargi, R. C., Babu, V. R., Rangaswamy, V., Patel, P., & Aminabhavi, T. M. (2008, February 11). Nano/micro technologies for delivering macromolecular therapeutics using poly(d,l-lactide-co-glycolide) and its derivatives. *Journal of Controlled Release*. http://doi.org/10.1016/j.jconrel.2007.09.013

Murli, C., Mishra, A. K., Thomas, S., & Sharma, S. M. (2012a). Ring-opening polymerization in carnosine under pressure. *Journal of Physical Chemistry B*, *116*, 4671–4676. http://doi.org/10.1021/jp300248b

Murli, C., Mishra, A. K., Thomas, S., & Sharma, S. M. (2012b). Ring-opening polymerization in carnosine under pressure. *Journal of Physical Chemistry B*, *116*(15), 4671–4676. http://doi.org/10.1021/jp300248b

Murli, C., & Song, Y. (2010). Pressure-Induced polymerization of acrylic acid: A raman spectroscopic study. *Journal of Physical Chemistry B*, *114*(30), 9744–9750. http://doi.org/10.1021/jp1034757

Oswald, I. D. H., Chataigner, I., Elphick, S., Fabbiani, F. P. A., Lennie, A. R., Maddaluno, J., … Smith, R. I. (2009). Putting pressure on elusive polymorphs and solvates. *CrystEngComm*, *11*(2), 359–366. http://doi.org/10.1039/B814471K

Oswald, I. D. H., & Urquhart, A. J. (2011). Polymorphism and Polymerisation of Acrylic and Methacrylic Acid at High Pressure. *Crystengcomm*, *13*(14), 4503–4507. http://doi.org/10.1039/c1ce05295k

Patyk, E., Skumiel, J., Podsiadło, M., & Katrusiak, A. (2012). High-pressure (+)-sucrose polymorph. *Angewandte Chemie - International Edition*, *51*(9), 2146–2150. http://doi.org/10.1002/anie.201107283

Piermarini, G. J., Block, S., Barnett, J. D., & Forman, R. A. (1975). Calibration of the pressure dependence of the R1 ruby fluorescence line to 195 kbar. *Journal of Applied Physics*, *46*(6), 2774–2780. http://doi.org/10.1063/1.321957

Pillai, C. K. S., & Sharma, C. P. (2010). Review paper: absorbable polymeric surgical sutures: chemistry, production, properties, biodegradability, and performance. *Journal of Biomaterials Applications*, *25*(4), 291–366. http://doi.org/10.1177/0885328210384890

Satthaphut, N., Sutcliffe, O. B., & Oswald, I. D. H. (2014). Putting the squeeze on mephedrone hydrogen sulfate. *Zeitschrift Fur Kristallographie*, *229*(2), 101–111. http://doi.org/10.1515/zkri-2013-1639

Seryotkin, Y. V, Drebushchak, T. N., & Boldyreva, E. V. (2013). A high-pressure polymorph of chlorpropamide formed on hydrostatic compression of the ??-form in saturated ethanol solution. *Acta Crystallographica Section B: Structural Science, Crystal Engineering and Materials*, *69*(1), 77–85. http://doi.org/10.1107/S2052519212051147

Sheldrick, G. M. (2001). SADABS. *University of Gottingen, Germany, Bruker AXS Madison, Wisconsin, USA*.

Solhaug, J. H., & Heimann, P. (1975). Polyglycolic acid (PGA, Dexon) sutures in neck surgery. *Acta Chirurgica Scandinavica*, *141*, 326–328.

Webb, J., & Anderson, B. (1978). Problems with crystals. *Journal of Chemical Education*, *55*(10), 644. http://doi.org/10.1021/ed055p644

Wood, P. A., Francis, D., Marshall, W. G., Moggach, S. A., Parsons, S., Pidcock, E., & Rohl, A. L. (2008). A study of the high-pressure polymorphs of L-serine using

ab initio structures and PIXEL calculations. *CrystEngComm*, *10*(9), 1154–1166. http://doi.org/10.1039/B801571F

Chapter 4 – Analysis of hydrogenous glycolide at high pressure using Neutron powder diffraction

4.1 Introduction

The work in this chapter follows on from that in Chapter 3, in which the behaviour of glycolide under high pressure was studied, demonstrating that particle size was an important factor in whether the phase transformation was observed or not. It was observed that a portion of single crystal showed no change in the Raman spectrum, however a corner of the crystal which had been crushed on loading showed the transformation. The Raman spectra of Forms I and II of glycolide are shown in Figure 4.1.

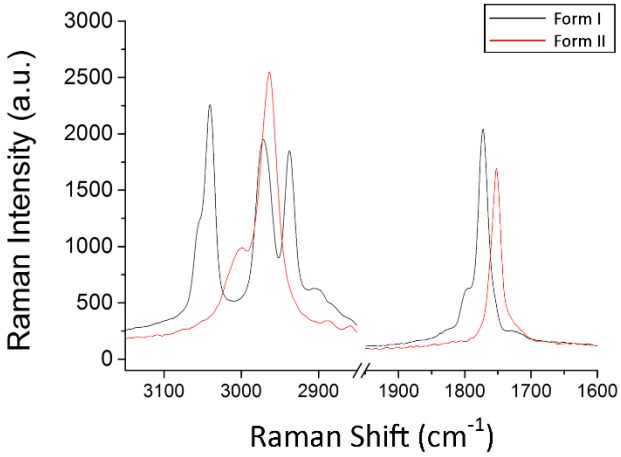

Figure 4.1 - Raman spectra of Forms I and II of glycolide, focussing on the C-H stretch region and the ester linkage region.

It was subsequently observed that the single crystal underwent a reconstructive phase transition at 0.4 GPa, resulting in the degradation of the single crystal. Consequently, it was not possible to collect SXRD data on the previously unobserved Form II, although it was noted that Form II remained stable upon decompression to ambient conditions. A large volume press (described in section 3.5) was employed to produce Form II in gram quantity with the recovered material being used to seed crystal growth from a solution in acetone. The resulting crystals were analysed via SXRD, allowing the structure of Form II to be fully solved. The structures of both polymorphs are shown in Figure 4.2. The highly puckered ring structure in Form I is

seen to flatten significantly over the phase transition, with Form II showing a near-planar ring sitting over an inversion centre.

The unit cell parameters of this single crystal were Pawley-refined against XRD data collected on a powdered sample of glycolide at 0.12 GPa (see Figure 4.3). This confirmed that the polymorph obtained through seeding of a solution in acetone with glycolide recovered from the large volume press was the same as that observed in the DAC. The lower pressure at which Form II was observed (c.f. the 0.4 GPa at which the transition was observed in a single crystal sample in Chapter 3) suggests an effect relating to the impact of particle size on the phase transition.

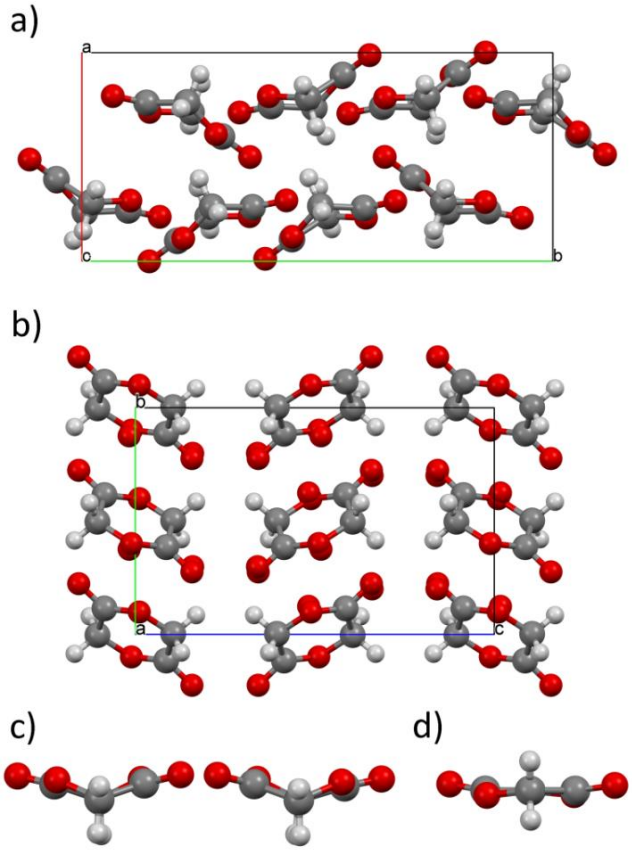

Figure 4.2- Packing diagrams of a) Form I and b) Form II of glycolide. c) The two molecules in Form I exhibit a highly puckered twist-boat conformation whilst d) the molecule in Form II is almost planar.

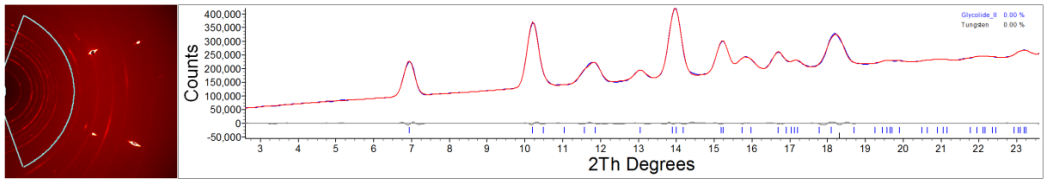

Figure 4.3 - Powder X-ray diffraction pattern of glycolide at 0.12 GPa.

Table 4.1 summarises the unit cell parameters of Forms I and II of glycolide, from SXRD analysis.

Table 4.1 - Unit cell parameters of Forms I and II of glycolide

Unit Cell Parameter	**Form I**	**Form II**
a (Å)	6.7039(2)	5.2399(2)
b (Å)	14.9481(4)	7.4388(3)
c (Å)	9.6177(2)	11.7763(4)
α (°)	90	90
β (°)	98.9365(18)	90
γ (°)	90	90
Unit Cell Volume (Å^3)	952.10(2)	459.02(2)
Space Group	$P2_1/n$	P*bca*
Z	8	4

The initial experiment in chapter 3 highlights the lack of precision with which the pressure can be controlled, resulting in the relatively large steps in pressure between data collections. Furthermore, the inability to collect in-situ data in the large volume press meant it was not possible to precisely measure the pressure at which the phase transition occurred in the powdered sample used in these experiments.

After the powder diffraction pattern of Form II was obtained at 0.12 GPa, a further PXRD data collection at 0.9 GPa showed the existence of a previously unknown third polymorph of glycolide (Figure 4.4). The simple diffraction pattern, showing four prominent reflections does not match the diffraction patterns of either of the known polymorphs (Figure 4.4 c.f. Figure 4.3).

Based on this evidence, time was granted to study the system on the PEARL beamline at the ISIS Neutron and Muon source. Other research has shown phase transitions

as well as polymerisation (Oswald & Urquhart, 2011) occurring upon decompression with this possibility to be investigated using neutron diffraction.

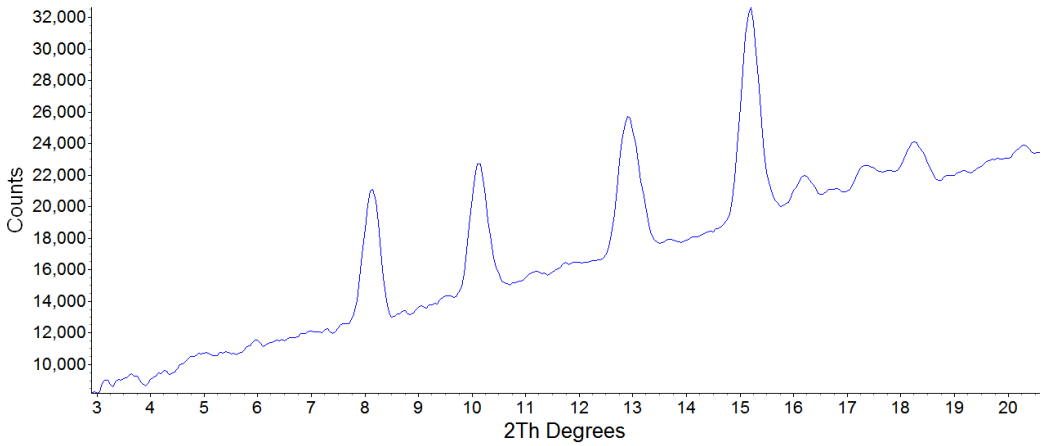

Figure 4.4 - Diffraction of a third form of glycolide, collected at 0.9 GPa.

4.2 Experimental

A comparative advantage of collecting data on the PEARL beamline is the high degree of control over the pressure exerted on the sample. With the load increased in increments of 2 – 3 tonnes, one can better control the step size in pressure increase. In addition to this, relatively small quantities of data can be collected and subsequently analysed separately or summed together allowing the phase transitions observed to be studied much more closely.

Typically, samples studied using neutron diffraction are deuterated in order to reduce the background associated with the inelastic scattering of ^{1}H nuclei (as discussed in Section 1.2 of this thesis). Recent advances at the PEARL beamline have included the development of Zirconium-Toughened Alumina (ZTA) anvils. The ZTA anvils do not absorb neutrons, and so contribute less background giving an improved signal-to-noise ratio when compared to their tungsten carbide (WC) predecessors.

Due to difficulties encountered when trying to deuterate the glycolide sample prior to this experiment, the sample used for data collection was fully hydrogenous – $C_4H_4O_4$. This presented an opportunity not only study the behaviour of the glycolide sample under high pressure, but also to assess the quality of neutron diffraction data which may be collected using a fully hydrogenous sample in conjunction with the new ZTA anvils, and to compare this, for example, to the data collected on a deuterated sample with the WC anvils.

Glycolide (Sigma-Aldrich) was recrystallised from acetone prior to use. A titanium-zirconium (TiZr) encapsulated gasket and ZTA anvils were cooled, along with a 1:1 (v/v) mixture of pentane and isopentane to 263 K. The sample, gently ground using a mortar and pestle, was added to the gasket along with a small lead pellet (for use as a pressure calibrant), and the cooled PTM mixture. Pre-cooling of the components of the gasket-anvil assembly allowed easier loading of the cell since both components of the PTM are highly volatile. The gasket was loaded into the P-E cell and a load of 6 tonnes was applied to seal the gasket without applying significant pressure to the sample.

Data were collected as the load was increased, typically in increments of 3 tonnes, up to a maximum load of 66 tonnes (equating to a pressure of 5.00(2) GPa). Data were also collected upon decompression of the sample in order to study the transition to the unknown third form observed in the DAC experiment and the behaviour of this form as the sample was recovered to ambient conditions. Note that in the previous chapter, it was observed that it was possible to recover the high pressure Form II to ambient conditions.

Collection times were higher than for deuterated samples, but commensurate with those previously required for deuterated samples using the WC anvils. Longer data sets collected over approximately 7 hours, with exposure in the region of 1200 μA hours of radiation, were collected in steps of around 1 GPa. These data sets were Rietveld-fitted, with the shorter data sets (collected over 2 – 3½ hours) being Pawley-fitted. Data obtained at 0.388(10), 1.791(13), 2.579(15), 4.000(19) and 5.00(2) GPa

were sufficient to perform Rietveld analysis, as shown in the load versus pressure plot in Figure 4.5. During the decompression stage, the data collected at 4.28(3), 3.315(18), 2.985(16) and 1.274(14) GPa were also sufficient to permit Rietveld analysis.

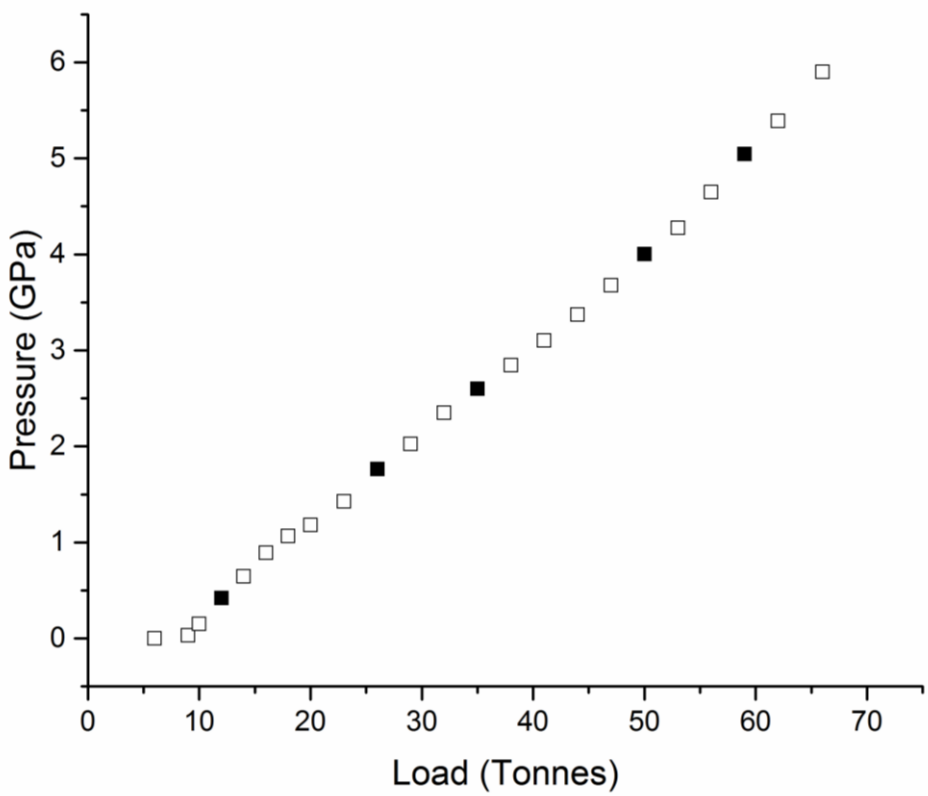

Figure 4.5 - The response of pressure to the applied load shows a linear response. Hollow shapes designate Pawley-fitted data, whilst the filled shapes designate Rietveld-fitted data.

4.3 Results and Discussion

4.3.1 Neutron Diffraction Data

The first data set, at a pressure of 0.000(19) GPa, showed the sample to be in its ambient form (Form I), with the next pressure point, 0.031(14) GPa, closely resembling the diffraction pattern of Form II. Visual inspection of the diffraction pattern observed at this pressure indicates the presence of Form I in smaller

quantities, as highlighted in Figure 4.6. The next increase in pressure, to 0.152(12) GPa, resulted in a clean diffraction pattern of Form II being observed.

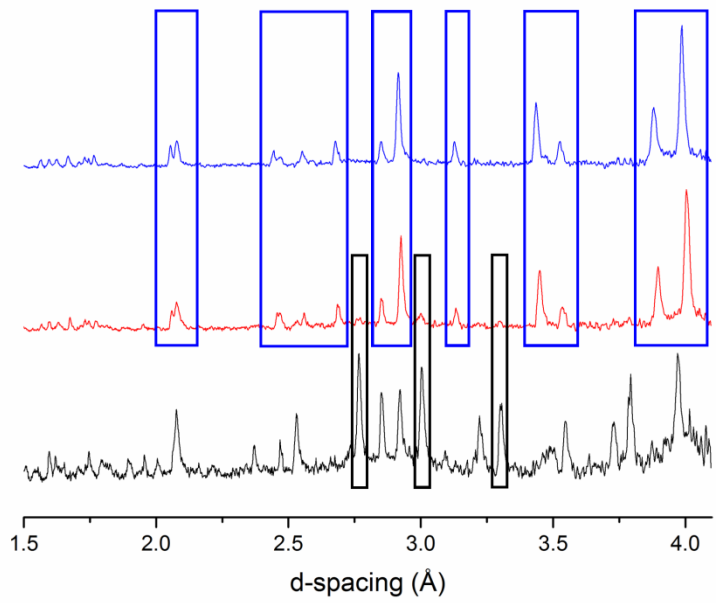

Figure 4.6 - Diffraction patterns of the data collected on glycolide-h4 at three lowest pressure points. The data collected at 0.000(19) GPa, 0.031(14) GPa and 0.152(12) GPa are represented by the black, red and blue plots, respectively. The black and blue boxes highlight the features of the diffraction patterns of Forms I and II, respectively, which are present in the data collected at 0.031(14) GPa.

The diffraction patterns collected upon compression of the sample from 0.388(10) GPa up to 5.00(2) GPa are shown in Figure 4.7 a. From visual observation, there are no significant changes in the diffraction patterns indicating that Form II is stable up to this pressure. Even upon decompression (Figure 4.7 b), there are no significant changes in the diffraction patterns that may have indicated a further phase transition or polymerisation. The diffraction pattern at 0.047 GPa, after complete removal of the mechanical load, visually matches those of Form II collected at higher pressures, showing that Form II can be successfully recovered to ambient conditions as reported in Chapter 3; the longevity of Form II under ambient conditions was not investigated due to restriction on time.

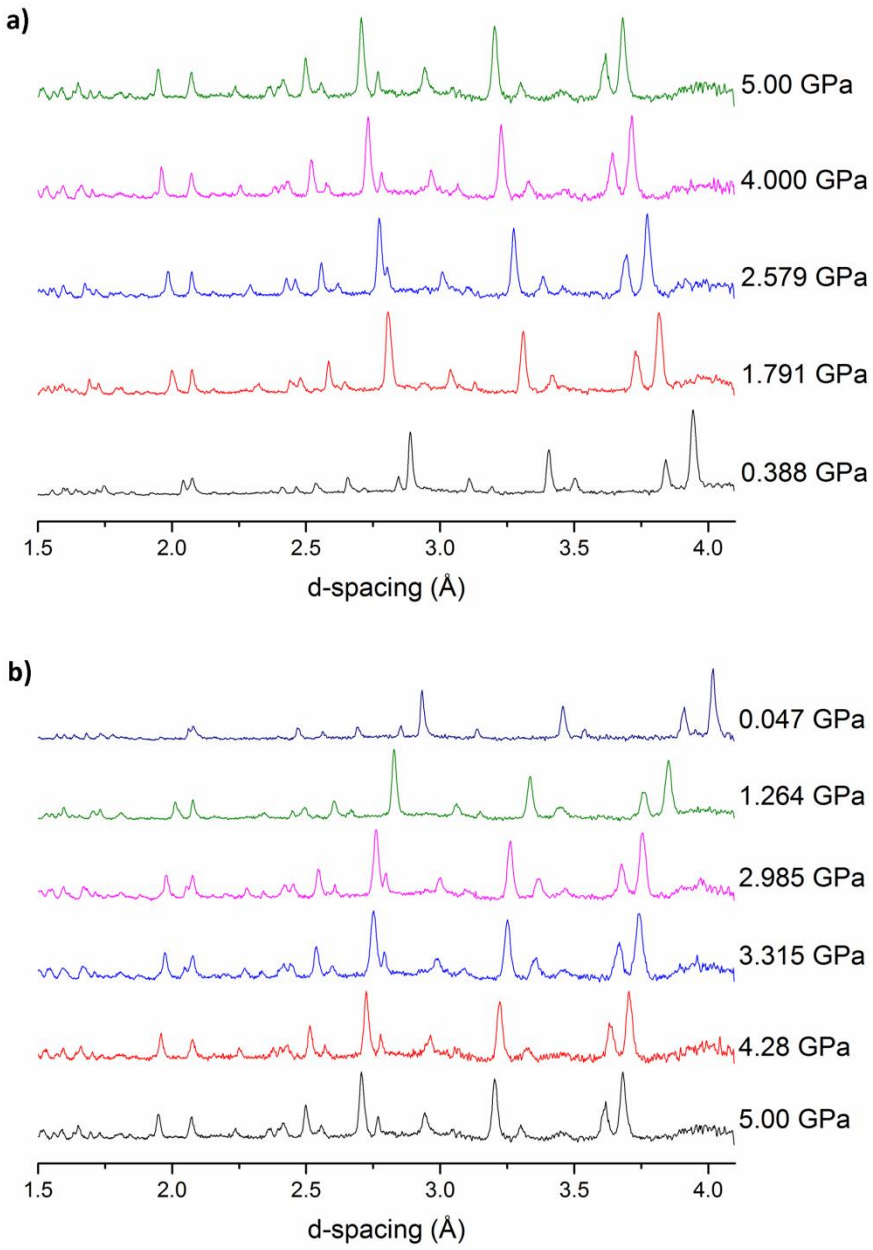

Figure 4.7 - Diffraction patterns of glycolide-h4 Form 2 upon a) compression and b) decompression.

Pawley refinements of the known structure of Form I (for the data collected at 0.000 GPa) and of the known structures of both Forms I and II (for the data collected at 0.031 GPa) showed these to be pure Form I and a mixed phase of Forms I and II, respectively. Subsequent Pawley and Rietveld refinements of the known structure of Form II for all data collected at higher pressures, as well as the data collected upon

decompression, generally showed good fits. The Rietveld fits of the data collected upon compression and decompression are shown in Figure 4.8 and 4.9, respectively.

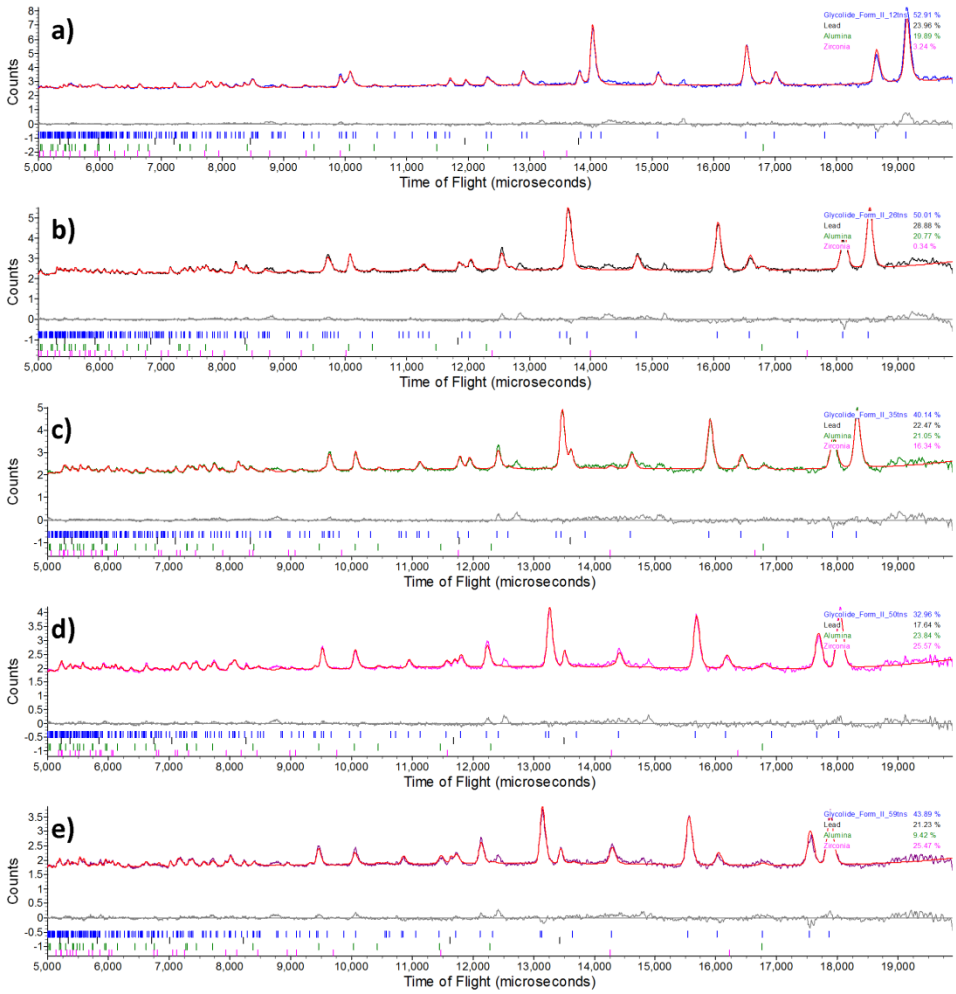

Figure 4.8 - Rietveld fits of the neutron diffraction data collected at a) 0.388 GPa, b) 1.791 GPa, c) 2.579 GPa, d) 4.000 GPa, and e) 5.00 GPa.

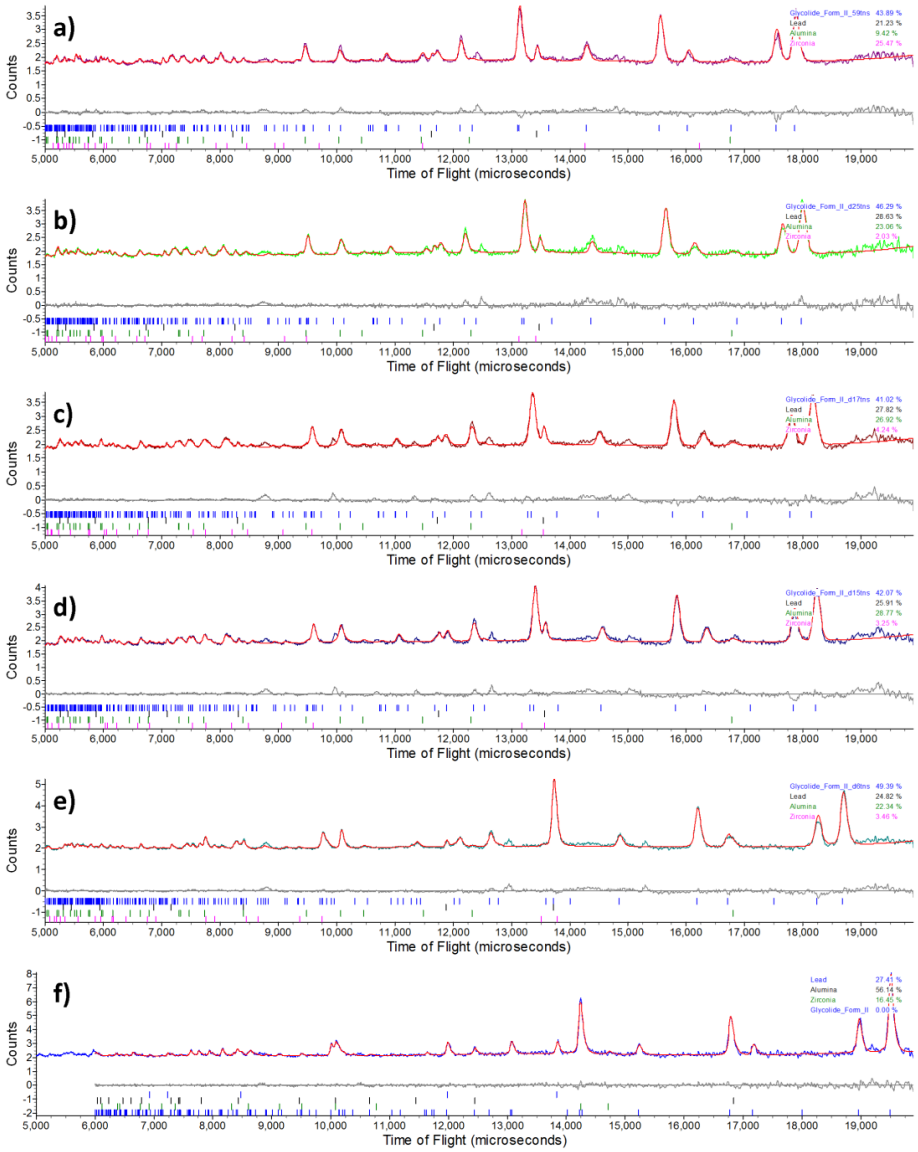

Figure 4.9 - Rietveld fits of the neutron diffraction data collected upon at a) 5.00 GPa, and upon decompression at b) 4.28 GPa, c) 3.315 GPa, d) 2.985 GPa, and e) 1.264 GPa. Plot f) shows the Pawley fit of the data collected after removal of the applied load (at which point the pressure refined to 0.047 GPa).

As seen in Figure 4.8, there are some small peaks in the diffraction patterns which are not accounted for by Form II of glycolide or any of the other known materials present (i.e. lead, alumina and zirconia). Figure 4.10 shows the progressive movement of these peaks against time of flight with increasing pressure, along with that of four assigned peaks of glycolide Form II and one assigned peak of lead. The equations of each of the third-order polynomial fits (in the format $y = ax^2 + bx + c$), as well as the shift in microseconds from 0.388 to 5.00 GPa, are shown in Table 4.2.

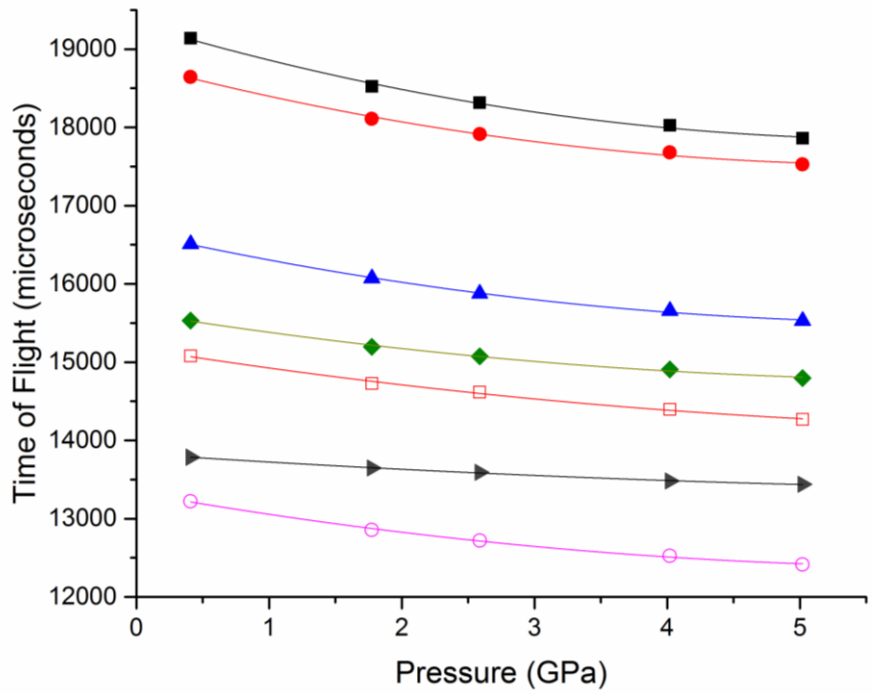

Figure 4.10 - Position of peaks with increasing pressure. The filled black squares, red circles, blue triangles and green diamonds represent the (111), (102), (112) and (022) reflections of glycolide Form II. The filled grey triangles represent the (111) reflection of lead. The hollow red squares and hollow pink circles represent two unassigned peaks.

Table 4.2 - Polynomial fits of each of the seven identified reflections.

Reflection	Material	Symbol	a	b	c	r^2	Shift (µs)
111	Form II	■	41.199	-504.529	19,321.157	0.993	1,279
102	Form II	●	38.480	-443.934	18,803.871	0.992	1,117
112	Form II	▲	31.331	-378.951	16,653.622	0.998	978
022	Form II	◆	17.931	-269.244	15,177.271	0.993	809
111	Lead	▶	6.941	-113.395	1,380.900	0.997	347
Misfit A	Unknown	□	21.526	-272.124	15,632.496	0.994	736
Misfit B	Unknown	○	23.709	-300.151	13,333.075	0.997	806

Since the time of flight is directly proportional to the interplanar distance (Figure 1.13), the extent to which a peak moves with applied pressure depends on the sample's compressibility. The marked difference between the degree to which the lead peak moves compared the four assigned Form II peaks and two unassigned peaks suggests that the substance reponsible for the two unassigned peaks is much closer to an organic material than the lead in its compressibility hence may be associated with the 3rd form that was observed in the X-ray DAC powder experiment. The d-spacing that this peak occurs at is approximately 3.13Å which corresponds to 13° 2θ (λ = 0.71073 Å). From Figure 4.3 there is a peak around this value which strengthens the argument that it is the appearance of the new form. Although there is no further evidence of the third phase of glycolide it can be assumed that it is likely to be denser and less compressible than Form II. The refined unit cell parameters are listed in Tables 4.3 (compression) and 4.4 (decompression), with those from the data collected upon compression illustrated in Figure 4.11.

Table 4.3 - Refined unit cell parameters of glycolide upon compression

Pawley / Rietveld	Load (tonnes)	Form	Pressure (GPa)	Space Group	a-axis (Å)	b-axis (Å)	c-axis (Å)	β (°)	Unit Cell Volume (Å^3)	Molecular Volume (Å^3)	R_wp
Pawley	6	1	0.000(19)	$P2_1/n$	6.7037(7)	14.9640(17)	9.619(3)	98.884(15)	953.3(3)	119.1625	1.288
Pawley	9	1	0.031(14)	$P2_1/n$	6.689(3)	14.942(9)	9.610(5)	98.77(6)	949.3(9)	118.6625	1.157
Pawley	9	2	0.031(14)	*Pbca*	5.2240(8)	7.4321(11)	11.780(2)	90	457.35(13)	114.3375	1.157
Pawley	10	2	0.152(12)	*Pbca*	5.1906(4)	7.4150(5)	11.7692(15)	90	452.98(7)	113.245	1.887
Rietveld	12	2	0.388(10)	*Pbca*	5.1176(4)	7.3666(4)	11.7168(10)	90	441.72(6)	110.43	1.693
Pawley	14	2	0.64(2)	*Pbca*	5.0604(6)	7.3184(6)	11.6661(19)	90	432.05(9)	108.0125	2.04
Pawley	16	2	0.891(15)	*Pbca*	5.0252(5)	7.2861(7)	11.6373(19)	90	426.09(9)	106.5225	1.932
Pawley	18	2	1.07(3)	*Pbca*	5.0053(6)	7.2666(8)	11.6161(19)	90	422.49(10)	105.6225	2.077
Pawley	20	2	1.18(2)	*Pbca*	4.9859(5)	7.2512(7)	11.5914(18)	90	419.07(9)	104.7675	1.916
Pawley	23	2	1.43(3)	*Pbca*	4.9552(6)	7.2155(7)	11.560(2)	90	413.33(10)	103.3325	2.21
Rietveld	26	2	1.791(12)	*Pbca*	4.9213(4)	7.1796(5)	11.5252(11)	90	407.22(6)	101.805	1.831
Pawley	29	2	2.02(2)	*Pbca*	4.8989(7)	7.1545(8)	11.494(2)	90	402.86(11)	100.715	2.234
Pawley	32	2	2.35(2)	*Pbca*	4.8772(7)	7.1270(8)	11.468(3)	90	398.64(12)	99.66	2.279
Rietveld	35	2	2.579(15)	*Pbca*	4.8574(4)	7.1027(5)	11.4474(11)	90	394.95(6)	98.7375	1.936
Pawley	38	2	2.85(2)	*Pbca*	4.8401(7)	7.0825(8)	11.426(2)	90	391.69(11)	97.9225	2.139
Pawley	41	2	3.10(3)	*Pbca*	4.8253(8)	7.0650(10)	11.409(3)	90	388.95(13)	97.2375	2.539
Pawley	44	2	3.37(2)	*Pbca*	4.8107(8)	7.0402(10)	11.381(3)	90	385.44(13)	96.36	2.472
Pawley	47	2	3.68(3)	*Pbca*	4.7924(8)	7.0212(10)	11.356(3)	90	382.13(13)	95.5325	2.421
Rietveld	50	2	4.000(19)	*Pbca*	4.7763(4)	6.9926(6)	11.3377(12)	90	378.66(6)	94.665	1.943
Pawley	53	2	4.28(2)	*Pbca*	4.7615(8)	6.9771(11)	11.322(3)	90	376.14(13)	94.035	2.197
Pawley	56	2	4.65(2)	*Pbca*	4.7453(7)	6.9536(10)	11.303(2)	90	372.96(11)	93.24	1.868
Rietveld	59	2	5.00(2)	*Pbca*	4.7319(5)	6.9302(6)	11.2791(14)	90	369.87(7)	92.4675	2.212
Pawley	62	2	5.39(3)	*Pbca*	4.7196(8)	6.9133(13)	11.262(3)	90	367.45(14)	91.8625	2.384
Pawley	66	2	5.90(3)	*Pbca*	4.7009(9)	6.8872(14)	11.236(3)	90	363.78(15)	90.945	2.606

Table 4.4 - Refined unit cell parameters of glycolide upon decompression

Pawley / Rietveld	Load (tonnes)	Form	Pressure (GPa)	Space Group	a-axis (Å)	b-axis (Å)	c-axis (Å)	β (°)	Unit Cell Volume (Å^3)	Molecular Volume (Å^3)	R_wp
Pawley	66	2	*Pbca*	5.90(3)	4.7009(9)	6.8872(14)	11.236(3)	90	363.78(15)	90.945	2.606
Pawley	35	2	*Pbca*	5.07(3)	4.7285(7)	6.9281(11)	11.283(3)	90	369.61(12)	92.4025	2.355
Pawley	30	2	*Pbca*	4.64(2)	4.7491(8)	6.9559(11)	11.293(3)	90	373.05(12)	93.2625	2.327
Rietveld	25	2	*Pbca*	4.28(3)	4.7648(7)	6.9751(9)	11.322(2)	90	376.28(10)	94.07	2.224
Pawley	20	2	*Pbca*	3.97(6)	4.7791(14)	7.0031(18)	11.352(5)	90	379.9(2)	94.975	4.366
Rietveld	17	2	*Pbca*	3.315(18)	4.8135(6)	7.0449(7)	11.3903(16)	90	386.25(8)	96.5625	2.187
Rietveld	15	2	*Pbca*	2.985(16)	4.8311(5)	7.0696(6)	11.4140(14)	90	389.84(7)	97.46	2.186
Pawley	13.5	2	*Pbca*	2.78(3)	4.8424(11)	7.0842(13)	11.438(4)	90	392.38(17)	98.095	3.254
Pawley	12	2	*Pbca*	2.64(2)	4.8554(9)	7.1032(10)	11.443(3)	90	394.67(14)	98.6675	2.758
Pawley	10	2	*Pbca*	2.19(3)	4.8895(10)	7.1464(12)	11.491(3)	90	401.54(15)	100.385	3.161
Pawley	8.5	2	*Pbca*	2.02(5)	4.8974(10)	7.1566(13)	11.505(3)	90	403.22(16)	100.805	3.153
Rietveld	6	2	*Pbca*	1.264(14)	4.9687(5)	7.2360(7)	11.5816(16)	90	416.40(8)	104.1	1.91
Pawley	0	2	*Pbca*	0.047(14)	5.2460(5)	7.4432(8)	11.7946(14)	90	460.55(9)	115.1375	2.283

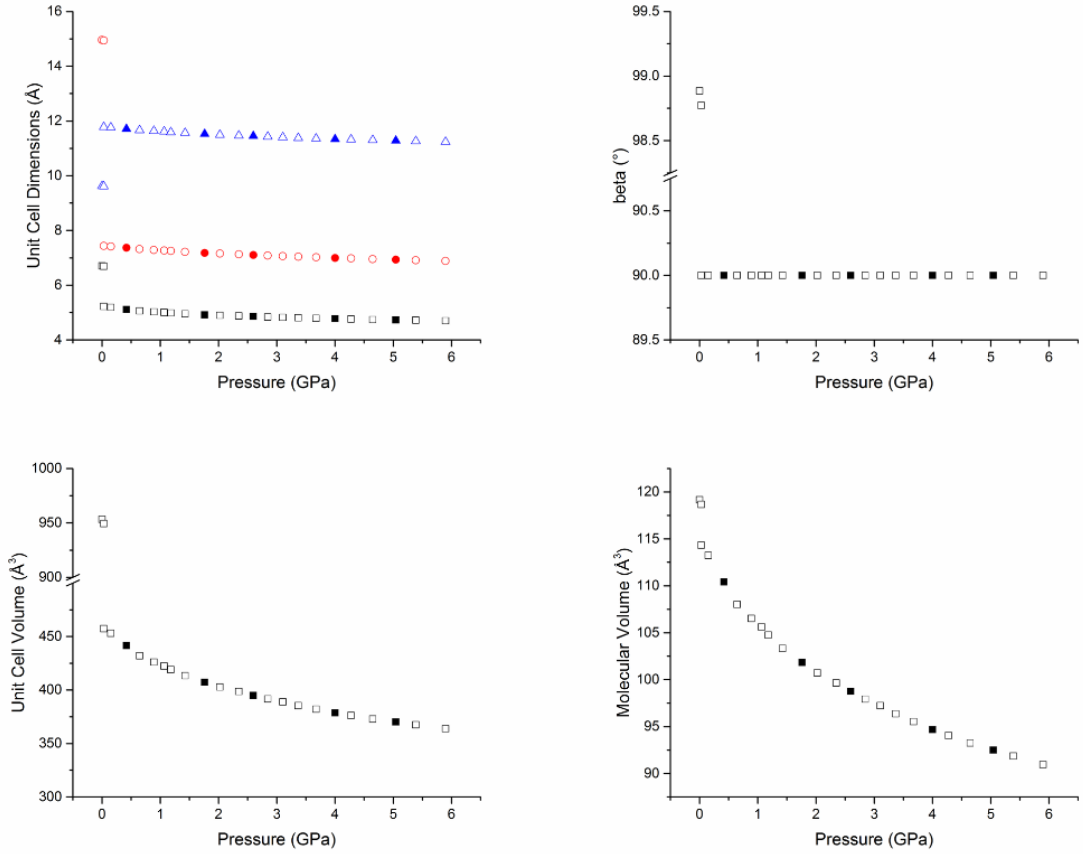

Figure 4.11 - Refined unit cell parameters of glycolide-h4 upon compression. In the top-left plot, showing all unit cell dimensions, black squares refer to the a-axis, red circles refer to the b-axis and blue triangles refer to the c-axis. Hollow shapes show Pawley-refined datasets, with filled shapes illustrating Rietveld-refined datasets.

4.3.2 PIXEL Calculations and Void Space Analysis

Form II is stable to the highest pressure at which data were collected (5.90 GPa). The unit cell volumes upon compression of Form II have been fitted to a 3rd order Birch-Murnaghan equation of state with V_0 = 461.9(9) Å^3, K_0 = 6.6(4) GPa, K' = 14.0(7) GPa, and K'' = -17.2. The *a*, *b* and *c*-axes compressed by 7.54%, 5.92% and 3.74%, respectively, upon compression from 0.388 GPa to 5.00 GPa, with a total contraction in the unit cell volume of 16.27%. Figure 4.12 shows the packing arrangement of Form II, projected along the *a*-axis, *b*-axis, and the diagonal between the *a*- and *b*-axes. From this figure, it can be seen that the crystal structure consists of stacked columns of molecules.

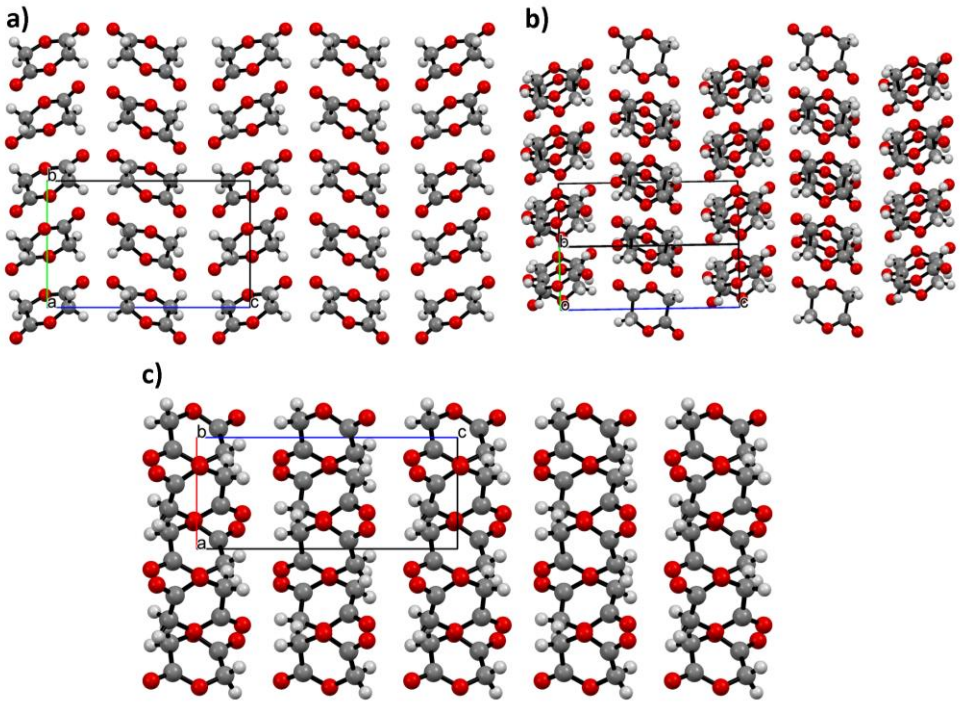

Figure 4.12 - Projections of the packing arrangement of Form II along a) the a-axis, b) the diagonal between the a- and b-axes, and c) the b-axis.

To understand the energies of the interactions involved the PIXEL method was used to track changes of molecule-molecule interactions with increasing pressure. The five most significant Form II molecule-molecule interactions at the first Rietveld-refined pressure point, 0.388 GPa, were tracked with increasing pressure. The symmetry operations of these five interactions, Interactions 1 – 5, are listed in Table 4.5 with the molecule pairs being illustrated in Figure 4.13. It should be noted that interactions listed in Table 4.5 are seen to be the most significant at all five pressure points collected on the PEARL beamline, and are also consistent with the strongest interactions calculated via the PIXEL method in Chapter 3.

Table 4.5 - The five strongest Form II molecule-molecule interactions, as calculated at 0.409 GPa

Interaction	**Symmetry Relation**
1	0.5+x,1.5-y,1-z
2	0.5+x,0.5-y,1-z
3	1+x,y,z
4	1-x,0.5+y,0.5-z
5	1-x,0.5+y,1.5-z

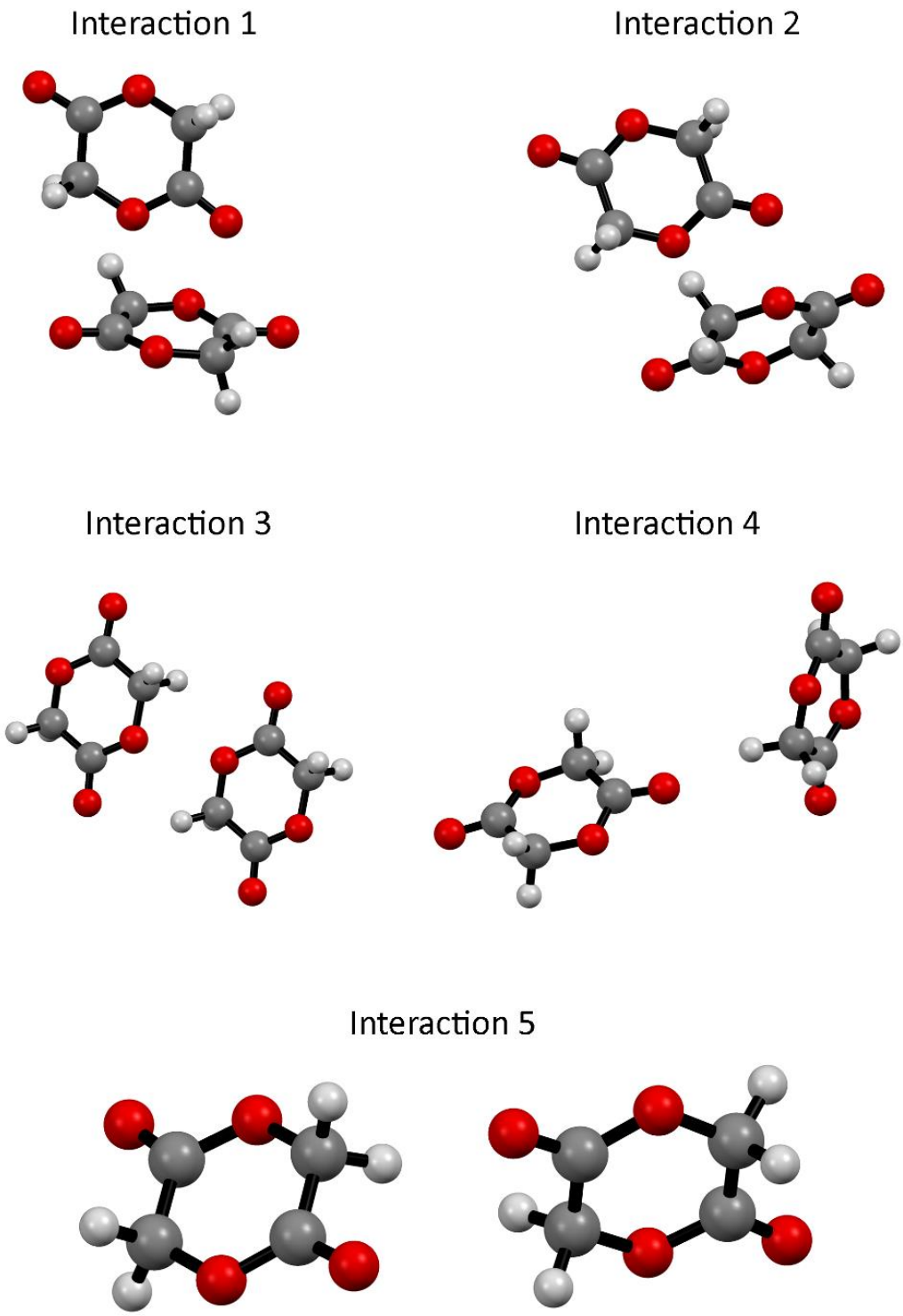

Figure 4.13 - Interactions 1 - 5 of glycolide Form II, as calculated at 0.409(10) GPa.

Table 4.6 shows the changes observed in the contributing terms of Interactions 1-5 upon increasing pressure.

Table 4.6 - Changes in Interactions 1 - 5 with increasing pressure

Pressure (GPa)	C_m-C_m Distance (Å)	E_c (kJ mol^{-1})	E_p (kJ mol^{-1})	E_d (kJ mol^{-1})	E_r (kJ mol^{-1})	E_{tot} (kJ mol^{-1})
Interaction 1						
0.409	4.424	-20.8	-6.5	-19.2	23.2	-23.3
1.774	4.28	-26.8	-9	-23.3	38.1	-21.1
2.588	4.223	-29.6	-10.2	-25.2	46	-19
4.02	4.144	-36	-12.8	-29.4	65.8	-12.4
5.02	4.085	-42.1	-15.6	-32.6	84.5	-5.8
Interaction 2						
0.409	4.546	-16.5	-5.8	-17.6	18.1	-21.8
1.774	4.425	-20.5	-8.1	-21.4	29.3	-20.7
2.588	4.383	-23.2	-9.5	-22.9	35.6	-20
4.02	4.327	-25.2	-10.2	-24.7	44.1	-15.9
5.02	4.309	-27.9	-11.1	-25.3	48.6	-15.8
Interaction 3						
0.409	5.118	-8.6	-1.8	-8.8	4.1	-15.1
1.774	4.921	-11.2	-3.1	-12.4	11	-15.7
2.588	4.857	-13.5	-3.9	-14.1	15.7	-15.8
4.02	4.776	-14.4	-4.6	-16.3	22.8	-12.4
5.02	4.732	-17.3	-6	-17.8	28.2	-12.8
Interaction 4						
0.409	6.956	-8.4	-1.8	-4	4.5	-9.7
1.774	6.833	-10.9	-2.8	-5	8.3	-10.4
2.588	6.783	-12.3	-3.2	-5.4	10.4	-10.5
4.02	6.716	-14.8	-4.2	-6	15.1	-10
5.02	6.68	-16	-4.7	-6.3	17.1	-9.9
Interaction 5						
0.409	6.884	-8.1	-1.8	-4.1	5.5	-8.5
1.774	6.746	-10.6	-2.6	-5	9.4	-8.7
2.588	6.688	-11.7	-3	-5.3	10.7	-9.2
4.02	6.605	-12.4	-3.6	-5.8	13.6	-8.2
5.02	6.557	-13.8	-4	-6.1	15.3	-8.7

Referring back to Figure 4.12, projection along the *a*-axis shows regular arrays of stacked molecules each separated by a gap of ~5.1 Å at 0.338 GPa (i.e. a unit cell). The top three interactions (1-3) are observed between the molecules that make up the layers in the *ab*-plane. Of these interactions, interaction 1 becomes the least stabilising over the course of the compression largely due to the rapid increase in

the repulsive component. Both this interaction and Interaction 2 are edge on face interactions however the difference in the intercentroid separation is the reason that Interaction 2 does not increase in energy as quickly (Figure 4.14). Projection along the *b*-axis shows neighbouring stacks of molecules that are linked through the three other interactions (Interactions 3-5). These are much more modest in their energy contribution to the crystal structure with very little variation in the total energy over the compression with any increase in the repulsion being cancelled by the increase in the coulombic energy (Table 4.6, Figure 4.14).

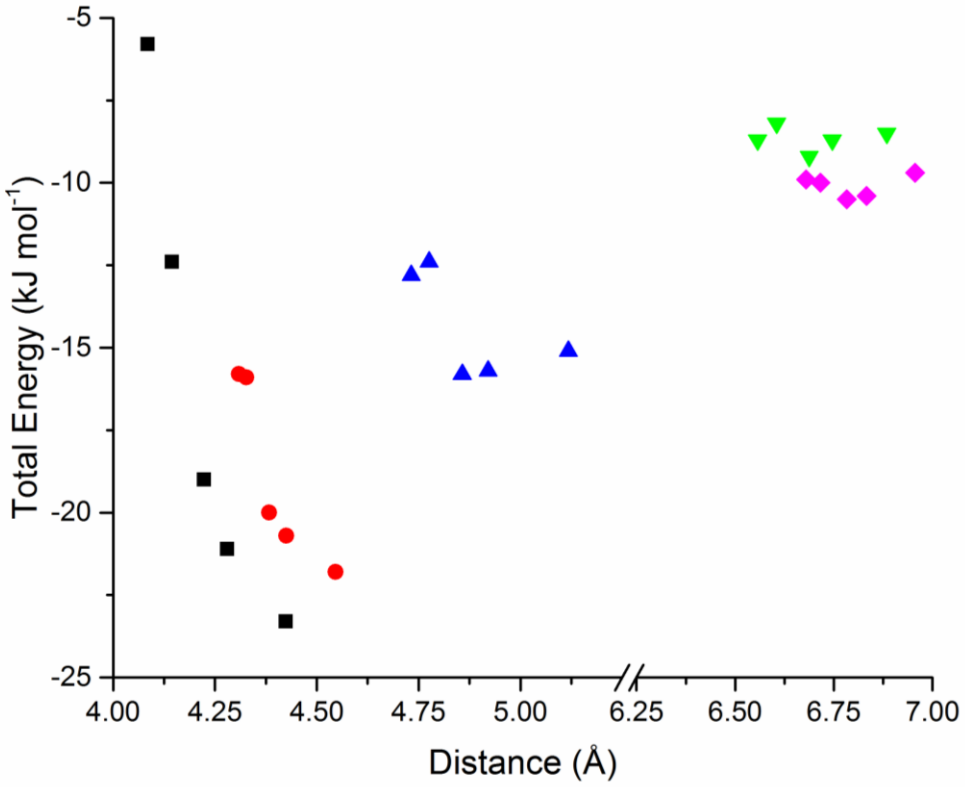

Figure 4.14 - The changes in total energy of the top five interactions as the Cm-Cm distance is varied. The black squares represent Interaction 1; red circles represent Interaction 2; blue triangles represent Interaction 3; pink diamonds represent Interaction 4; green triangles represent Interaction 5.

One stand-out feature from the energy calculations is a sudden change in the molecular conformation. Figure 4.15 plots the changes in the internal molecular energy of Form II and the total energy contribution of Interaction 3 against the C_m-C_m distance between the two molecules forming Interaction 3. It can be seen that

as the distance decreases, there is a sharp change in the total energy of Interaction 3. This coincides with a large step in the internal molecular energy, which destabilises considerably as the molecule undergoes a slight conformational change between 2.588 GPa and 4.02 GPa (the third and second data points from the left in Figure 0.11, respectively). The most significant difference between Interaction 3 at the third pressure point (2.588 GPa, with a C_m-C_m distance of 4.857 Å) and the fourth pressure point (4.02 GPa, with a C_m-C_m distance of 4.776 Å) is a jump in the repulsion term from +15.7 kJ mol^{-1} to +22.8 kJ mol^{-1} that coincides with a sharp change in the internal molecular energy from +4.1 kJ mol^{-1} to +20.8 kJ mol^{-1}. This sharp change in the internal molecular energy as pressure is increased indicates that the ring system is under significant strain at this pressure. Additional work would be required to investigate this further, but it may be found that subjecting Form II to higher still pressures could induce ring-opening polymerization as the internal strain becomes excessive.

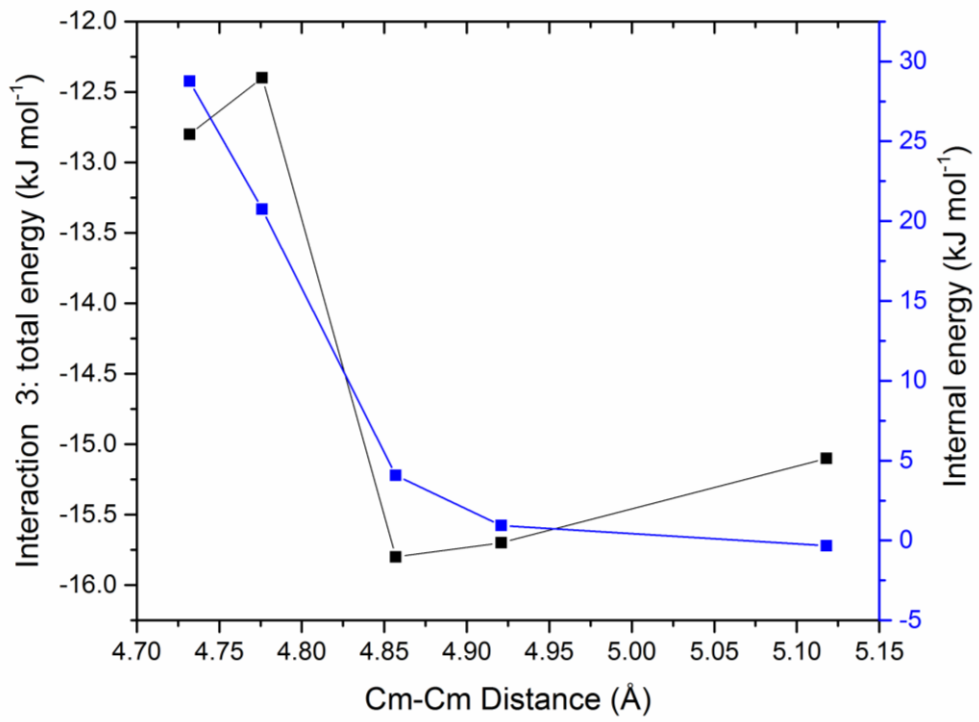

Figure 4.15 - Changes in the internal molecular energy of Form II (blue) and the total energy contribution of Interaction 3 (black) with the distance between the centres of mass of the two molecules forming Interaction 3.

In addition to the PIXEL calculations the voids in the structure were investigated as previous research has shown that pressure reduces the voids in the structure before invoking a polymorphic change. The voids within the unit cell, calculated using a 0.2 Å probe radius and a 0.1 Å grid spacing, were calculated for the structures of Form II at each of the refined pressures. Projections of these, along the *a*-axis, are shown in Figure 4.16. The unit cell volumes and associated void spaces upon increasing pressure are listed in Table 4.7. Overall the void volume reduces from 11% to 1% of unit cell volume. It is notable that at the same pressure at which there is a conformational change there is a plateau in the void volume hence the molecular rearrangement has helped to maintain the void space in the structure. As can be seen in Figure 4.16 the voids are reduced to only being present between the layers along the *c*-axis. By 1.8 GPa most of the voids within the *ab*-plane (i.e. the most stabilizing interactions) had disappeared.

Table 4.7 - Void space analysis of glycolide Form II upon increasing pressure.

Pressure (GPa)	**Unit Cell Volume (Å^3)**	**Change in Unit Cell Volume from 0.388 GPa**	**Void Space (Å^3)**	**Void Space (% of Unit Cell Volume)**
0.388(10)	441.72(6)	0.00%	51.48	11.7
1.791(12)	407.22(6)	-7.81%	17.68	4.3
2.579(15)	394.95(6)	-10.59%	9.19	2.3
4.000(19)	378.66(6)	-14.28%	10.66	2.8
5.00(2)	369.87(7)	-16.27%	4.39	1.2

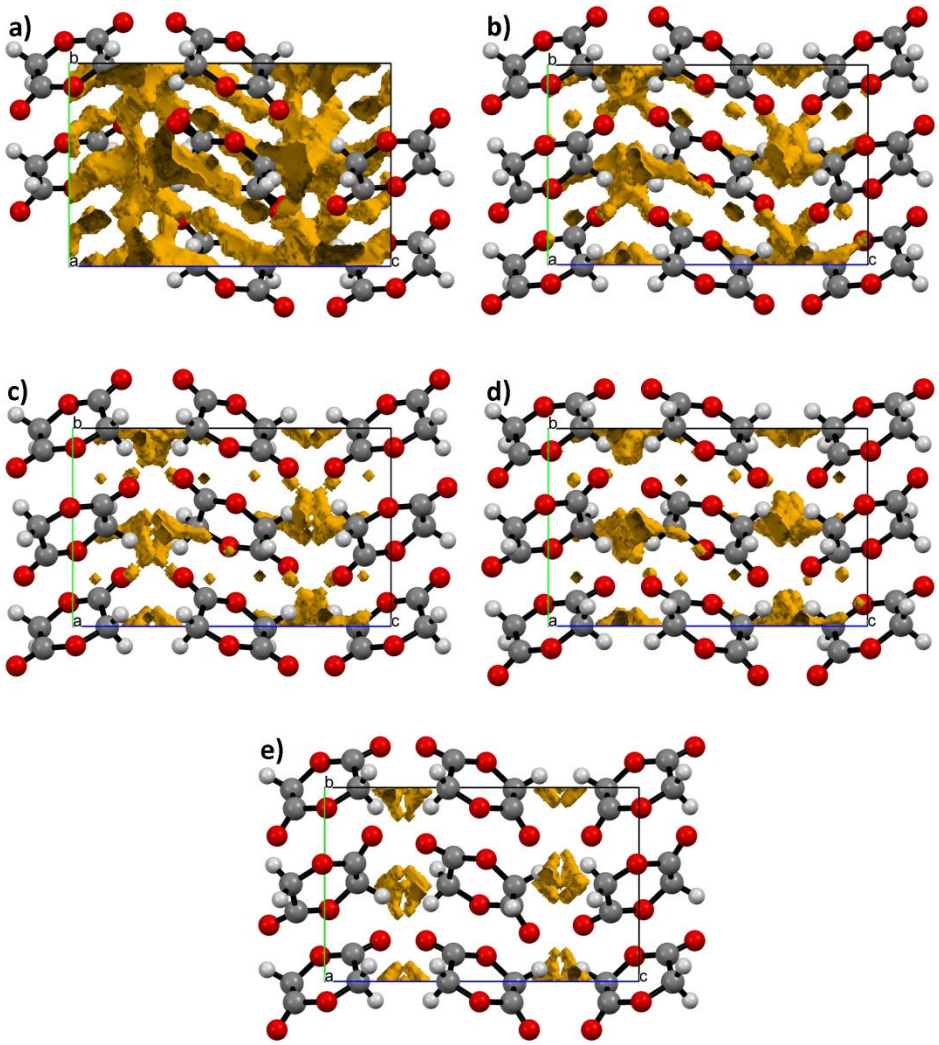

Figure 4.16 - Void space analysis of glycolide Form II upon increasing pressure at a) 0.388 GPa, b) 1.791 GPa, c) 2.579 GPa, d) 4.000 GPa and e) 5.00 GPa.

4.3.3 Non-occurrence of the Form II to Form III phase transition

Despite the presence of some peaks in the diffraction pattern which do not fit that of Form II (Figure 4.8), Form II is stable to the highest pressure reached and was recovered to ambient pressure without the completion of the phase transition seen in the DAC experiment. One possible explanation for this may be that sample size, which is much larger in the neutron diffraction experiment than in the DAC experiment, somehow hinders the occurrence of the phase transition. Alternatively, it may be a kinetic effect (Ridout, Price, Howard, & Probert, 2014) relating to the

time taken to compress or decompress the sample. In the neutron diffraction experiment, the sample was taken from ambient pressure to 5.90 GPa gradually over the course of 96 hours before being held at 5.90 GPa for around 2 hours. The decompression from 5.90 GPa to 4.28 GPa, 2.985 GPa, 1.264 GPa and to ambient conditions (refining to be 0.047 GPa) took approximately 5 hours, 20 hours, 31 hours and 40 hours, respectively. In contrast, the application and release of pressure in the DAC experiment in which the third unknown phase was observed took place in a matter of minutes, rather than hours. The more sudden change in pressure in the DAC may have been a factor in the transition to the third form of glycolide.

4.3.4 Significance of the use of hydrogenous material

The advantages of using deuterated samples over hydrogenous samples for neutron diffraction experiments are briefly discussed in Section 1.2 of this thesis. As well as its low incoherent scattering cross section (2.05 barns for deuterium c.f. 80.27 barns for hydrogen at a neutron wavelength of 1.8 Å), deuterium also has a comparably longer scattering length (6.67 fm c.f. -3.739 fm for hydrogen). However, there are also a number of arguments against sample deuteration being the default when collecting neutron diffraction data: in many cases, as with glycolide, sample deuteration is very difficult to achieve; in other cases, deuterated samples are subject to isotopic exchange during data collection; and perhaps even more critically, the proportionally large difference in atomic mass between hydrogen and deuterium compared to isotopes of heavier elements has been shown in some cases to result in structures of hydrogenous and deuterated samples of the same materials displaying differences in structure (including unit cell parameters) and properties such as electrical conductivity, and phase transition temperatures (Muraoka, Matsuo, & Kume, 1995; Syamaprasad & Vallabhan, 1982). With this in mind, there may be circumstances under which it is desirable or even essential to conduct neutron diffraction studies on hydrogenous samples.

Work on the use of hydrogenous samples to obtain Rietveld-quality neutron diffraction data has shown progress in recent years, with the work of Mark Weller and Paul Henry illustrating the ability to determine atomic positions of hydrogen atoms in sample systems including inorganic hydrates, organometallic compounds, and small organic molecules (Weller et al., 2009). In such experiments, whilst the data used to perform Rietveld refinements and hence solve atomic positions, it is often necessary to subtract the high background resulting from the inelastic scattering of hydrogen atoms.

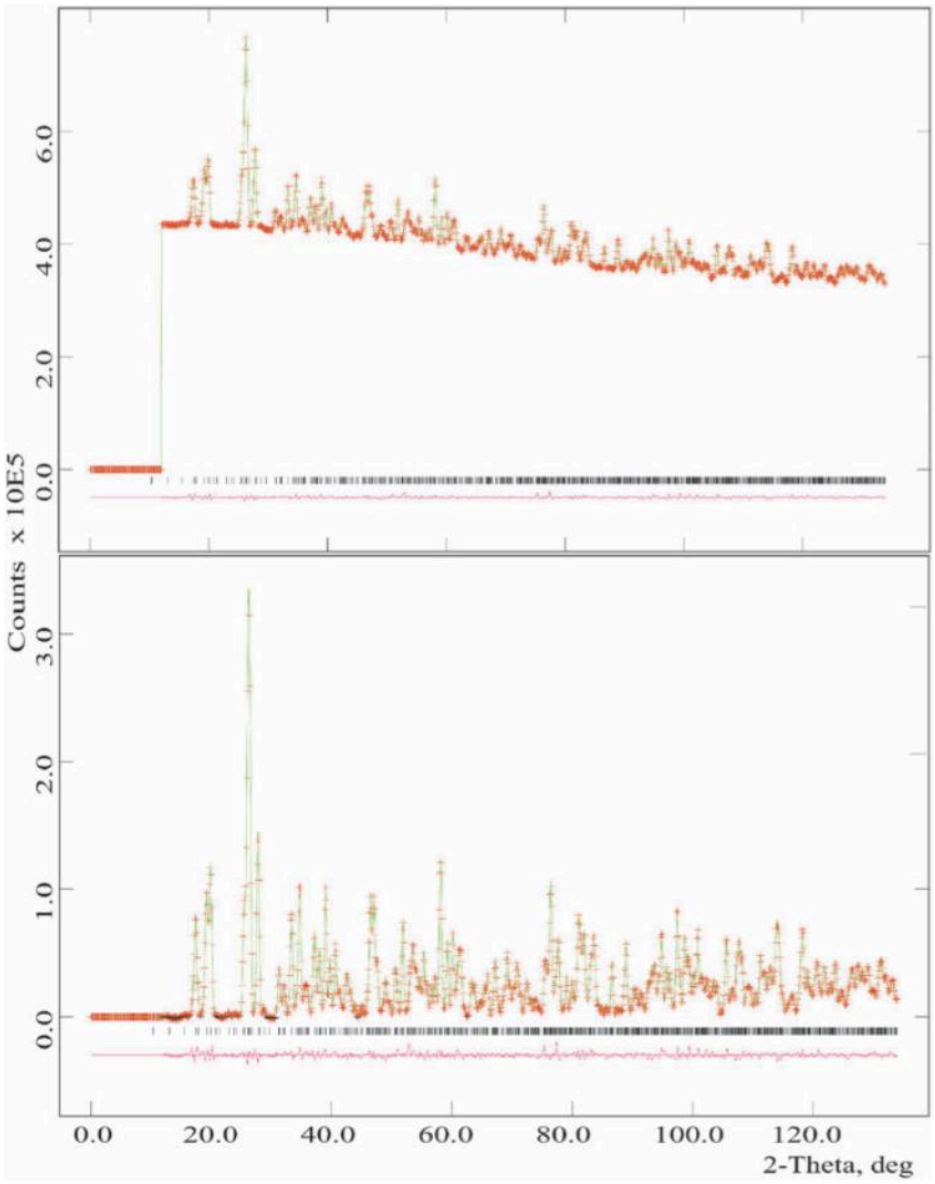

Figure 4.17 – Rietveld-fitted neutron diffraction data of Bi(NO3)3.5H2O collected on D20 at the ILL. The top image represents the data as-collected, with the bottom image showing the effect of background correction for the incoherent scattering of hydrogen (Weller et al., 2009)

In terms of advances on the PEARL beamline, the quality of the data obtained on the hydrogenous sample of glycolide during this work is comparable to that of the data collected on hydrogenous samples on the same beamline using the old WC anvils. Figure 4.19 shows the Rietveld fit of the data collected on a deuterated sample of Form I *L*-serine (Moggach, Marshall, & Parsons, 2006).

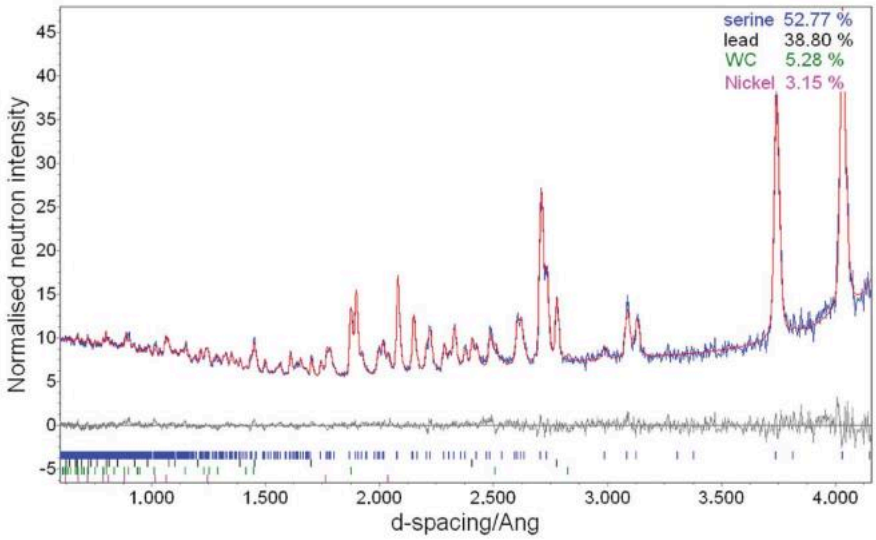

Figure 4.18 - Rietveld fit of L-serine-d7-I at 4.6 GPa. Data were collected on the PEARL beamline using WC backing discs (Moggach et al., 2006).

Comparing this diffraction (Figure 4.18) to that observed in Figure 4.7, it can be seen that with exception of the diffraction intensity at lower d-spacing drops off as a result of the hydrogen atoms, the quality of the data is broadly comparable. This represents a significant improvement on the high background previously obtained when using hydrogenous samples (Figure 4.17), enhancing the possibility of studying structural changes in materials with which it may be difficult to induce isotope exchange or where such a process results in any change in structure or properties.

4.4 Conclusions

Glycolide Form II was shown to be stable up to the highest pressure at which data were collected (5.90 GPa), and stable upon decompression to ambient pressure – as observed in Chapter 3. PIXEL calculations were used to track the molecule-molecule interactions upon increasing pressure, with the same five interactions remaining the most significant at all pressure points studied. Although no polymerisation was observed, it was noticed that the molecule underwent a conformational change at around 4.0 GPa at which point the internal strain on the ring structure increased.

Further work is needed to assess whether application of higher pressure may induce ring-opening polymerisation, as well as to solve the crystal structure of the third polymorph of glycolide observed via high pressure PXRD in the DAC experiment.

4.5 References

Moggach, S. A., Marshall, W. G., & Parsons, S. (2006). High-pressure neutron diffraction study of L-serine-I and L-serine-II, and the structure of L-serine-III at 8.1 GPa. *Acta Crystallographica. Section B, Structural Science*, *62*(Pt 5), 815–25. http://doi.org/10.1107/S010876810601799X

Muraoka, H., Matsuo, T., & Kume, Y. (1995). Deuteration effect in the phase transition of (NH4)2PbCl6. *Solid State Communications*, *93*(6), 529–531. http://doi.org/10.1016/0038-1098(94)00735-7

Oswald, I. D. H., & Urquhart, A. J. (2011). Polymorphism and Polymerisation of Acrylic and Methacrylic Acid at High Pressure. *Crystengcomm*, *13*(14), 4503–4507. http://doi.org/10.1039/c1ce05295k

Ridout, J., Price, L. S., Howard, J. A. K., & Probert, M. R. (2014). Polymorphism arising from differing rates of compression of liquids, *14*(7), 3384–3391. http://doi.org/10.1021/cg500331u

Syamaprasad, U., & Vallabhan, C. P. . (1982). Effect of deuteration on the electrical conductivity, dielectric constant and phase transitions in LiNH4SO4. *Physics Letters A*, *89*(1), 37–40. http://doi.org/10.1016/0375-9601(82)90141-4

Weller, M. T., Henry, P. F., Ting, V. P., Wilson, C. C., Henry, P. F., Weller, M. T., … Weller, M. (2009). Crystallography of hydrogen-containing compounds: realizing the potential of neutron powder diffraction. *Chemical Communications*, *45*(21), 2973. http://doi.org/10.1039/b821336d

Chapter 5 – Pressure transmitting medium dependent polymorphism of acrylamide – a neutron diffraction study

5.1 Introduction

Acrylamide, C_3H_5NO, is the amide analogue of acrylic acid. It is a white powder at room temperature with a melting point of 82 – 86 °C. The majority of acrylamide is used as the precursor to its polymer, polyacrylamide (PAM), which is used in a variety of applications including treatment of waste water, as a soil conditioner and in gel electrophoresis, as well as finding biomedical applications such as drug delivery and as a soft tissue filler in cosmetic surgery (Yang, Song, Chen, Zhang, & Wang, 2008).

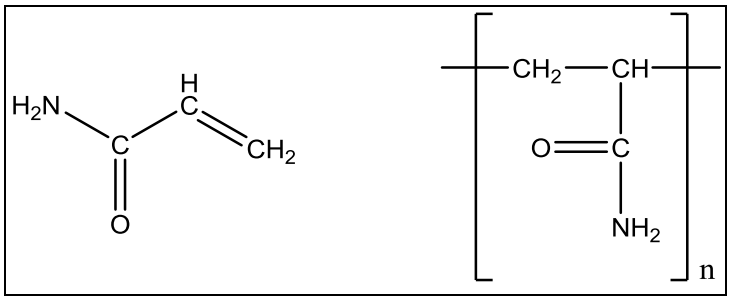

Figure 5.1 – Acrylamide (left) and polyacrylamide (right).

Previous work, including that of our group, has shown that polymorphism and solid-state polymerisation of small organic molecules can be induced by the application of pressure (Oswald & Urquhart, 2011). The aims of this study were to observe and understand the structural changes in acrylamide induced by high pressure and to establish whether polymerisation can be achieved by the application of high pressure, as has been seen in acrylic acid.

Acrylamide is a crystalline solid, with previous research showing it to crystallise in space group $P2_1/n$, with the unit cell parameters shown in Table 5.1, such that the orientation of the molecules allows the ethylene moieties to be in close proximity to one another.

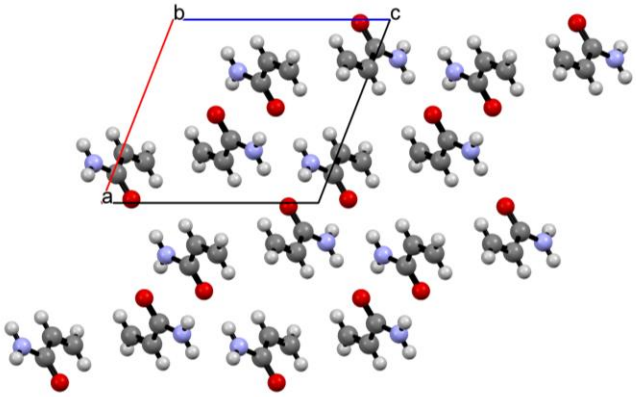

Figure 5.2 - Crystal structure of acrylamide (Zhou et al., 2007)

Table 5.1 - Unit cell parameters of acrylamide (Zhou et al., 2007).

Unit Cell Parameter	**Value**
a / Å	8.2062(16)
b / Å	5.7480(11)
c / Å	9.0527(18)
α / °	90.00
β / °	111.37(3)
γ / °	90.00
Unit Cell Volume / $Å^3$	397.65(4)
Space Group	$P2_1/n$
Z	4
Z’	1
R-factor / %	4.15

5.2 Experimental

5.2.1 Characterisation of Acrylamide under Ambient Conditions

Acrylamide (Sigma Aldrich) was recrystallised from chloroform via slow solvent evaporation and analysed by SXRD to confirm its crystal structure. Diffraction quality was poor, although sufficient to show that the crystal structure matched that reported in the literature.

5.2.2 Neutron Diffraction Experiments

Having encountered problems resulting from the poor diffraction of X-rays using the laboratory source, six days of beam time on the PEARL beam line at the ISIS Neutron Source were granted in order to study further the behaviour of acrylamide under high pressure. During this time, acrylamide was examined at high pressure in three different PTMs – a 1:1 (v/v) mixture of pentane and isopentane, a 4:1 (v/v) mixture of methanol and ethanol, and isopropyl alcohol (IPA). The PTMs, as well as the acrylamide sample, were all deuterated in order to prevent the high background associated with the inelastic scattering component of ^{1}H nuclei, as discussed in Chapter 1 of this thesis.

5.2.2.1 General Procedures

A small sample of acrylamide in drops of PTM was ground using a mortar and pestle before being loaded into the Paris-Edinburgh cell along a small pellet of lead. The lead was loaded to allow the pressure of the sample to be calculated *in-situ* through its equation of state. The PTM was added with a Pasteur pipette before the cell was sealed and loaded into position. The mechanical load was added, typically in increments of 2-3 tonnes. At each pressure point, data were typically collected for a minimum exposure of around 50 µA of data which equated to around 20 minutes for the approximate mean intensity of 150 – 160 µA per hour of ISIS.

5.2.2.2 Loading 1: A 1:1 (v/v) pentane and iso-pentane

Neutron diffraction data of acrylamide-d_5, in a 1:1 (v/v) mixture of deuterated pentane and isopentane, were collected at regular pressure increments up to 5.5 GPa by applying a load

of 68 tons to the TiZr gasket. Data were also collected during the decompression stage of the experiment to observe any phase changes the sample may undergo whilst the pressure is being released, as has previously been seen in methacrylic acid (Oswald & Urquhart, 2011).

The data obtained at each pressure interval were Pawley fitted in order to track the changes in unit cell upon compression and decompression (Tables 5.2 and 5.3, respectively). Where the data had been collected over an extended time period and were of sufficient quality, Rietveld refinements were conducted. Rietveld refinements were conducted on the data collected at the following pressure points: -0.008 GPa (6 tonnes); 0.574 GPa (27 tonnes); 1.049 GPa (33 tonnes); 1.554 GPa (39 tonnes); 2.175 GPa (45 tonnes); 3.794 GPa (54 tonnes); 5.588 GPa (68 tonnes); and during the decompression stage at 1.723 GPa (6 tonnes). Figure 5.3 shows the response of the load applied to the pressure that the sample experienced. After a slow initial response, the cell responded well at higher pressures.

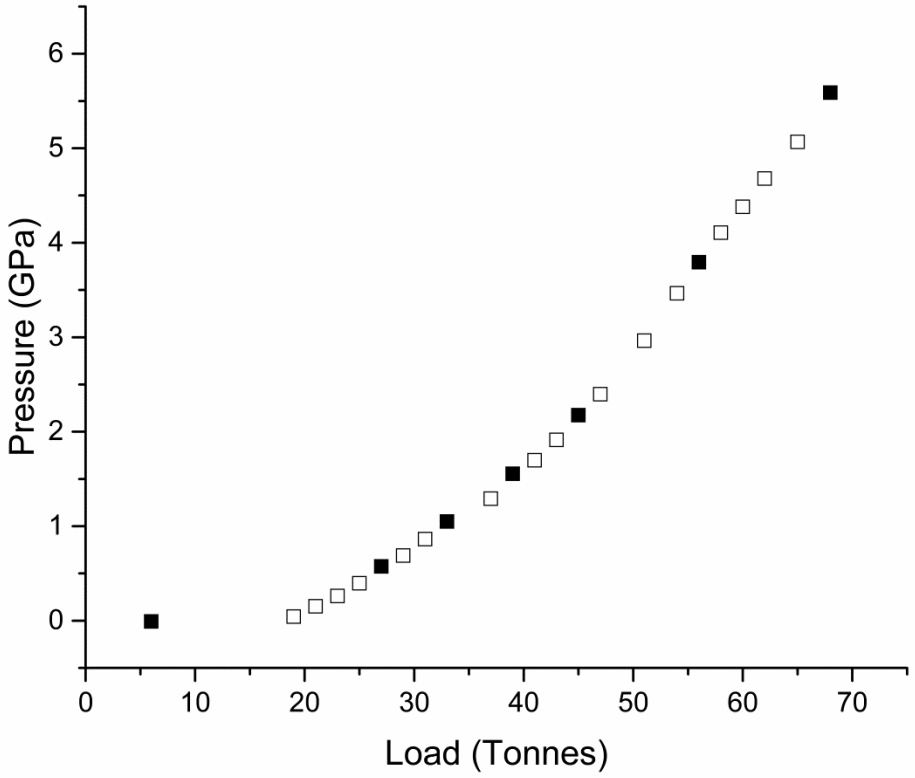

Figure 5.3 – The response of pressure to the applied load during the experiment using pentane/iso-pentane as the PTM. The filled squares show the pressure points at which the data were suitable for Rietveld refinements to be performed.

The second phase of acrylamide, herein designated Form II, was identified by simple compression of Form I. Diffraction data were collected on the I19 beamline at Diamond Light Source in order to assist structure solution since neutron diffraction quality were initially poor. The data were collected using Rigaku CrystalClear software before the frames were converted to Bruker .sfrm format.

5.2.2.3 Loading 2: A 4:1 (v/v) Methanol/Ethanol Mixture

Acrylamide-d_5 was studied in a 4:1 (v/v) mixture of deuterated methanol and ethanol, up to a pressure of 5.5 GPa. Data were collected at regular pressure intervals, with the mechanical load typically added in increments of 2-3 tonnes. Data obtained were Pawley fitted and, where the data collected were of sufficient quantity, Rietveld fitted – as per the previous loading in the pentane/iso-pentane environment.

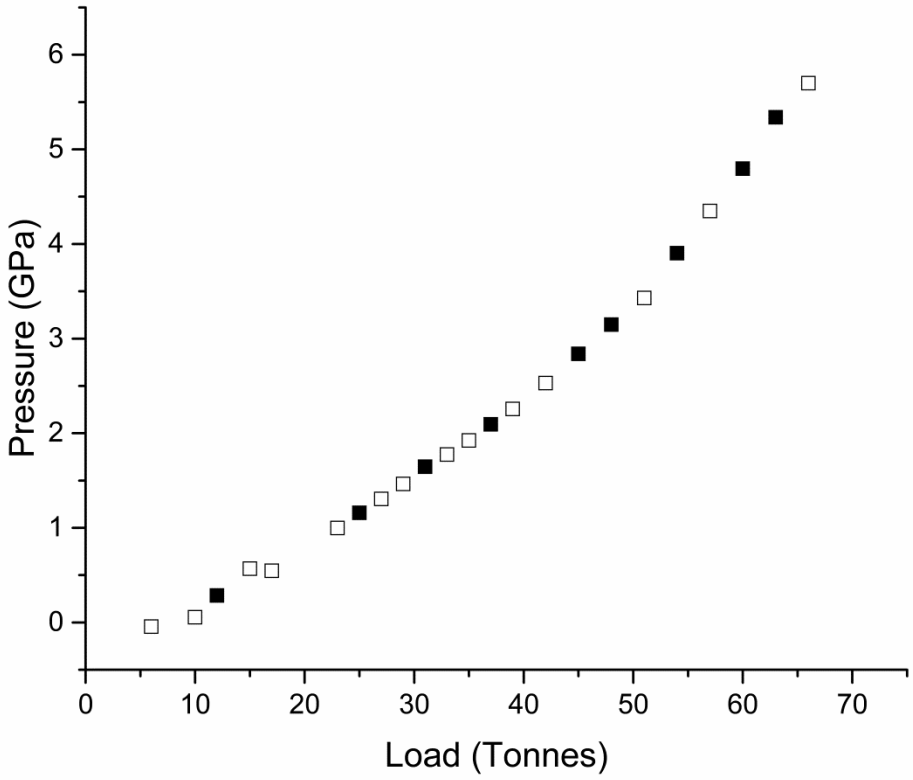

Figure 5.4 – The response of pressure to the applied load during the experiment using MeOD/EtOD as the PTM.

The data collected fitted the known ambient-pressure form of acrylamide (Form I) at lower pressures, until the sample underwent a phase transition. The high pressure form was observed at 1.159 GPa, under a load of 25 tonnes, and matched neither of the known polymorphs (Forms I and II). The phase transition to this new polymorph, herein designated Form III, was reconstructive in nature and so whilst the experiment started with a good, well-orientated powder, this deteriorated over the phase transition and became somewhat orientated. The identification of the unit cell and hence the structure was not possible from the PEARL data due, in part, to the fact it is a medium-resolution instrument and that the high d-spacing reflections (>4 Å) were not available at the time of data collection. It should be noted that during the writing of this thesis, processes have been developed to integrate these reflections.

Single Crystal Growth & refinement – Form III

The problems encountered whilst attempting to index the powder data meant that another method had to be employed in order to solve the structure of Form III. A DAC was loaded with acrylamide powder (Form I, gently ground with mortar and pestle), along with a 4:1 (v/v) mixture of methanol and ethanol. Both the sample and the PTM were hydrogenous, rather than the deuterated samples used in the neutron diffraction experiments. A single crystal was grown through temperature annealing, with SXRD data of the obtained crystal being collected. The data were refined using the usual procedures, as set out in Chapter 2, in order to solve the structure of Form III. This structure was then used to refine the neutron diffraction data obtained on the PEARL beamline, in order to observe the behaviour of Form III under pressure.

5.2.2.4 Loading 3 – Iso-propyl alcohol (IPA)

The Paris-Edinburgh cell was loaded as per the previous two loadings, with deuterated IPA being used as the PTM. Data were obtained up to 5.21 GPa (67 tonnes), again in increments of 2-3 tonnes. A phase transition was observed at approximately 1.4 GPa, to a phase which did not match either of the previously observed high pressure forms (Forms II and III).

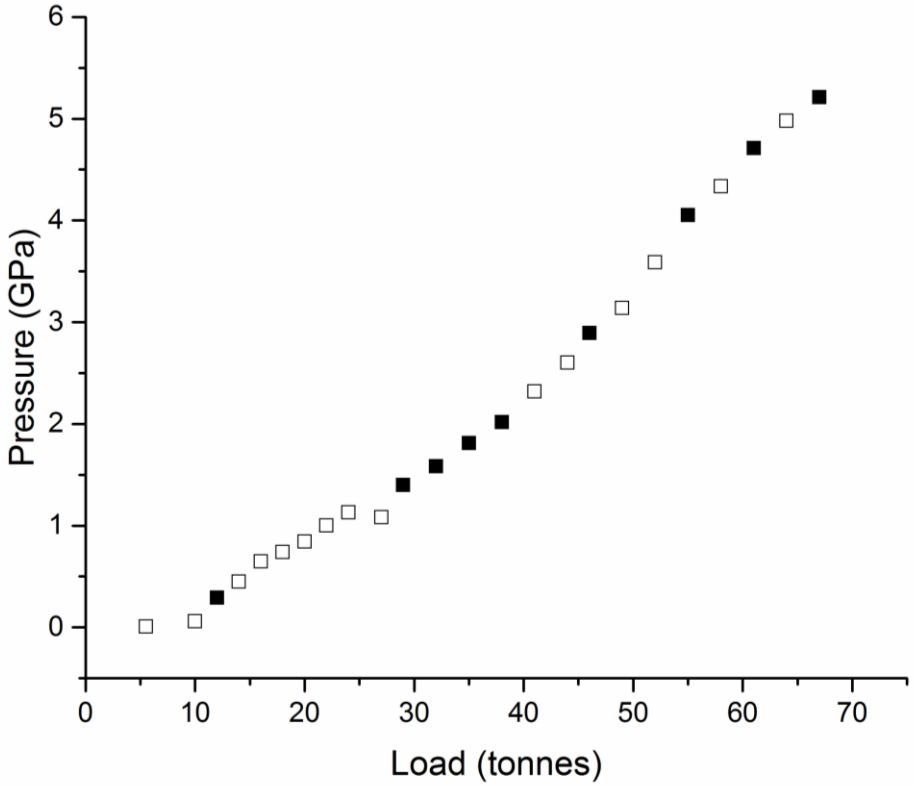

Figure 5.5 - The response of pressure to the applied load during the collection of data on acrylamide in an environment of IPA. The filled shapes represent the longer data collections intended for Rietveld refinement, with the hollow shapes representing shorter collections intended for Pawley refinement.

5.2.3 PIXEL Calculations

PIXEL calculations (Gavezzotti, 2003) allow the crystal structure to be analysed in terms of intermolecular interactions, were conducted on the refined crystal structures to observe any changes in intermolecular forces as pressure is increased. The PIXEL method required the electron density in an isolated molecule to be calculated, and distributed across so-called pixels of electron density. The intermolecular interactions, broken down into coulombic energy, polarisation energy, dispersion energy and repulsion energy, are then calculated by summing the energies between pairs of pixels in neighbouring molecules. It should be noted that these calculations do not take into account the conformational energies of the molecules.

5.3 Results and Discussion

5.3.1 Ambient Pressure Form (Form I)

The Raman spectrum of acrylamide (recrystallised from acetone) was collected using a 532 nm laser, and is shown in Figure 5.6. An axis break has been introduced from 2750 cm^{-1} to 1750 cm^{-1} as there are no significant Raman bands of interest in this region.

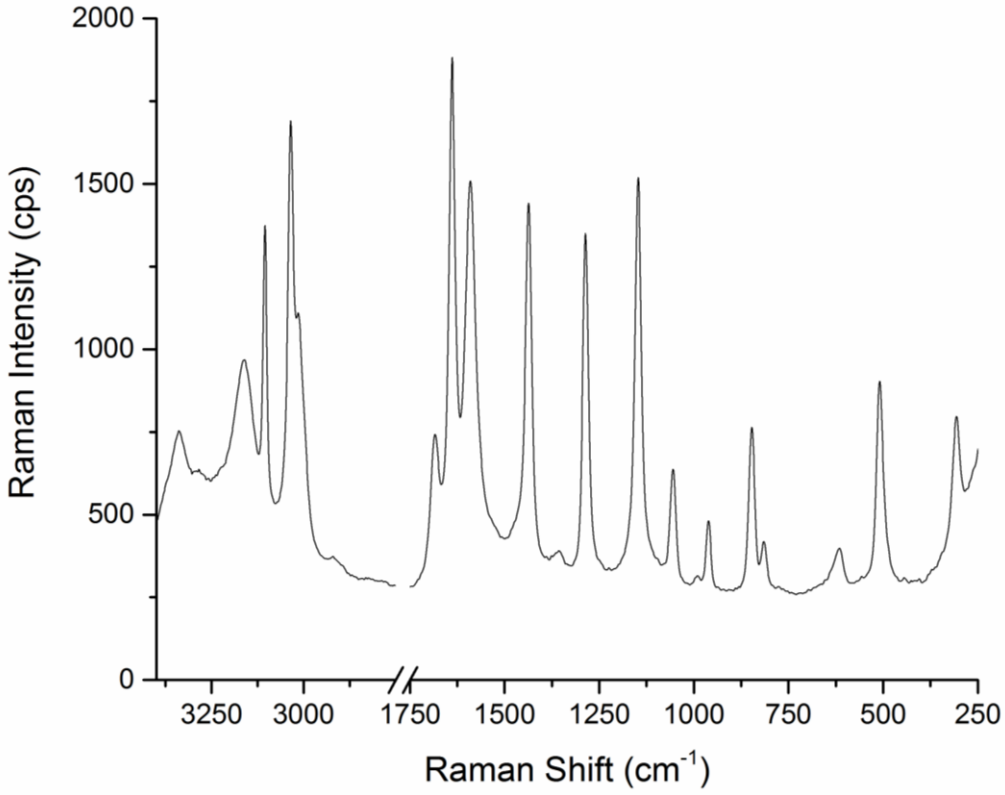

Figure 5.6 - Raman spectrum of acrylamide, recrystallised from acetone.

The crystalline structure of the ambient pressure form (Form I), is dominated by the hydrogen-bonded amide dimer, as seen in Figure 5.7 a). The N-O distance in the dimer interaction is 2.856 Å, with the N-D--O angle measuring 176.26°. Figure 5.7 b) illustrates the herring bone packing arrangement of acrylamide molecules in the greater lattice structure.

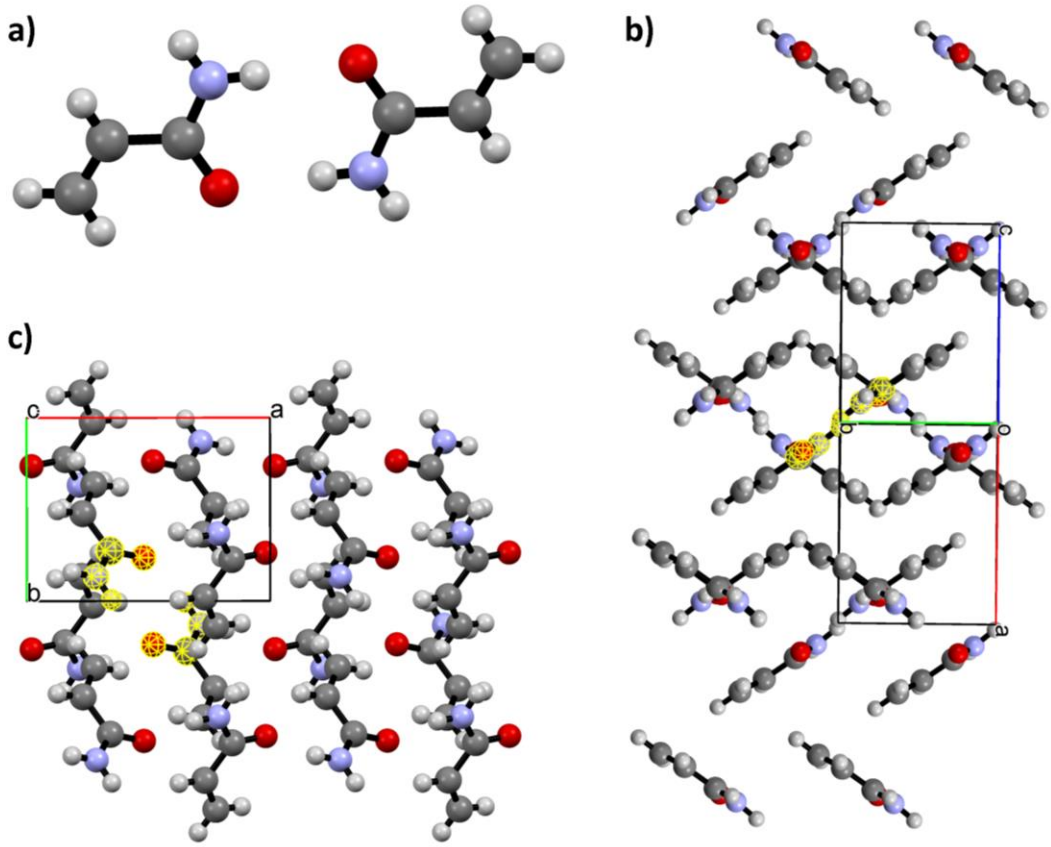

Figure 5.7 - Packing features of Form I of acrylamide. The dominant amide dimer interaction is shown in a), while b) and c) illustrate the wider packing arrangement with the atoms involved in an amide dimer interaction highlighted.

5.3.2 Loading 1 – Acrylamide in a 1:1 (v/v) pentane : iso-pentane environment

Figure 5.8 shows the data collected on increasing pressure. From these diffraction patterns it can clearly be seen that there is a smooth compression of the structure until 1.049 GPa, before significant differences in the diffraction pattern collected at 1.554 GPa are observed indicating a phase transition. Figure 5.9 shows the data collected at 1.359 GPa, representing a mixed phase containing both Form I and the high pressure form (herein designated Form II).

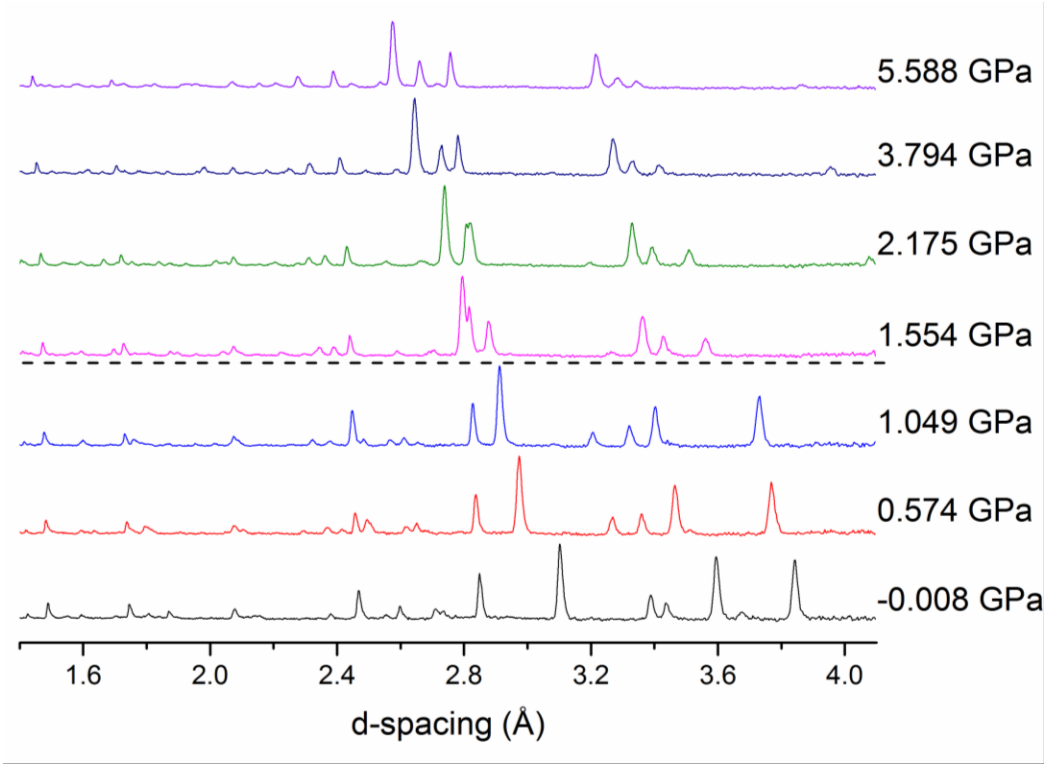

Figure 5.8 - Diffraction patterns of acrylamide in pentane/iso-pentane environment with increasing pressure. The dotted line represents the phase transition from Form I to Form II.

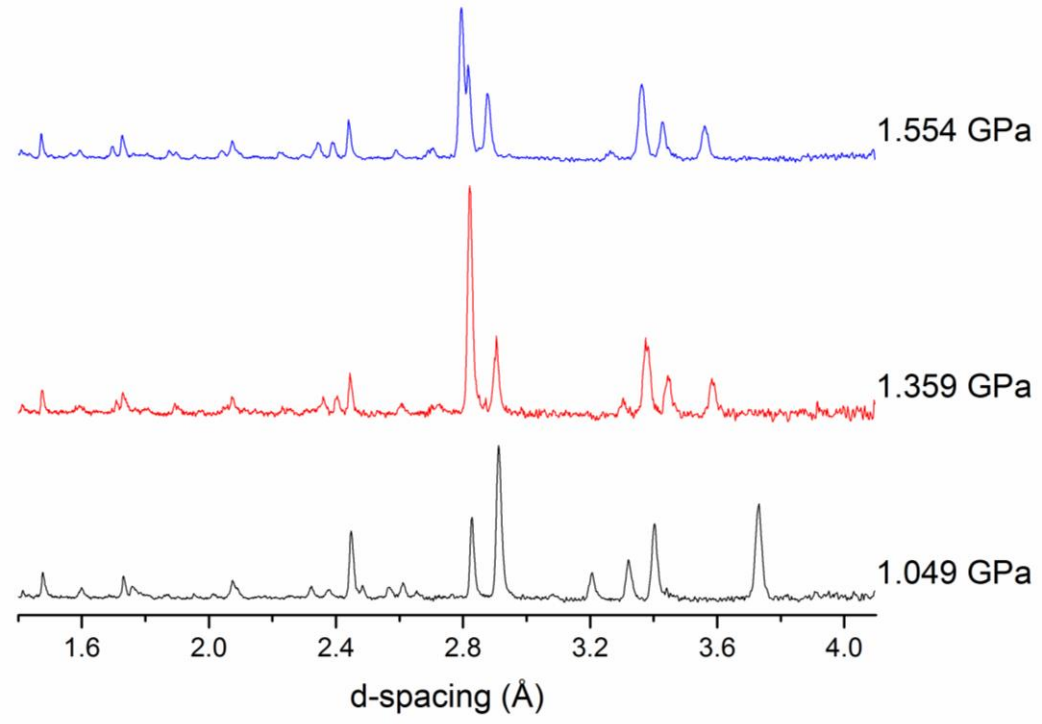

Figure 5.9 - Diffraction patterns of Form I (1.049 GPa) and Form II (1.554 GPa). The diffraction data at 1.359 GPa represents a mixed phase.

As seen in Figures 5.8, a significant change in the diffraction pattern is observed in the data collected from 1.554 GPa upwards, illustrating the phase change from Form I to Form II. Identification of this phase directly from the neutron diffraction data was not possible but fortunately this new phase was solved using data previously obtained from I19 beamline at the DIAMOND Light Source. Data had been collected at 2.27 GPa, with the solution matching the data collected at PEARL. Using this model as a starting model the high pressure datasets were used for either Pawley or Rietveld refinement with the final unit cell parameters presented in Table 5.2.

The Rietveld fits of the neutron diffraction data collected at -0.008 GPa and 1.049 GPa – a) and b) in Figure 5.10, respectively – show a good fit with the known crystal structure of Form I, while the Pawley fit of the data collected at 1.359 GPa, plot c), shows the presence of small quantities of Form I. At 1.359 GPa, the diffraction pattern is dominated by that of Form II, with the diffraction at 1.554 GPa showing that the phase transition from Form I to Form II was complete by this point. The data collected at 5.558 GPa – plot e) – shows that Form II is stable up to this point.

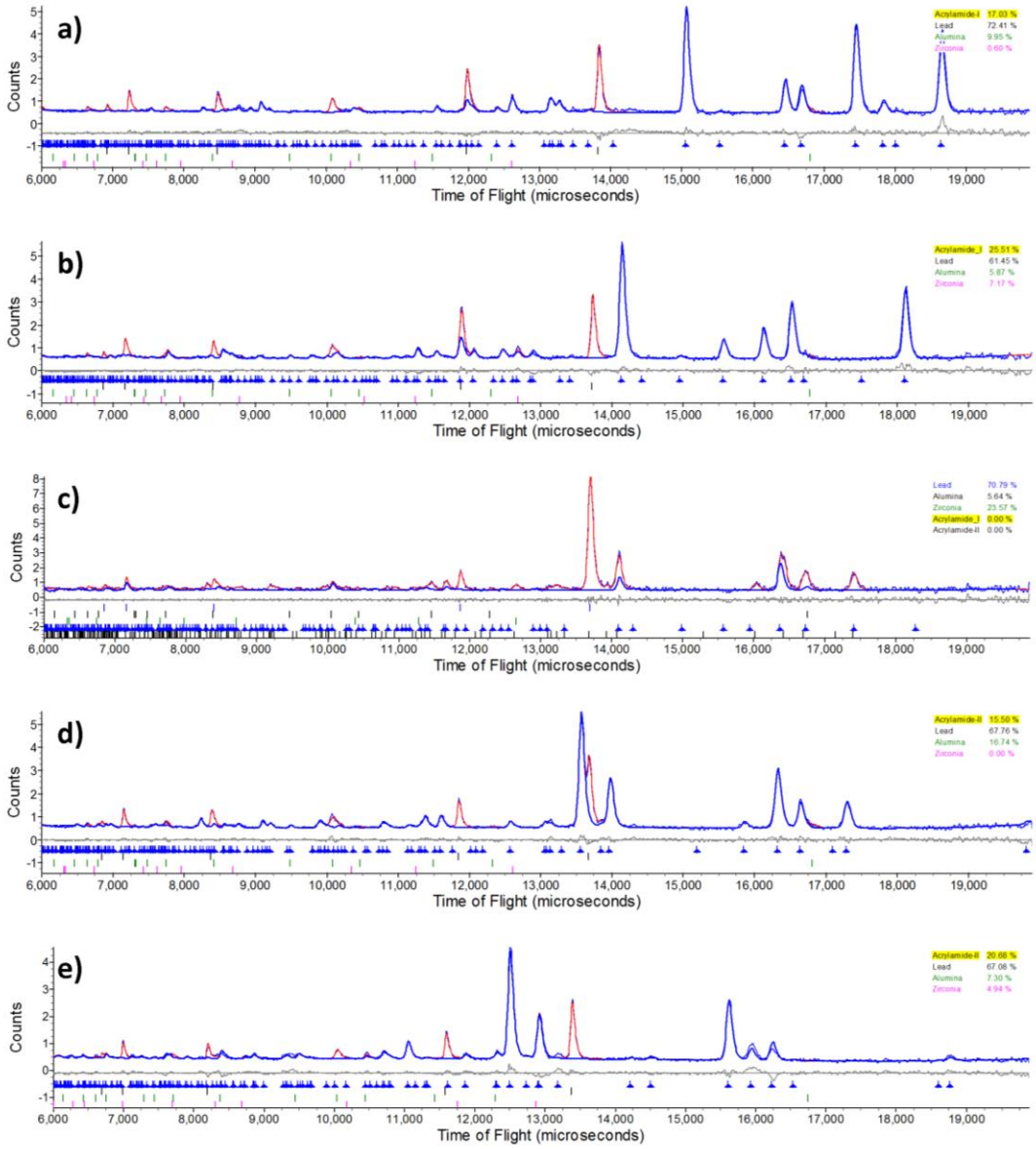

Figure 5.10 - Rietveld fits of the neutron diffraction data collected upon compression compression of acrylamide in pentane:iso-pentane environment at: a) -0.008 GPa, b) 1.049 GPa, d) 1.554 GPa and e) 5.558 GPa. The Pawley fit showing the presence of both polymorphs at 1.359 GPa is shown in c).

Neutron diffraction data collected during the decompression of the sample showed no signs of polymerisation or of any further phase transitions until the phase transition was reversed, allowing Form I to be recovered at ambient pressure. The neutron diffraction patterns collected during decompression are shown in Figure 5.11. The dotted lines represent the shift from pure Form II (at 1.723 GPa) to a pattern consisting of elements of the diffraction patterns of both Forms I and II (1.135 GPa), and then to pure Form I at ambient pressure.

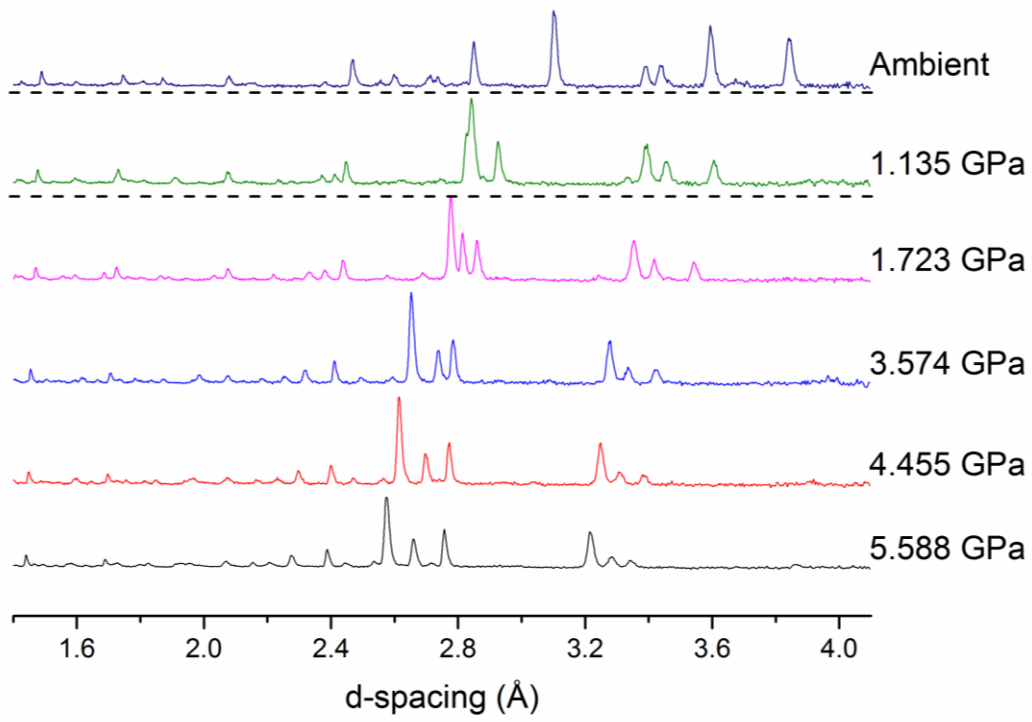

Figure 5.11 - Diffraction data of acrlyamide in pentane/iso-pentane environment during sample recovery to ambient pressure. The dotted lines represent the transition from Form II to a mixed phase of Forms I and II, and then to a clean sample of Form I.

Rietveld fits of the data collected at 5.558 GPa and 1.723 GPa are shown in Figure 5.12, along with Pawley fits of the data collected at 1.135 GPa and the sample recovered to ambient pressure (0.004 GPa). The diffraction at 1.135 GPa shows Form II to be stable upon decompression to this point, albeit with some indication of the presence of Form I in small quantities. The data collected after the mechanical load had been completely removed (with the pressure refining to 0.004 GPa) showed that the sample had completely converted back to Form I.

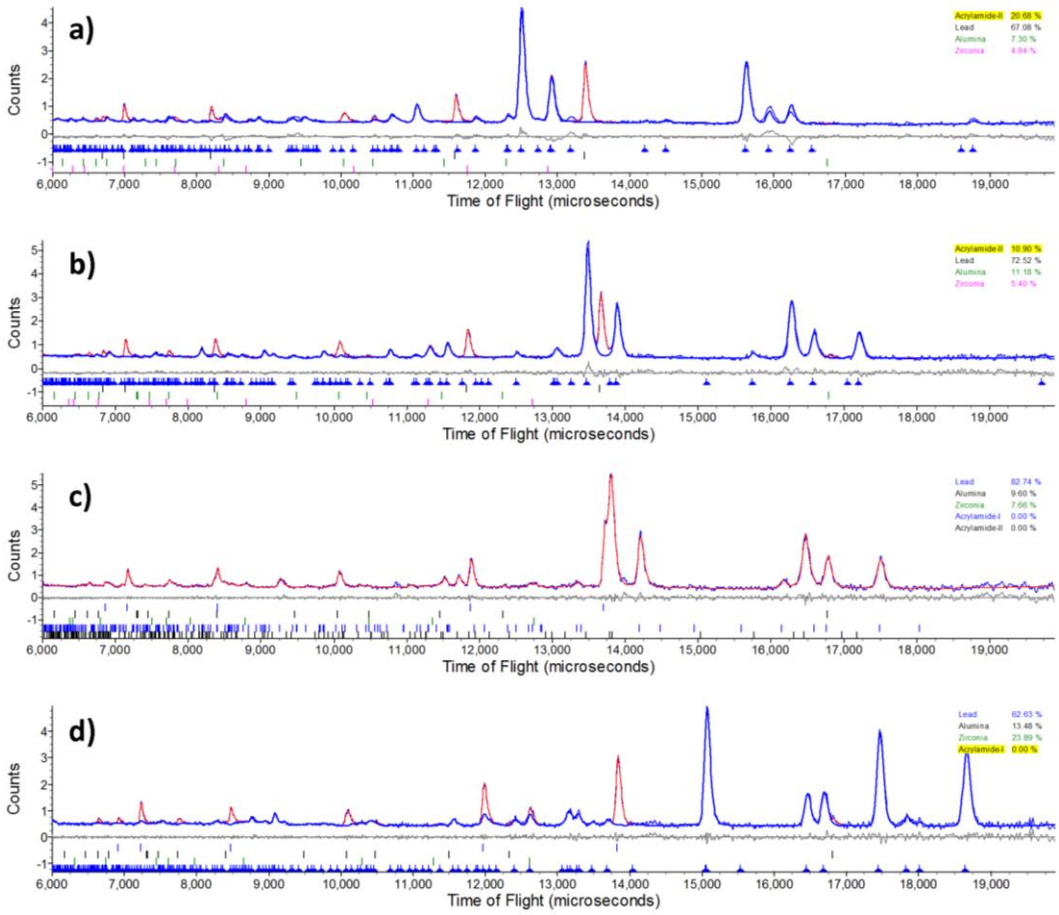

Figure 5.12 - Rietveld fits of neutron diffraction data taken upon decompression of acrylamide in pentane:iso-pentane environment at a) 5.558 GPa and b) 1.723 GPa. The Pawley fits of data collected at c) 1.135 GPa and d) 0.004 GPa are also shown.

Table 5.2 - Unit cell parameters of acrylamide in the pentane/isopentane PTM

Pawley / Rietveld	Load (tonnes)	Form	Pressure (GPa)	Space Group	a-axis (Å)	b-axis (Å)	c-axis (Å)	β (°)	Unit Cell Volume (Å^3)	R_wp
R	6	1	-0.008(4)	$P2_1/n$	8.4030(5)	5.8039(8)	9.3424(9)	113.438(7)	418.04(8)	5.717
P	19	1	0.043(9)	$P2_1/n$	8.3683(13)	5.790(2)	9.298(2)	113.182(18)	414.1(2)	7.751
P	21	1	0.151(9)	$P2_1/n$	8.3046(8)	5.7412(14)	9.2411(18)	112.682(12)	406.53(14)	7.471
P	23	1	0.26(2)	$P2_1/n$	8.2400(8)	5.6986(14)	9.1713(18)	112.216(11)	398.68(13)	7.28
P	25	1	0.395(8)	$P2_1/n$	8.1828(7)	5.6455(13)	9.1236(17)	111.788(16)	391.37(13)	6.78
R	27	1	0.574(3)	$P2_1/n$	8.1175(4)	5.5986(6)	9.0587(7)	111.298(5)	383.57(6)	3.899
P	29	1	0.689(6)	$P2_1/n$	8.0803(6)	5.5669(11)	9.0279(16)	111.034(9)	379.03(11)	6.698
P	31	1	0.863(9)	$P2_1/n$	8.0324(7)	5.5296(14)	8.9796(16)	110.711(11)	373.06(12)	6.912
R	33	1	1.049(4)	$P2_1/n$	7.9809(4)	5.4854(7)	8.9431(8)	110.334(6)	367.12(6)	4.583
P	37	1	1.050(4)	$P2_1/n$	7.9808(4)	5.4853(7)	8.9432(8)	110.333(6)	367.11(6)	4.607
P	37	2	1.290(17)	$P2_1/c$	8.063(9)	5.409(7)	8.872(6)	110.37(7)	362.8(7)	6.541
R	39	2	1.290(17)	$P2_1/c$	6.910(3)	5.435(3)	9.774(7)	106.58(4)	351.8(4)	6.541
P	41	2	1.554(4)	$P2_1/c$	6.8418(5)	5.4080(7)	9.7506(9)	106.698(6)	345.56(6)	4.874
P	43	2	1.697(6)	$P2_1/c$	6.7969(14)	5.3883(10)	9.7443(15)	106.696(7)	341.83(11)	4.754
R	45	2	1.914(6)	$P2_1/c$	6.7491(8)	5.3578(10)	9.7386(12)	106.701(16)	337.30(9)	5.075
P	47	2	2.175(4)	$P2_1/c$	6.6913(4)	5.3295(5)	9.7327(8)	106.711(5)	332.42(5)	4.314
P	51	2	2.396(10)	$P2_1/c$	6.6529(12)	5.3060(13)	9.7305(18)	106.745(13)	328.92(12)	5.031
P	54	2	2.963(11)	$P2_1/c$	6.5583(7)	5.2504(12)	9.7177(11)	106.788(9)	320.35(9)	5.008

R	56	2	3.464(13)	$P2_1/c$	6.5003(9)	5.2114(11)	9.7102(17)	106.857(12)	314.80(10)	5.538
P	58	2	3.794(6)	$P2_1/c$	6.4499(6)	5.1837(8)	9.6945(12)	106.852(7)	310.21(7)	5.936
P	60	2	4.107(10)	$P2_1/c$	6.4165(11)	5.1595(12)	9.680(3)	106.868(12)	306.70(13)	6.923
P	62	2	4.379(7)	$P2_1/c$	6.3819(7)	5.1476(11)	9.6781(14)	106.906(8)	304.20(9)	5.271
P	65	2	4.680(7)	$P2_1/c$	6.3520(7)	5.1300(13)	9.6731(11)	106.959(7)	301.50(9)	5.143
R	68	2	5.068(8)	$P2_1/c$	6.3129(7)	5.1099(9)	9.663(2)	106.991(6)	298.11(9)	5.02
R	6	2	5.588(8)	$P2_1/c$	6.2701(6)	5.0875(10)	9.6504(14)	107.075(8)	294.27(8)	6.619

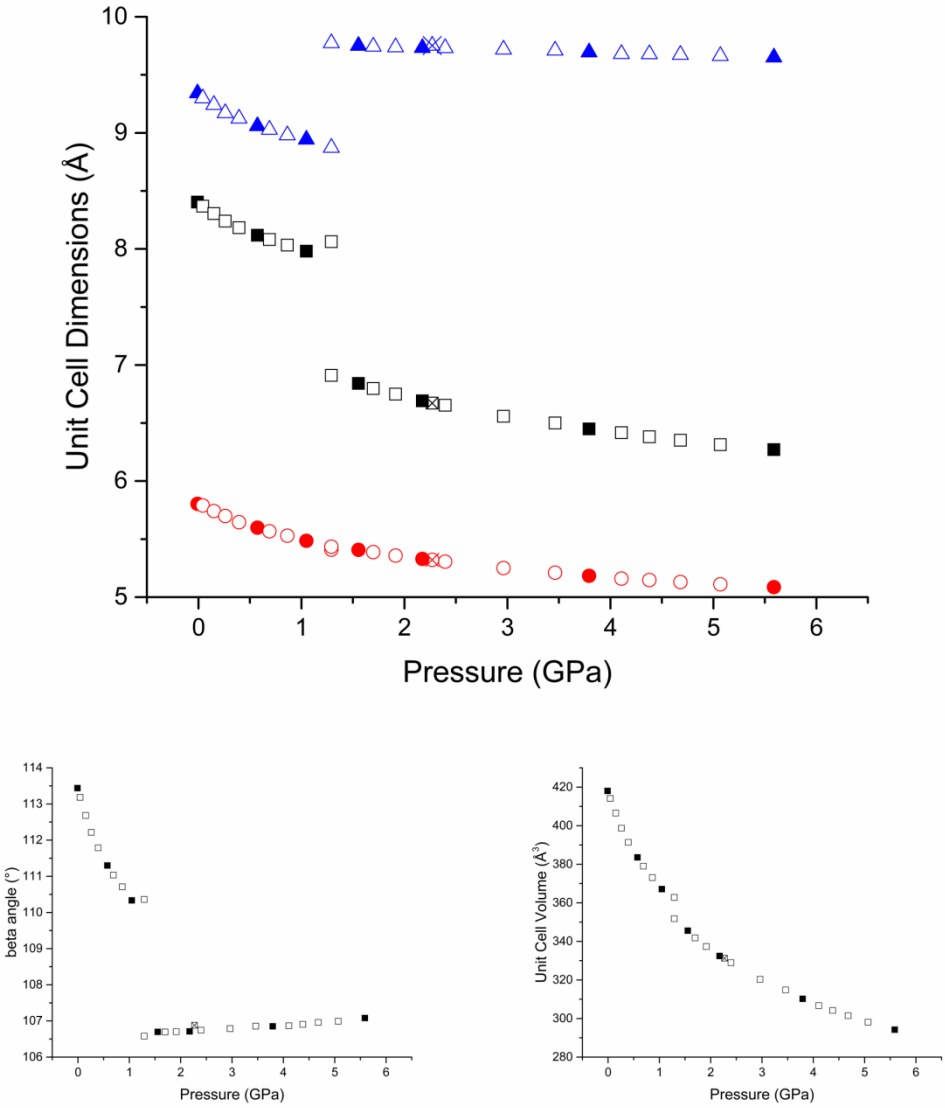

Figure 5.13 - Unit cell parameters of acrlyamide in the pentane/isopentane environment. In the plot showing unit cell dimensions, the black squares, red circles and blue triangles represent the *a*, *b*, and *c* axes, respectively. Filled shapes illustrate the data sets which were Rietveld-fitted; hollow shapes show the Pawley-fitted data. The hollow shapes with crosses in the centre show the data collected on the I19 beamline at DIAMOND, used to help structure solution for Form II.

Figure 5.13 illustrates the changes in the unit cell parameters of acrylamide obtained during the experiment. The polymorph transition can clearly be seen in the plots showing the length of the *a*-axis, *c*-axis and *β*-angle, whilst a step in the curve showing unit cell volume against pressure is also observed which indicates that it is a First-Order polymorph transition. From one data point to the next, within each polymorph, a gradual decrease is seen across each of the unit cell axes, and the unit cell volume. The size of the β-angle shows a smooth decrease

with increasing pressure in Form I, before decreasing markedly over the phase transition followed by a gradual increase in the angle with increasing pressure after the phase transition.

5.3.3 Loading 2 – Acrylamide-d_5 in a 4:1 (v/v) MeOD : EtOD environment

Figure 5.14 shows the diffraction patterns collected upon compression of acrylamide-d_5 in a 4:1 MeOD:EtOD environment up to 5.338 GPa. As the time available to us was limited, it was decided that collecting data on the known Form I was not a priority and so only two extended data sets of this polymorph was collected in order to allow Rietveld refinement to be conducted. These data were collected at ambient pressure (refining to -0.045 GPa) and 0.285 GPa. The dotted line in Figure 5.15 represents a phase transition from the ambient pressure polymorph, Form I, to a previously unseen polymorph, herein designated Form III.

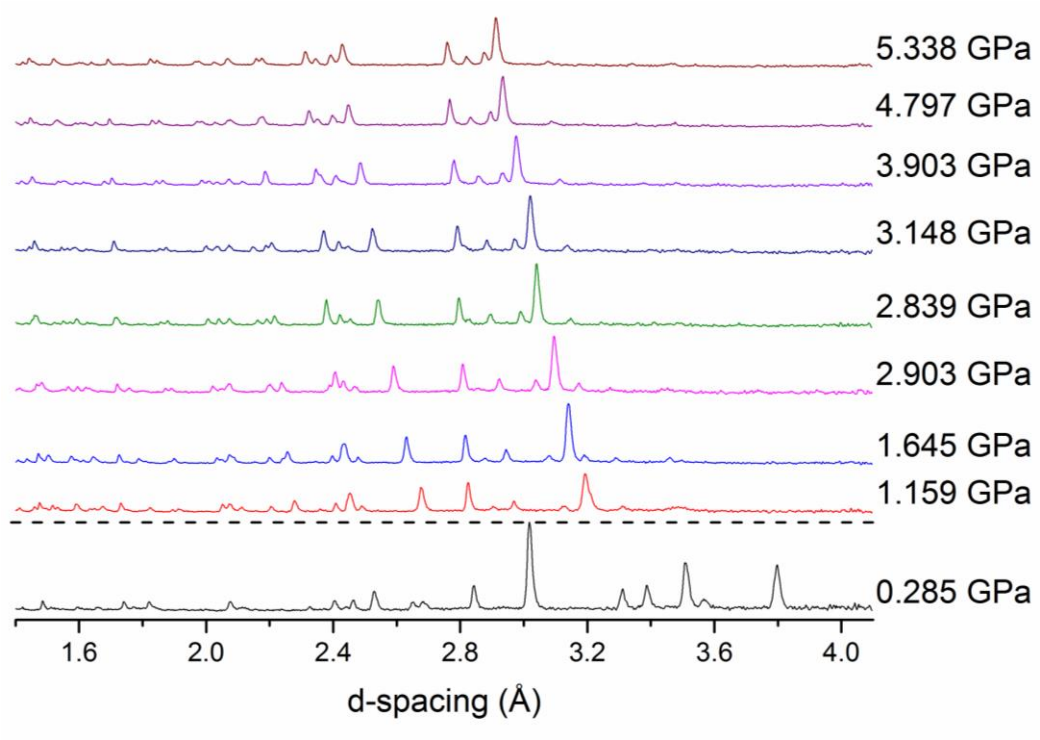

Figure 5.14 – Neutron diffraction data collected upon compression of acrylamide-d_5 to 5.388 GPa in a 4:1 MeOD:EtOD environment.

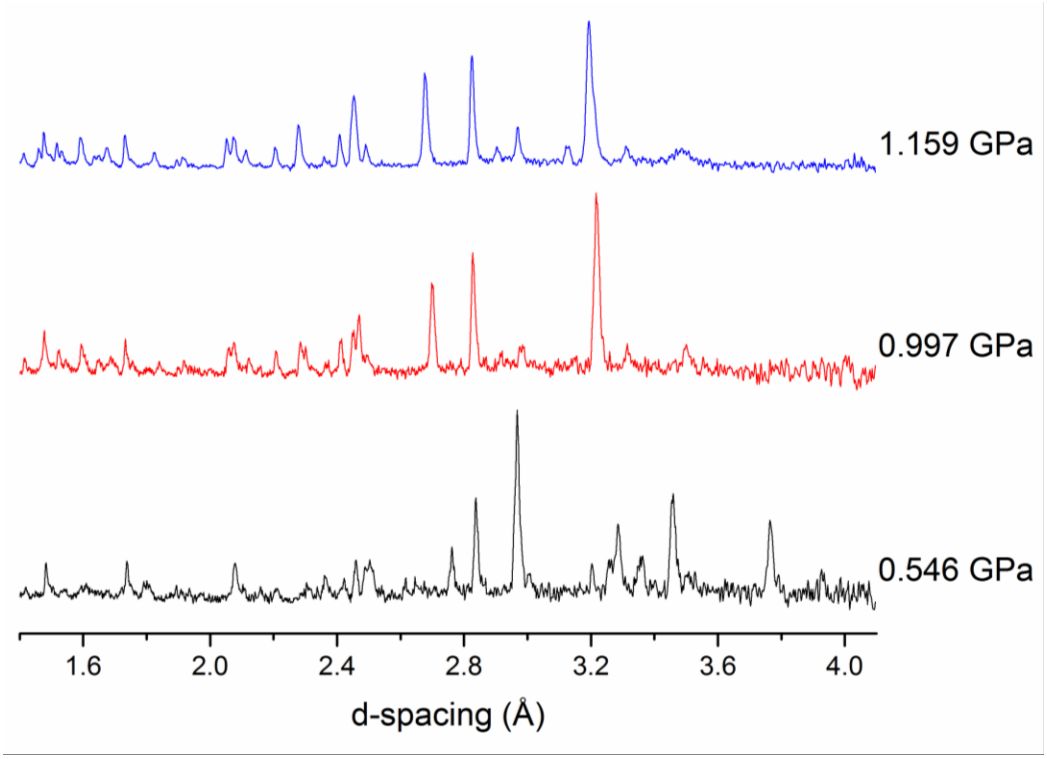

Figure 5.15 – Neutron diffraction patterns of acrylamide upon compression in a 4:1 MeOD:EtOD environment, showing the phase transition from Form I to Form III.

A subsequent replication of this experiment in a DAC (using a hydrogenous sample and PTM rather than the deuterated sample and environment used in the study at ISIS), growing a single crystal at pressure through temperature annealing, allowed the structure of Form III to be fully solved using SXRD. Fitting the neutron diffraction data collected at ISIS against the solved Form III structure confirmed the polymorphs observed in each of the experiments were the same, allowing the behaviour of Form III to be studied through examination of the neutron diffraction data. Figures 5.16 show the Rietveld-fitted neutron diffraction data of acrylamide in the 4:1 MeOD-EtOD environment against Forms I and III.

Data were collected between the Rietveld-refined datasets of Form I at 0.285 GPa and Form II at 1.159 GPa. These data were Pawley-refined, with the diffraction patterns collected at 0.546 GPa, 0.997 GPa and 1.159 GPa shown in Figure 5.15. These three diffraction patterns represent Form I, a mixed phase of Forms I and III, and Form III, respectively. A Pawley fit of the data collected at 0.997 GPa, along with Rietveld fits of Form I at -0.045 GPa and 0.285 GPa, and of Form III at 1.159 GPa and 5.388 GPa are shown in Figure 5.16. These fits show

that at 0.997 GPa, Form III is the dominant polymorph, and is then stable up to the highest pressure at which a Rietveld refined data set was collected, 5.338 GPa.

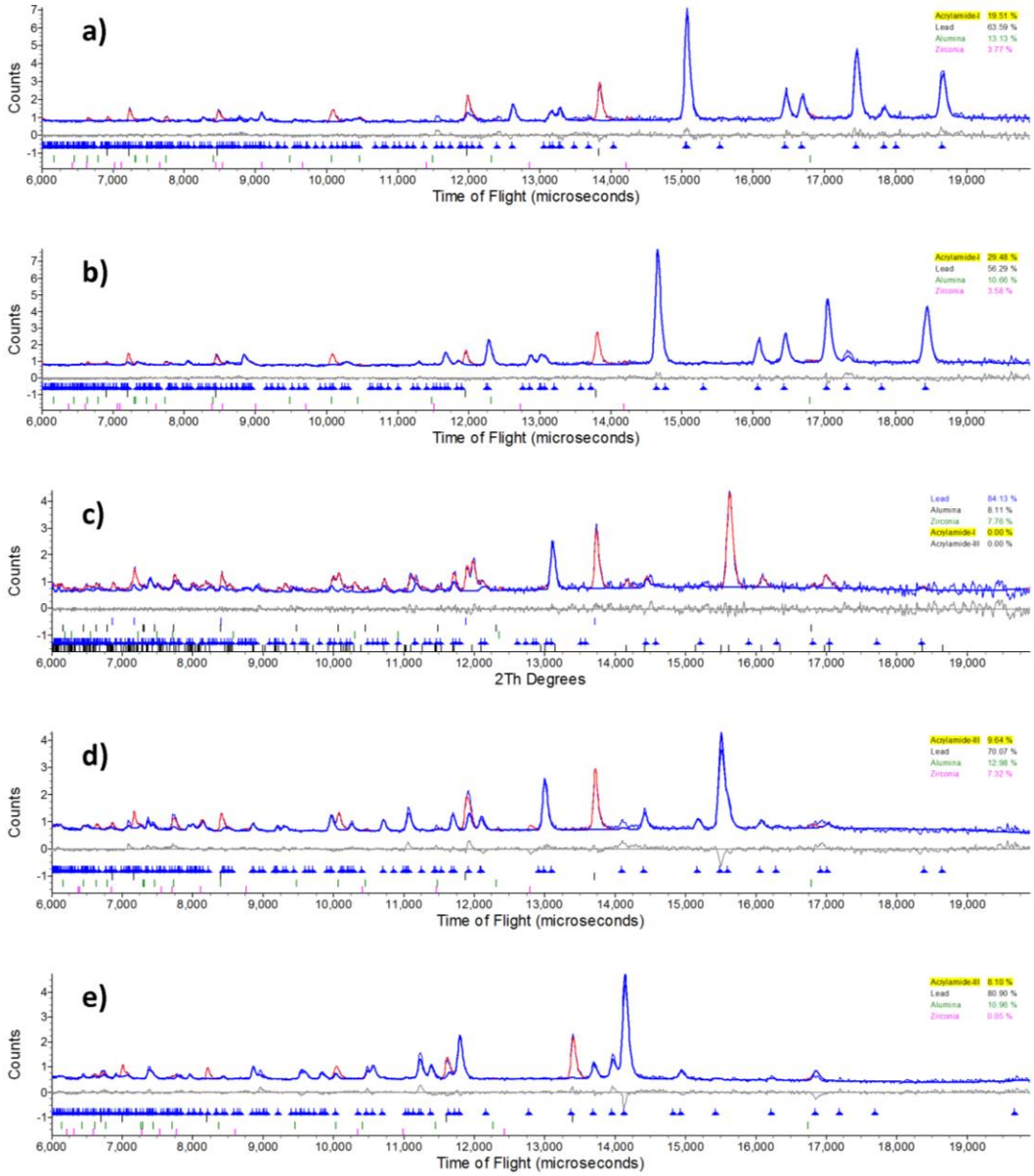

Figure 5.16 - Rietveld refinements of the data collected upon compression of acrylamide in the 4:1 MeOD:EtOD environment at a) -0.045 GPa, b) 0.285 GPa, d) 1.159 GPa and e) 5.338 GPa. The Pawley fit of the data at 0.997 GPa is shown in d), where both Forms I and III are present.

Neutron diffraction data collected during the decompression of the sample back to ambient pressure showed, as in the first loading, no signs of polymerisation. Similarly, the phase transition was reversed upon decompression, allowing Form I to be recovered upon removal

of the applied mechanical load and associated pressure. The diffraction patterns collected upon decompression are shown in Figure 5.17. From visual observation, it appears as though sample III is stable as low as 0.679 GPa, before the data after complete removal of the applied mechanical load show the sample recovered to be Form I.

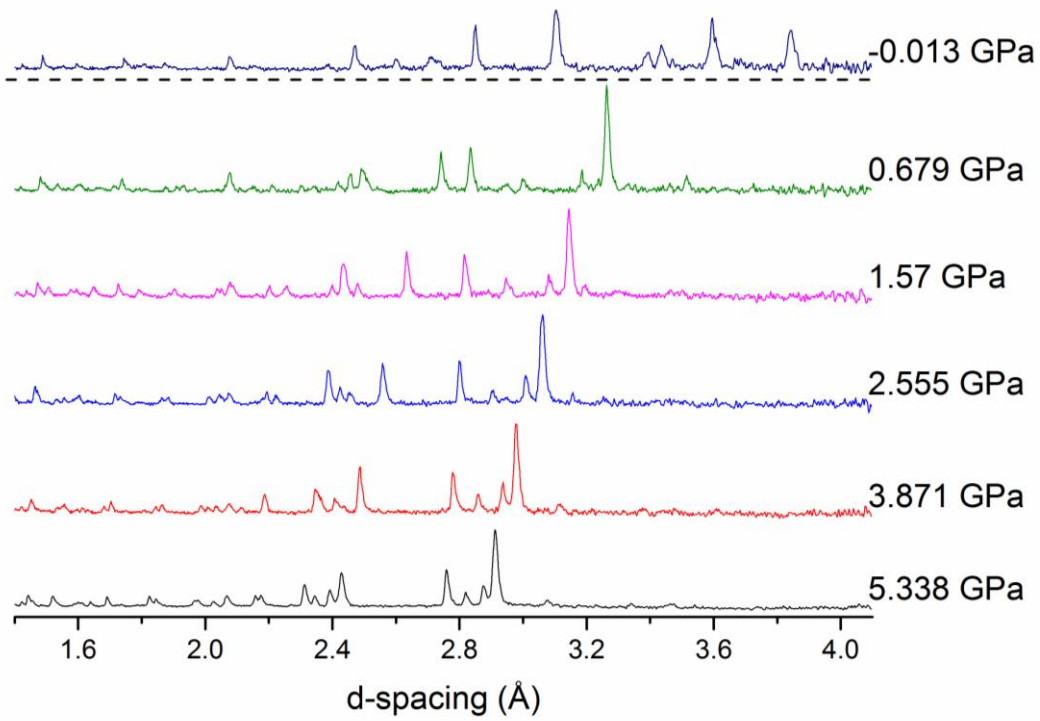

Figure 5.17 – Neutron diffraction data collected upon decompression of acrylamide in the 4:1 MeOD:EtOD environment.

Figure 5.18 shows a Rietveld refinement of the neutron diffraction data collected at 5.338 GPa along with Pawley refinements collected upon decompression at 2.555 GPa, 0.679 GPa and -0.013 GPa. These fits reflect the visual observation made above, showing that the diffraction data collected at 0.679 GPa is that of a clean sample of Form II, with Form I then being observed when the sample was recovered to ambient conditions.

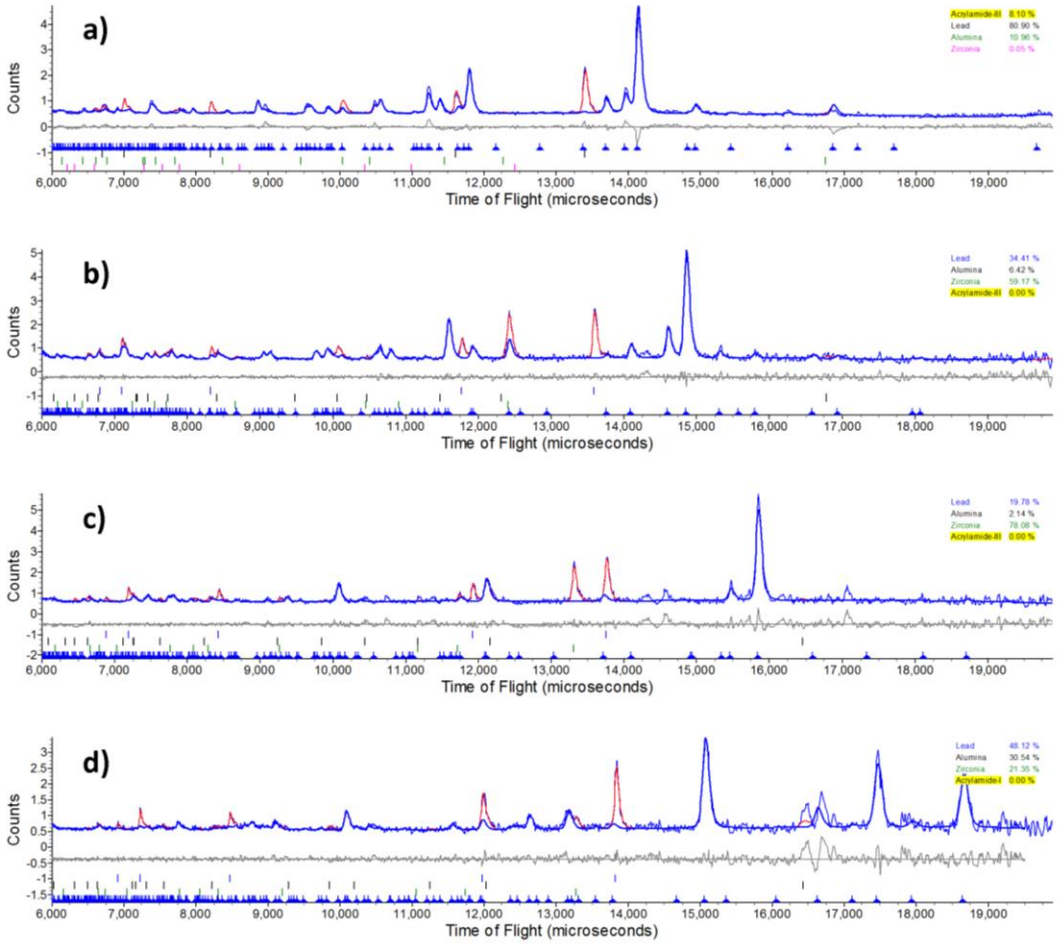

Figure 5.18 - a) shows the Rietveld refinement of the neutron diffraction data collected from the acrylamide sample at 5.338 GPa in the 4:1 MeOD:EtOD environment, while b), c) and d) show the Pawley fits of the data collected upon decompression, at 2.555 GPa, 0.679 GPa and -0.013 GPa, respectively.

Table 5.3 shows a comprehensive summary of the refined unit cell parameters of acrylamide upon compression in the 4:1 MeOD-EtOD environment. Since the phase transition results in the number of molecules in the unit cell, Z, increasing from 4 to 8, the change in the molecular volume as opposed to the unit cell volume is a more appropriate way of showing the compression of the sample under pressure. This shows a steady compression of the material across both phases (Figure 5.19).

Table 5.3 - Unit cell parameters of acrylamide in the 4:1 MeOD/EtOD environment

Pawley / Rietveld	Load (tonnes)	Form	Pressure (GPa)	Space Group	a-axis (Å)	b-axis (Å)	c-axis (Å)	β (°)	Unit Cell Volume (Å^3)	R_wp
P	6	I	-0.040(6)	$P2_1/n$	8.4061(8)	5.8031(11)	9.3443(12)	113.441(9)	418.21(11)	5.77
P	10	I	0.054(13)	$P2_1/n$	8.2195(13)	5.537(3)	9.2585(6)	111.305(14)	392.6(2)	7.965
R	12	I	0.285(6)	$P2_1/n$	8.2178(4)	5.6726(7)	9.1557(8)	112.019(6)	395.68(6)	4.407
P	15	I	0.567(6)	$P2_1/n$	8.1131(5)	5.5938(12)	9.0557(13)	111.254(7)	383.03(10)	4.238
P	17	I	0.546(11)	$P2_1/n$	8.1016(15)	5.598(3)	9.039(3)	111.161(19)	382.3(3)	7.202
P	23	I	0.997(10)	$P2_1/n$	8.141(2)	5.613(10)	9.038(12)	111.23(12)	385.0(9)	6.168
P	23	III	0.997(10)	C_2/c	7.667(16)	6.6473(6)	13.649(4)	97.92(4)	689.0(14)	6.168
R	25	III	1.159(6)	C_2/c	7.6706(10)	6.6397(7)	13.5852(11)	97.694(7)	685.67(13)	5.262
P	27	III	1.304(8)	C_2/c	7.6592(14)	6.6269(10)	13.518(2)	97.942(11)	679.5(2)	4.572
P	29	III	1.463(7)	C_2/c	7.6441(13)	6.6185(8)	13.4498(16)	98.179(10)	673.54(16)	4.423
R	31	III	1.645(6)	C_2/c	7.6362(9)	6.5996(7)	13.3756(10)	98.479(6)	666.71(12)	5.354
P	33	III	1.775(9)	C_2/c	7.625(2)	6.5907(10)	13.3264(14)	98.705(10)	662.0(2)	5.785
P	35	III	1.924(9)	C_2/c	7.6203(13)	6.5800(14)	13.2657(12)	98.940(7)	657.07(19)	5.552
R	37	III	2.093(8)	C_2/c	7.6101(9)	6.5654(8)	13.2074(11)	99.256(7)	651.30(12)	6.2
P	39	III	2.257(7)	C_2/c	7.5997(12)	6.5552(8)	13.1611(10)	99.401(9)	646.86(14)	4.575
P	42	III	2.529(8)	C_2/c	7.5841(8)	6.5370(8)	13.0772(14)	99.747(9)	638.97(12)	4.751
R	45	III	2.839(7)	C_2/c	7.5731(7)	6.5133(5)	13.0035(9)	100.131(5)	631.40(9)	4.772

R	48	III	3.148(7)	C_2/c	7.5586(7)	6.4916(6)	12.9270(9)	100.424(5)	623.83(9)	4.83
P	51	III	3.429(9)	C_2/c	7.5461(13)	6.4732(8)	12.8635(11)	100.763(9)	617.30(14)	4.597
R	54	III	3.903(8)	C_2/c	7.5321(6)	6.4460(7)	12.7706(9)	101.153(6)	608.33(9)	4.901
P	57	III	4.349(9)	C_2/c	7.5124(7)	6.4248(7)	12.6935(8)	101.505(5)	600.35(9)	2.991
R	60	III	4.797(8)	C_2/c	7.4981(6)	6.4039(7)	12.6162(8)	101.837(5)	592.90(9)	4.687
R	63	III	5.338(11)	C_2/c	7.4846(6)	6.3793(9)	12.5424(11)	102.187(7)	585.37(11)	5.896
P	66	III	5.700(13)	C_2/c	7.4751(10)	6.3585(8)	12.4960(15)	102.447(8)	579.98(13)	5.027

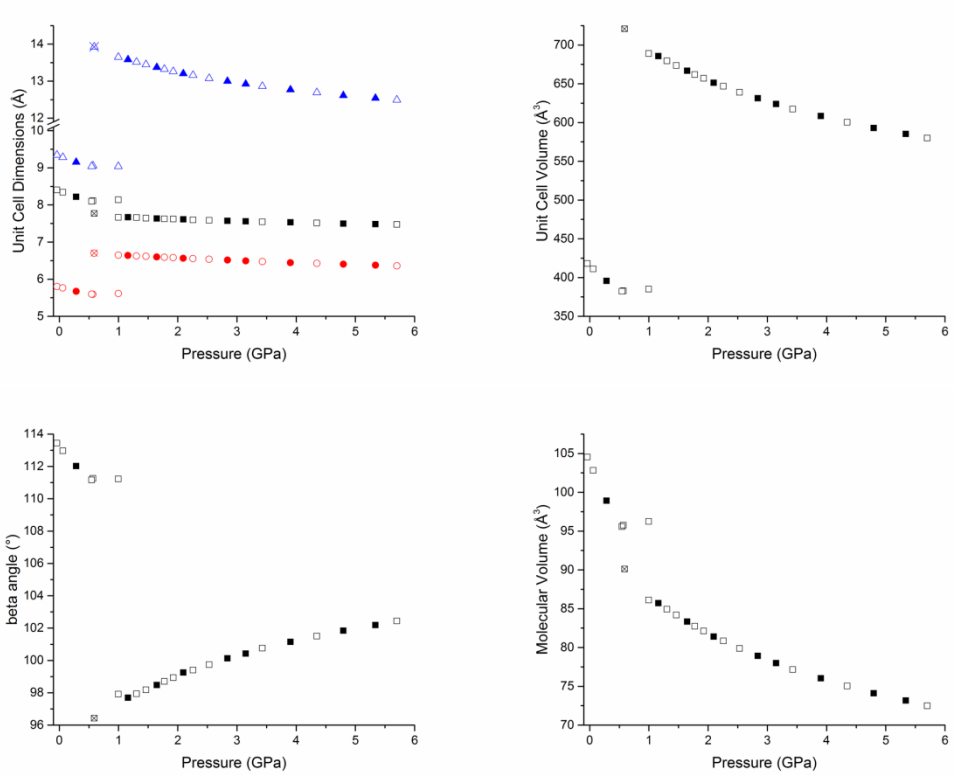

Figure 5.19 - Unit cell parameters of acrylamide in the 4:1 (v/v) MeOD/EtOD environment. In the plot showing unit cell dimensions, the black squares, red circles and blue triangles represent the a, b, and c axes, respectively. Filled shapes signify Rietveld-refined data, whilst hollow shapes signify Pawley-refined data. Hollow shapes with crosses in the centre signify the SXRD data subsequently collected in a DAC, used to assist in solving the neutron diffraction data.

5.3.4 Loading 3 – Acrylamide-d_5 in iso-propyl alcohol (IPA)

Neutron diffraction data were collected upon compression of acrylamide-d_5 in IPA to 5.21 GPa. The diffraction patterns observed are shown in Figure 5.20, with the dotted line between 0.74 and 1.40 GPa representing a phase transition from the ambient pressure polymorph, Form I, to a previously unknown polymorph, herein designated Form IV. Data were collected between 0.74 and 1.40 GPa, showing the phase transition from Form I to Form IV. The patterns observed across the phase transition are shown in Figure 5.21. It should be noted that as the sample undergoes a phase transition to a denser polymorph, the pressure in the cell decreases.

Diffraction patterns collected upon decompression are shown in Figure 5.22. From visual observation of the patterns shown, it can be seen that the high pressure polymorph, Form IV, is stable upon decompression to 1.025 GPa. The pattern at 0.39 GPa appears to show

elements of Forms I and IV, whilst the diffraction data collected upon recovery to ambient pressure shows a clean sample of Form I.

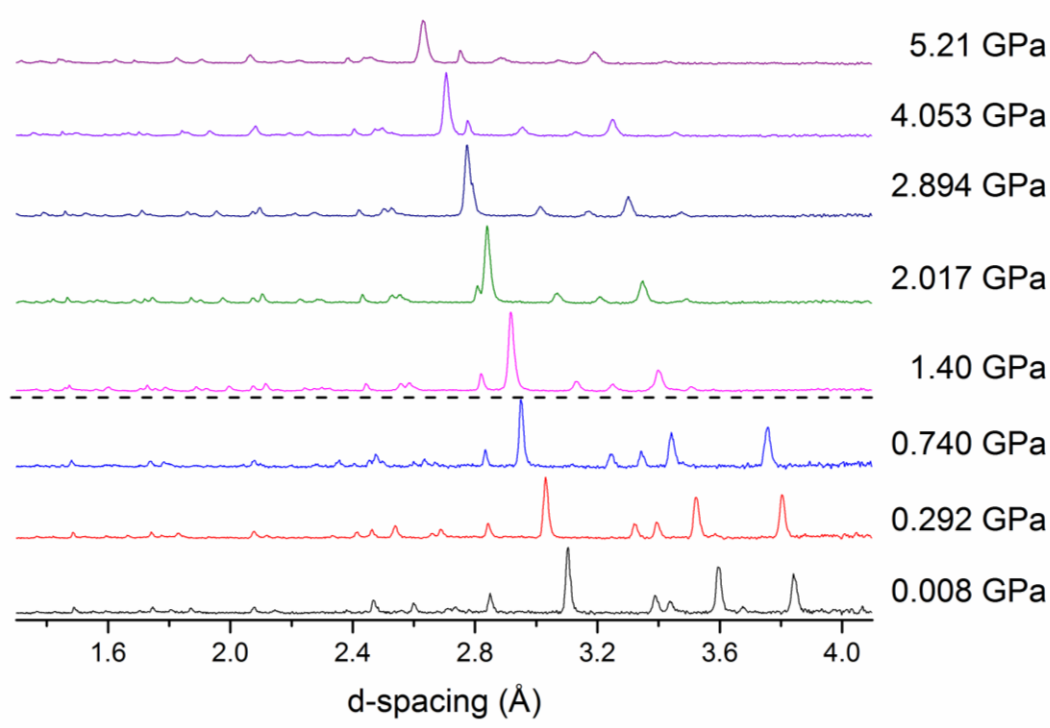

Figure 5.20 - Neutron diffraction data collected upon compression in iso-propyl alcohol.

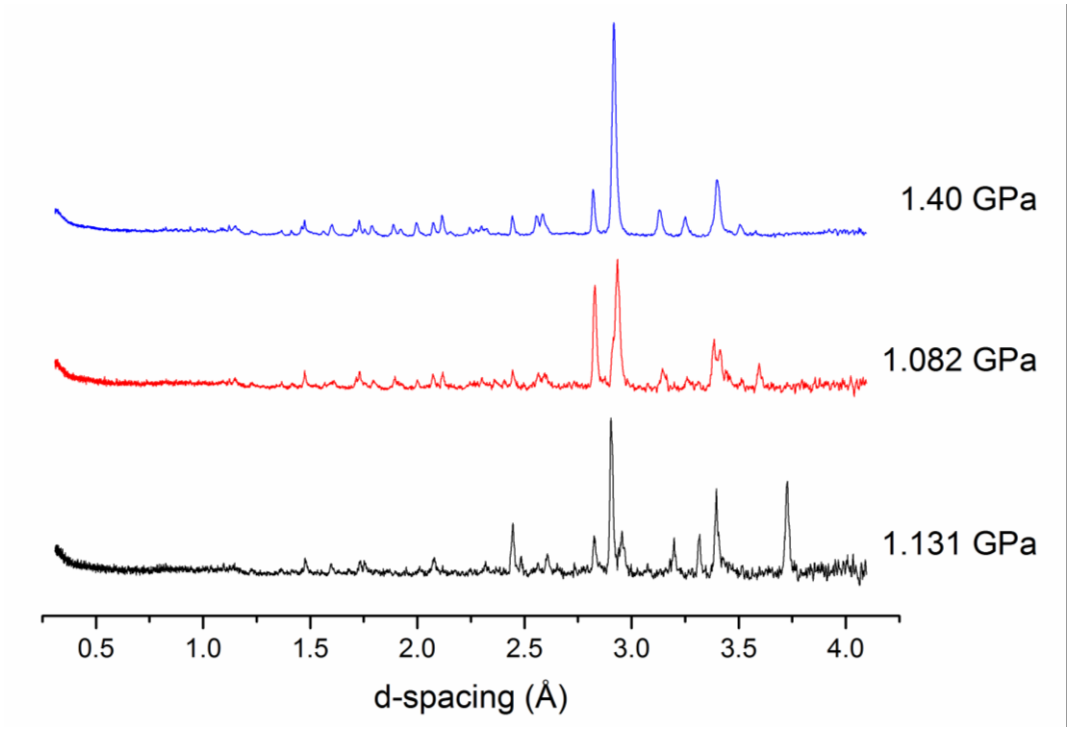

Figure 5.21 - Neutron diffraction data collected upon compression, showing the sample undergoing a phase transition.

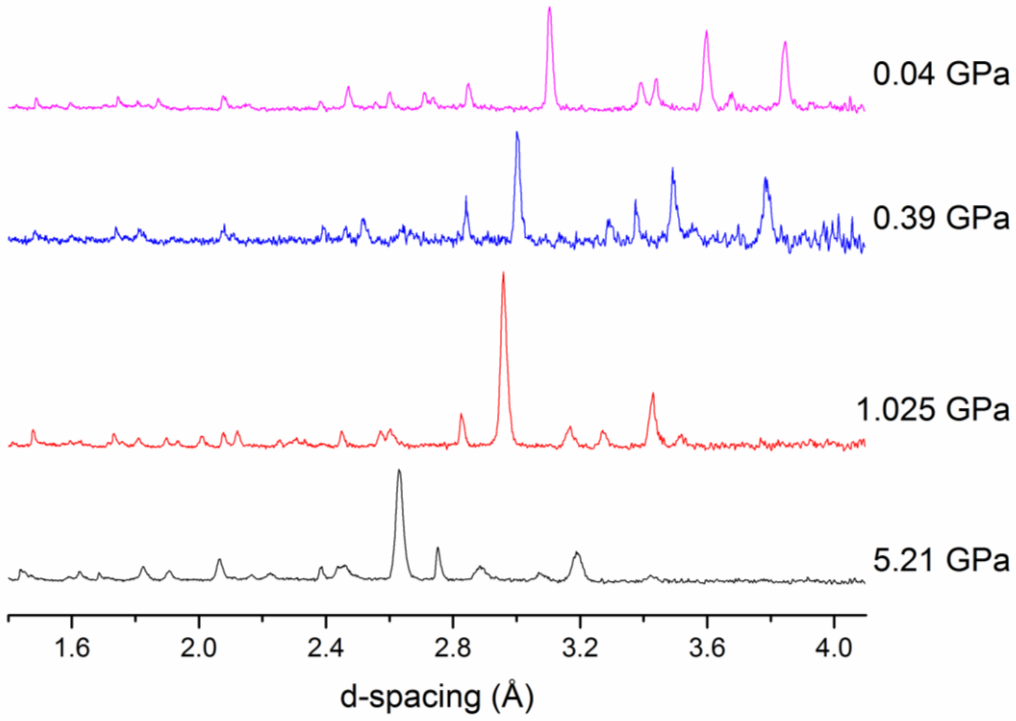

Figure 5.22 - Neutron diffraction data collected upon decompression, showing the sample reverting back to its ambient pressure form upon recovery to ambient pressure.

Pawley and Rietveld fits were performed on the data collected before the phase transition, and on those data collected upon decompression. Figure 5.26 shows the Rietveld-fitted data collected at 0.292 GPa, as well as the Pawley-fitted data collected at 0.008 GPa, 1.131 GPa and 1.082 GPa upon compression. The Pawley-fitted data collected upon decompression to 0.04 GPa is also shown.

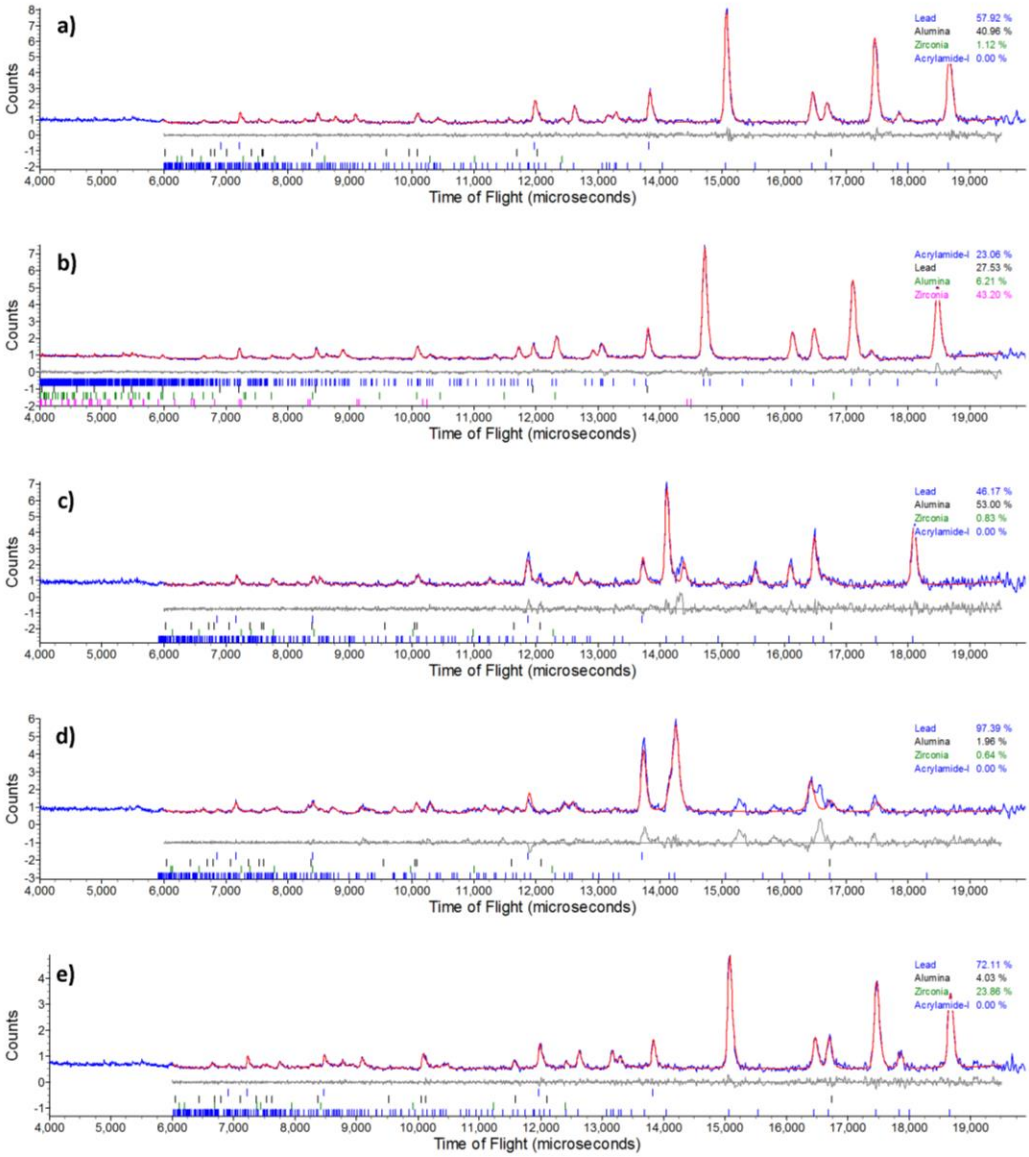

Figure 5.23 - Fits of data collected upon compression at: a) 0.008 GPa, b) 0.292 GPa, c) 1.131 GPa, and d) 1.082 GPa. Plot e) shows the fit of the data collected upon decompression to 0.04 GPa.

Figure 5.26 shows that the sample was in the ambient form, Form I, in the first two pressure points illustrated. In plot c), the sample has begun to undergo a phase transition, resulting in a number of mis-fitting peaks which are more evident as the phase transition progresses. In plot d), the pressure refined to be lower than that of plot c), showing the unknown high pressure form to be denser than the ambient-pressure form. Upon decompression to ambient pressure, Form I is recovered. Refined unit cell parameters of Form I are given in Table 5.4, and illustrated in Figure 5.24.

Table 5.4 - Unit cell parameters of Form I upon compression in the iso-propyl alcohol environment .

Pawley / Rietveld	Load (tonnes)	Form	Pressure (GPa)	Space Group	a-axis (Å)	b-axis (Å)	c-axis (Å)	β (°)	Unit Cell Volume (Å^3)	R_wp
Pawley	5.5	I	0.008(9)	$P2_1/n$	8.4061(8)	5.8035(14)	9.3447(15)	113.444(12)	418.24(13)	5.168
Pawley	10	I	0.06(2)	$P2_1/n$	8.3568(9)	5.7484(14)	9.3057(12)	113.209(13)	410.85(4)	12.717
Rietveld	12	I	0.292(5)	$P2_1/n$	8.2456(4)	5.6940(7)	9.1806(8)	112.234(5)	398.99(6)	4.133
Pawley	14	I	0.450(11)	$P2_1/n$	8.1567(6)	5.6284(14)	9.0984(17)	111.571(8)	388.45(13)	6.535
Pawley	16	I	0.649(12)	$P2_1/n$	8.1091(10)	5.5941(15)	9.0497(19)	111.199(19)	382.74(15)	7.771
Pawley	18	I	0.740(9)	$P2_1/n$	8.0687(5)	5.5580(12)	9.0126(15)	110.944(8)	377.47(11)	5.92
Pawley	20	I	0.843(12)	$P2_1/n$	8.0369(7)	5.5254(13)	8.9889(14)	110.741(14)	373.30(11)	7.373
Pawley	22	I	1.003(15)	$P2_1/n$	7.9966(7)	5.4950(15)	8.9541(16)	110.426(11)	368.71(13)	8.061
Pawley	24	I	1.131(17)	$P2_1/n$	7.9674(9)	5.4811(15)	8.9171(14)	110.251(13)	365.34(13)	8.905
Pawley	27	I	1.082(13)	$P2_1/n$	8.082(4)	5.4768(17)	8.8323(11)	110.48(4)	366.3(2)	8.716

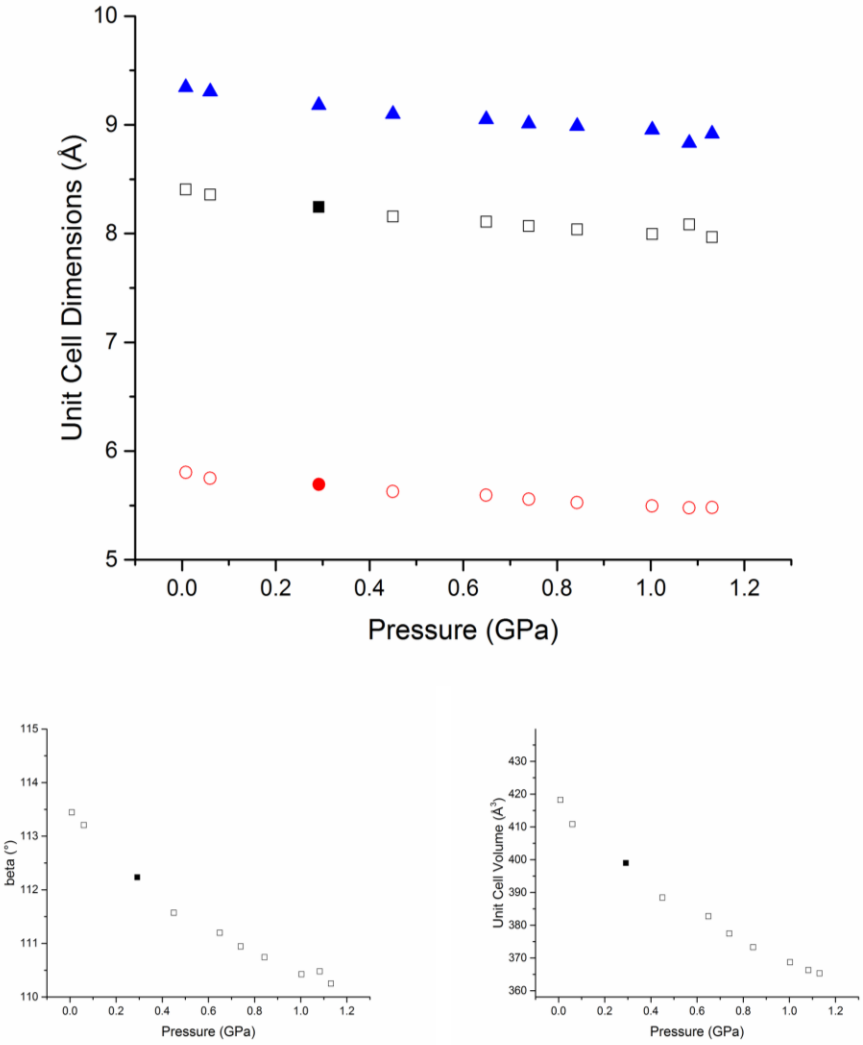

Figure 5.24 - Refined unit cell parameters of Form I of acrylamide upon compression in IPA.

5.3.4.1 Structure Solution of Form IV

Attempts to solve the structure of Form IV were unsuccessful, with further work required in order for this to be achieved. This may include further attempts to grow a crystal at high pressure through temperature annealing (as per the method used to solve the structure of Form III), or computational methods. One limitation of attempting to solve the structure computationally is that the contents of the asymmetric unit must be known. In order to assist, examination of Form IV via spectroscopic techniques may allow the presence or absence of a second acrylamide molecule in the asymmetric unit to be determined depending on, for example, whether the amide signal in the Raman spectrum is present as a split band or a

single band. A further limitation of this is that, at present, it is not possible to know whether the high pressure form observed, Form IV, is a polymorph or a solvate.

5.4 Summary of Observations

In summary, the high pressure behaviour of acrylamide has been observed in three different environments – a 1:1 (v/v) mixture of pentane and iso-pentane, a 4:1 (v/v) mixture of methanol and ethanol, and iso-propyl alcohol (IPA). In each environment, acrylamide is seen to undergo a reversible phase transition upon compression, with the high pressure forms observed in each of the media being distinct from each other. The diffraction patterns of each of the four forms are shown in Figure 5.25.

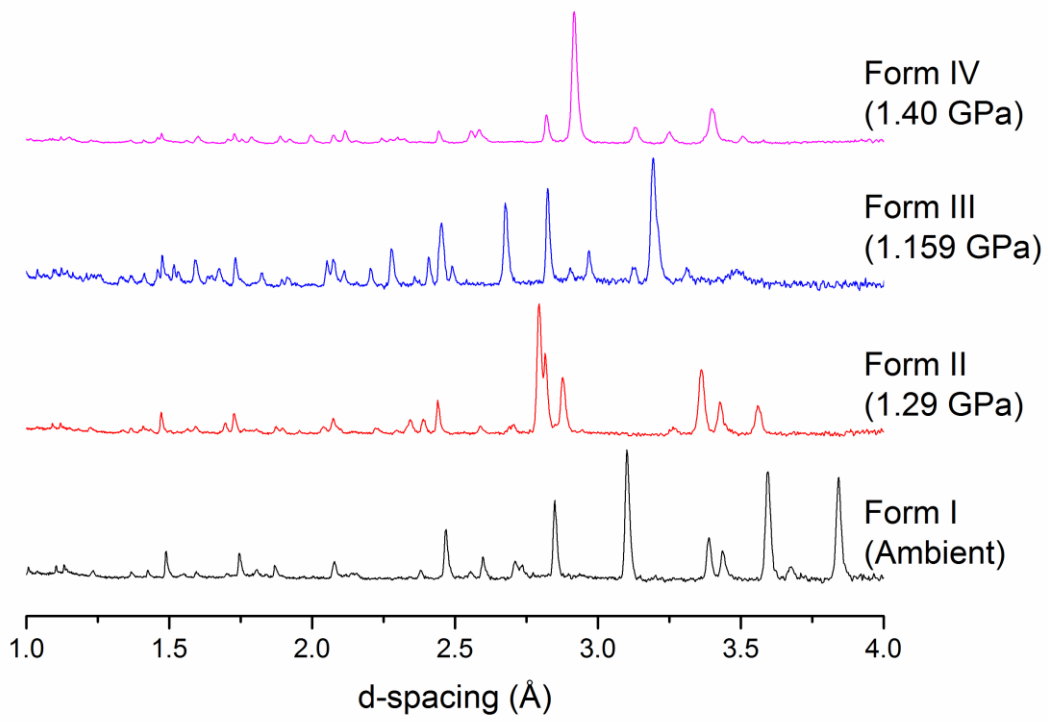

Figure 5.25 - Neutron diffraction patterns of each of the four forms of acrylamide.

The observation of different high pressure forms in each of the media may be linked to the degree to which acrylamide is soluble in the medium used, which varies significantly across

the three media used. Acrylamide is insoluble in the pentane:iso-pentane environment, freely soluble in the methanol:ethanol environment and moderately soluble in IPA.

The structures of the high pressure forms in the pentane:iso-pentane environment and in the methanol:ethanol environment (Forms II and III, respectively) were successfully solved, whilst that of Form IV (the high pressure form in the iso-propyl alcohol environment) was not successfully solved.

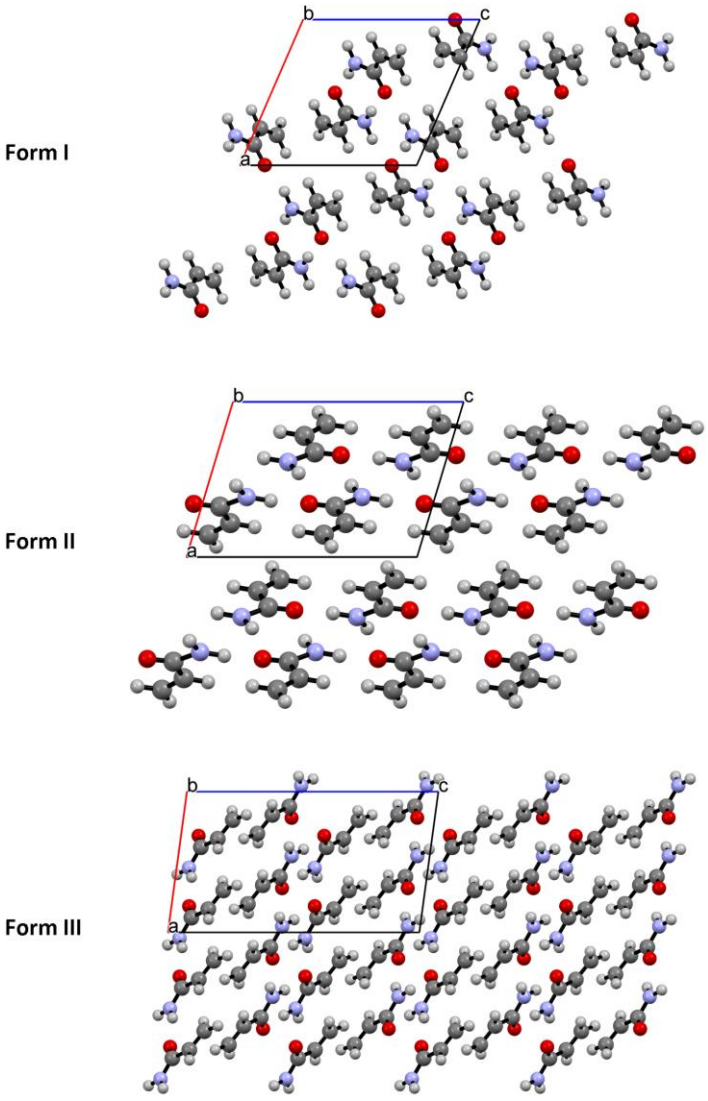

Figure 5.26 - Packing arrangement of Forms I, II and III of acrylamide.

With each of the forms having been observed over a range of pressures, compression of the unit cell was used to fit a 3rd order Birch-Murnaghan equation of state to each polymorph

(Table 5.5). From this table, it can be seen that the predicted molecular volumes of Forms II and III at ambient pressure, V_0, are 97.6% and 82.1% that of Form I, respectively. Hence, it can be seen that Form III is significantly denser than Form II. Form III has a higher bulk modulus than Form II, and hence compresses slightly less when comparisons are made over a similar pressure range (Table 5.6).

Table 5.5 - 3rd order Birch-Murnaghan equations of state of Forms I, II and III of acrylamide.

Polymorph	**V_0 (Å^3)**	**K_0**	**K'**	**K''**
Form I	417.5(4)	4.60(17)	9.6(6)	-8.9
Form II	407.4(3)	4.66(8)	8.9(2)	-7.1
Form III	774.2(6)	5.2(7)	11.0(11)	-11.3

Table 5.6 - Comparison of the rates of compression of Forms I, II and III of acrylamide

Unit Cell Parameter	**Lowest Pressure (GPa)**	**Highest Pressure (GPa)**	**Compression (%)**
Form I (observed between ambient pressure and 0.1.291 GPa)			
a-axis (Å)	8.4030	8.063	4.0
b-axis (Å)	5.8039	5.409	6.8
c-axis (Å)	9.3424	8.872	5.0
Volume (Å^3)	418.04	362.8	13.2
Form II (observed between 1.291 GPa and 5.588 GPa)			
a-axis (Å)	6.910	6.2706	10.2
b-axis (Å)	5.435	5.0868	6.8
c-axis (Å)	9.774	9.6502	1.3
Volume (Å^3)	351.8	294.24	19.6
Form III (observed between 0.997 GPa and 5.338 GPa)			
a-axis (Å)	7.667	7.4844	2.4
b-axis (Å)	6.6473	6.3792	4.0
c-axis (Å)	13.649	12.5431	8.1
Volume (Å^3)	689.0	585.36	15.0

Calculation of the void spaces in each form with increasing pressure allows one to visualise how the compression of the unit cell occurs. In Form I, compression of each of the axes is relatively similar, while compression of the *a*-axis and *c*-axis are by far the most significant in Forms II and III, respectively. The void spaces, in each case calculated using a 0.2 Å probe radius and an approximate probe spacing of 0.1 Å, of Forms I, II and III at each Rietveld-fitted pressure point can be seen in Figures 5.29 – 5.31. Figure 5.32 plots the void space as a percentage of the unit cell volume against pressure for Forms I, II and III of acrylamide.

From Figures 5.27 – 5.29, it can be seen that as Form I compresses, the void spaces in each axis are reduced relatively evenly. In contrast, the void spaces Form II's *a*-axis compress much more quickly than those in its *c*-axis. Similarly, the voids in Form III's *c*-axis are reduced much more quickly than those in it's *a*-axis. This can be explained in each case by the proximity of the molecules to each other and the direction of the intermolecular bonds.

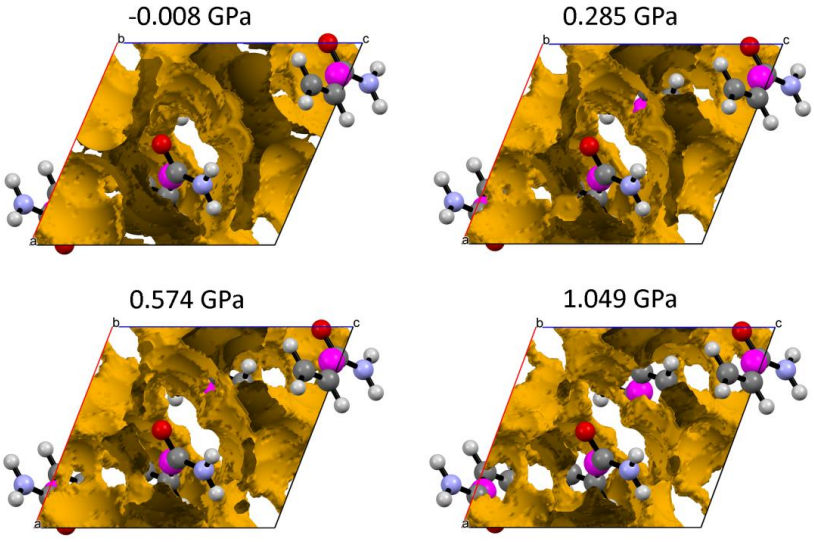

Figure 5.27 – Void space for Form I. From lowest to highest pressure, the void spaces were 31.5%, 26.4%, 24.4% and 20.3% of the unit cell.

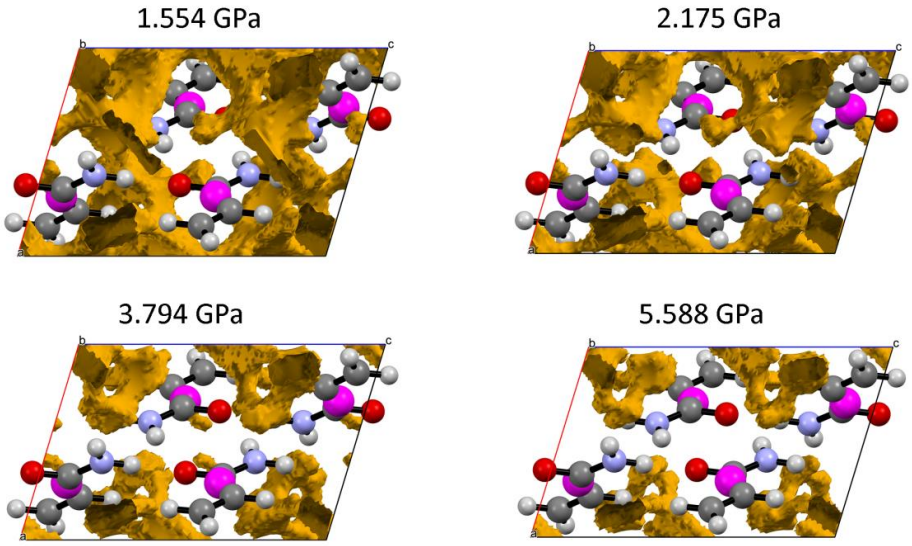

Figure 5.28 - Void space for Form II. From lowest to highest pressure, the void spaces were 15.8%, 12.7%, 7.9% and 5.4% of the unit cell.

Figure 5.29 - Void space for Form III. From lowest to highest pressure, the void spaces were 14.9%, 12.8%, 10.9%, 9.1%, 8.4%, 7.3%, 6.1%, and 5.3% of the unit cell.

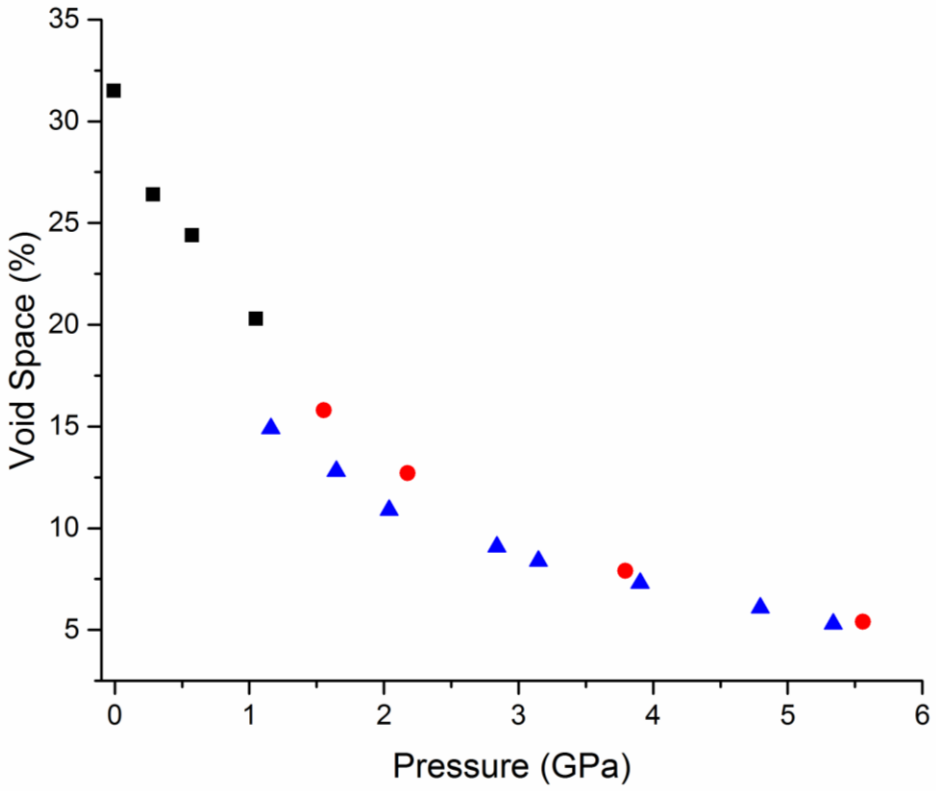

Figure 5.30 - Void space analysis of Form I (black squares), Form II (red circles) and Form III (blue triangles) of acrylamide with increasing pressure.

Figure 5.30 shows the reduction in void space as a function of pressure for each of the three polymorphs of acrylamide. It can be seen that at lower pressures, around 1 – 2 GPa, Form III has significantly lower void space than Form II, indicating its higher density. Due to the higher compressibility of Form II, this difference is much less significant by the top of the observed pressure range, with the two forms having comparable densities.

5.5 PIXEL Calculations

5.5.1 Form I

PIXEL calculations were carried out at four pressure points: -0.008(4) GPa, 0.285(6) GPa, 0.574(3) GPa and 1.049(4) GPa. The structure at 0.285 GPa had been refined from data collected during the experiment with the 4:1 (v/v) mixture of methanol and ethanol as the PTM. The other three structures were all refined from data collected using the 1:1 (v/v)

mixture of pentane and iso-pentane is the PTM. During data collection, it had been decided that due to the length of time required to collected sufficient data for a Rietveld analysis, the priority should not lie with collecting data on known phases. For this reason, limited data were collected on Form I during the experiments using the 4:1 methanol/ethanol mixture or the IPA as PTMs.

The most significant intermolecular interactions were observed at each pressure point. It was observed that the dominant interactions were the same at all four of these pressure points. The changes in the five strongest intermolecular interactions at the lowest pressure data point, -0.008(4) GPa, herein labelled Interactions 1.1 – 1.5, are summarised below.

Table 5.7 - The strongest five interactions in Form I of acrylamide, as calculated in the -0.008 GPa data set

Interaction	**Symmetry Relation**
1.1	-x,1-y,2-z
1.2	0.5+x,0.5-y,0.5+z
1.3	-x,-y,2-z
1.4	0.5-x,-0.5+y,1.5-z
1.5	1-x,-y,2-z

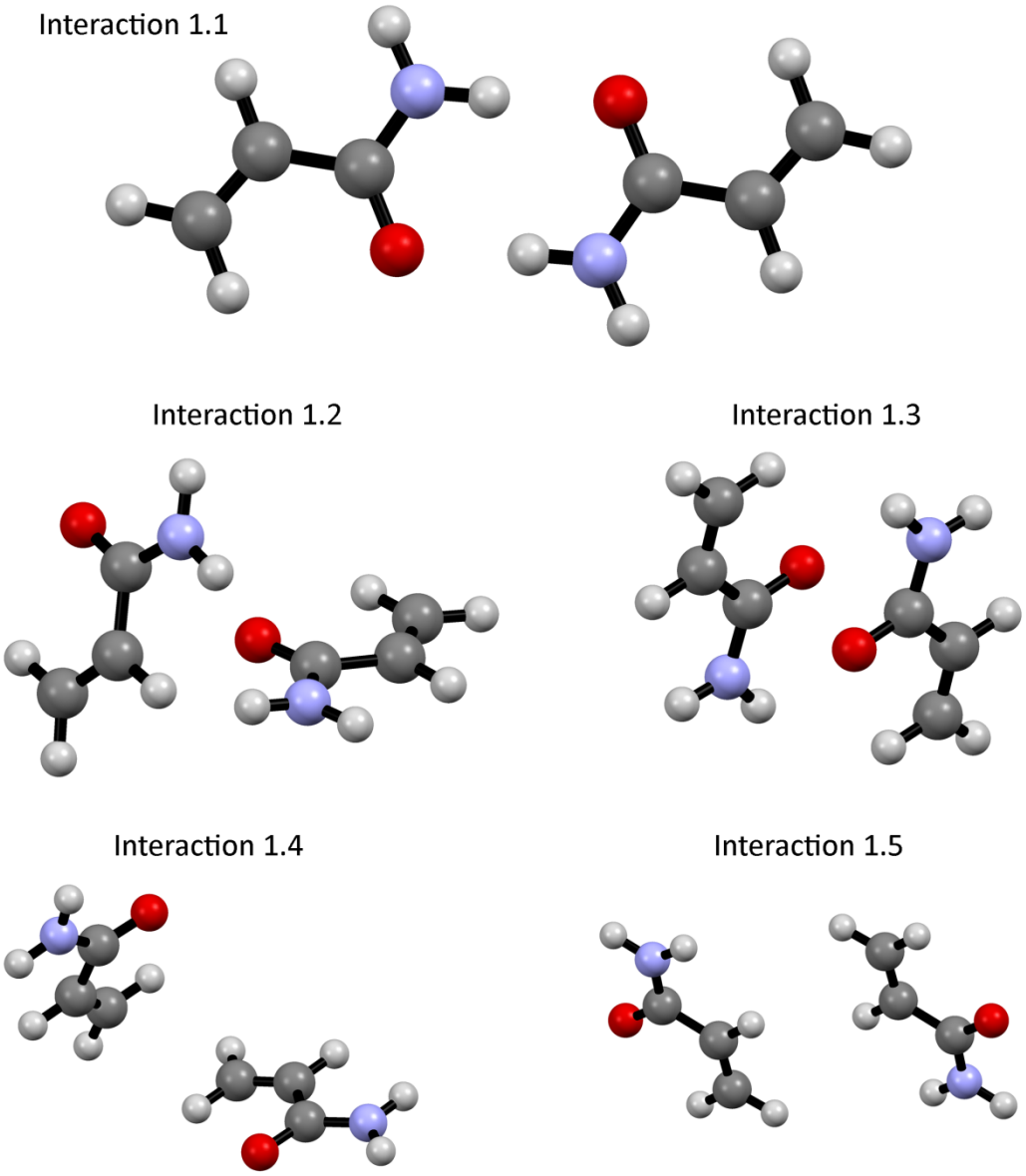

Figure 5.31 - The pairs of molecules forming Interactions 1.1 – 1.5. Interaction 1.1 is dominated by the hydrogen bonding of the amide dimer; Interaction 1.2 is dominated by the single hydrogen bonding interaction between the amide groups; Interaction 1.3 is dominated by the anti-parallel carbonyl-carbonyl interaction; Interactions 1.4 and 1.5 can be largely explained by the proximity of the carbon backbones of the neighbouring molecules.

Table 5.9 summarises the changes in Interactions 1.1 – 1.5 across the observed pressure range. In the table, C_m-C_m denotes the distance between the centres of mass of the two molecules whilst E_c, E_p, E_d and E_r are the coulombic, polarisation, dispersion and repulsion energy terms, respectively. E_{tot} represents the overall energy for the molecule-molecule interaction (i.e. the sum of the four components described above).

Table 5.8 - Changes in Interactions 1.1 - 1.5 with pressure

Pressure (GPa)	**C_m-C_m** Distance (Å)	**E_c** (kJ mol^{-1})	**E_p** (kJ mol^{-1})	**E_d** (kJ mol^{-1})	**E_r** (kJ mol^{-1})	**E_{tot}** (kJ mol^{-1})
Interaction 1.1						
-0.008	4.961	-92.4	-34.2	-20.2	87.9	-59
0.285	5.071	-78.4	-26.6	-17.8	61.6	-61.1
0.573	4.93	-95.3	-33.2	-19.6	94.6	-53.5
1.049	5.006	-82.8	-27.9	-18.4	73.2	-55.8
Interaction 1.2						
-0.008	4.98	-42.4	-15.2	-12.5	39.5	-30.6
0.285	5.005	-44.2	-16.1	-12.1	42.7	-29.7
0.573	4.978	-46.4	-17.2	-12.7	46.6	-29.7
1.049	4.993	-48	-17.9	-12.5	49	-29.3
Interaction 1.3						
-0.008	3.65	-1.6	-2	-9.8	3.4	-10
0.285	3.566	-1.4	-2.6	-11.2	5.2	-9.9
0.573	3.511	-1.7	-2.8	-12.3	6.8	-9.9
1.049	3.467	-2.4	-3	-12.9	7.7	-10.7
Interaction 1.4						
-0.008	5.498	-2.9	-0.8	-6.1	2.8	-7.1
0.285	5.361	-3.1	-1.1	-7.4	4.1	-7.5
0.573	5.33	-3.4	-1.5	-8.4	6	-7.2
1.049	5.185	-3.8	-2	-9.9	8.4	-7.3
Interaction 1.5						
-0.008	5.782	-1.1	-0.7	-7	2.4	-6.4
0.285	5.446	-2.7	-1.3	-10.3	6.3	-8
0.573	5.432	-2.7	-1.3	-9.8	5.7	-8.2
1.049	5.204	-4.5	-2.1	-12.1	9.7	-9

As can be seen from the Table 5.9, Interaction 1.1 becomes slightly weaker as pressure increases to 1.049 GPa, counteracting the marginal increase in the attractive forces in Interactions 1.2, 1.3, 1.4 and 1.5 over this pressure range. The combined energies of these five interactions at -0.008 GPa is -113.1 kJ mol^{-1}, compared to -112.1 kJ mol^{-1} at the top pressure of 1.049 GPa.

The most interesting behaviour is observed in Interactions 1.1 and 1.5. The E_{tot} value for Interaction 1.1, dominated by the amide dimer interaction, remains relatively steady as pressure is increased, destabilising only slightly. As the amide groups approach each other, the coulombic energy contribution increases slightly as the hydrogen bonding strengthens, with a larger opposite effect observed on the repulsion term due to the proximity of the electron density between the two molecules, weakening the overall stabilising contribution of this interaction at 0.573 GPa when compared to -0.008 GPa. A further increase in the pressure, to 1.049 GPa shows that the molecules have in fact been pushed further apart, resulting in a decrease in the contribution of the repulsion term and a net increase in the strength of this interaction.

The most significant change in Interaction 1.5, Figure 5.32, is in the repulsion component. This can be explained by the proximity of the carbons in the neighbouring molecules. As the molecules (and their respective electron density clouds) are forced closer together at higher pressures, the repulsion energy contribution increases.

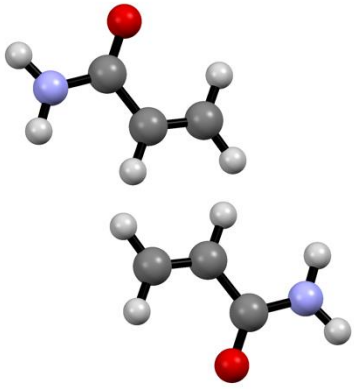

Figure 5.32 – The molecules involved in Interaction 1.5.

At the other end of the scale, those intermolecular interactions found to have overall repulsive energies become marginally more repulsive towards the upper end of this pressure range. At the lowest pressure, -0.008 GPa, the strongest repulsive interactions have E_{tot} values of +2.9 kJ mol^{-1}, with this increasing to +3.1 kJ mol^{-1} at the highest pressure data set of 1.049 GPa.

5.5.2 Form II

PIXEL calculations were carried out at four pressure points: 1.554(4) GPa, 2.175(4) GPa, 3.794(6) GPa and 5.588(8) GPa. Data were also collected, and the structure subsequently solved, at 1.722(4) GPa during the decompression phase of the experiment, but PIXEL analysis has not been included here since a single pressure point upon decompression would provide limited insight into the patterns observed. All structures were refined from data collected during the experiment using the 1:1 (v/v) mixture of pentane and isopentane as the PTM. The most significant intermolecular interactions at each pressure point were observed. As with Form I, the dominant intermolecular reactions observed at the lowest pressure data set (1.554 GPa, in this case) remained dominant across the pressure range studied. The changes in the five strongest interactions at 1.554 GPa, herein labelled Interactions 2.1 – 2.5, are summarised below.

Table 5.9 - The five strongest intermolecular interactions, as calculated at 1.554 GPa

Interaction	**Symmetry Relation**
2.1	1-x,1-y,1-z
2.2	x,1.5-y,-0.5+z
2.3	1-x,2-y,1-z
2.4	-x,2-y,1-z
2.5	-x,0.5+y,0.5-z

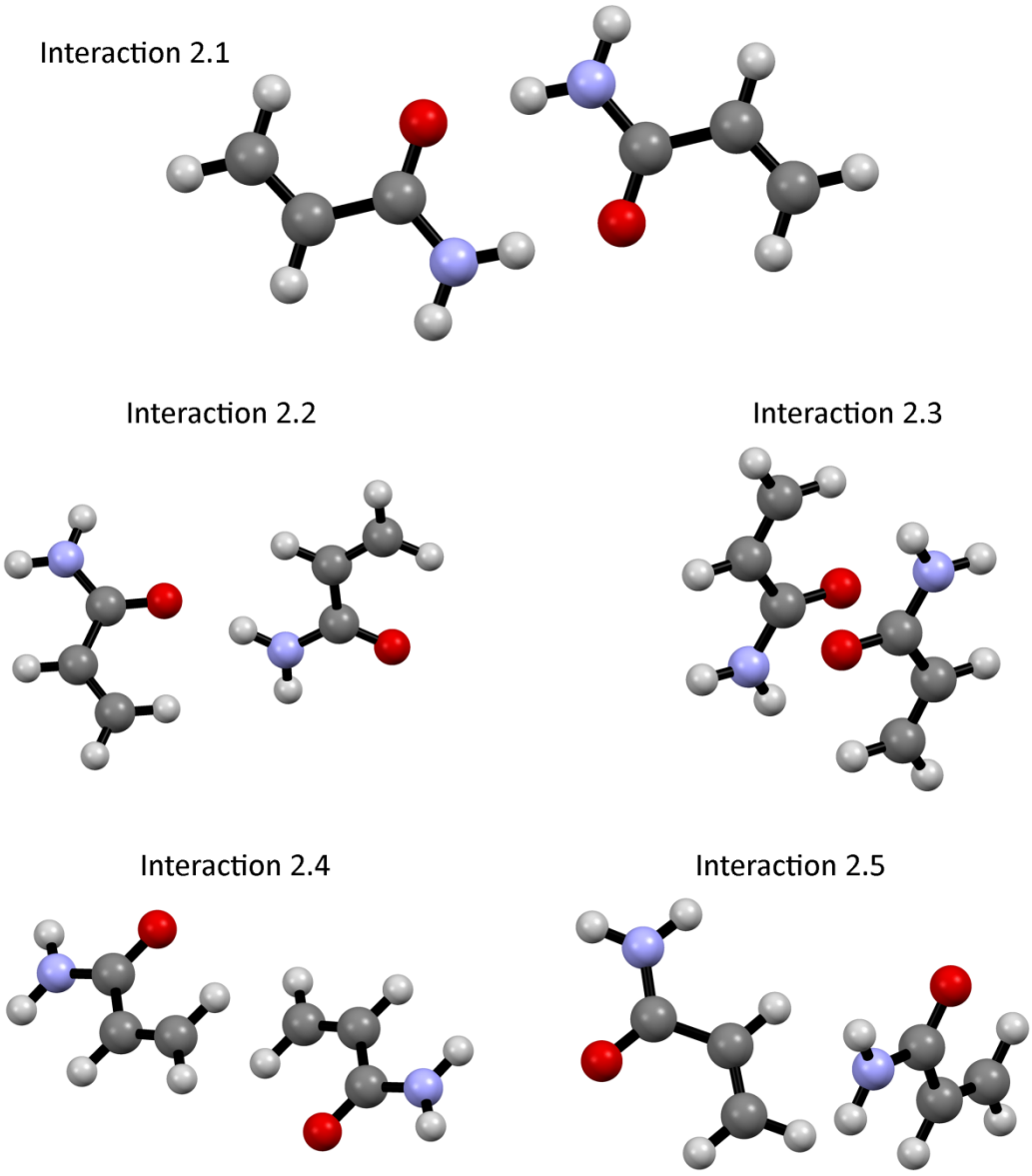

Figure 5.33 - The pairs of molecules forming Interaction 2.1 – 2.5. Interactions 2.1, 2.2 and 2.3 are comparable to Interaction 1.1, 1.2 and 1.3, respectively, in terms of their dominant contributing features. Interactions 2.4 and 2.5 are comparable to Interactions 1.5 and 1.4, respectively.

Table 5.10 - Changes in Interactions 2.1 – 2.5 with pressure

Pressure (GPa)	**C_m-C_m Distance** (Å)	**E_c** (kJ mol^{-1})	**E_p** (kJ mol^{-1})	**E_d** (kJ mol^{-1})	**E_r** (kJ mol^{-1})	**E_{tot}** (kJ mol^{-1})
Interaction 2.1						
1.554	4.928	-86.2	-31	-19.8	83.2	-53.8
2.175	4.813	-103.5	-41.1	-21.6	117.2	-49
3.794	4.644	-100.8	-44.6	-22.6	136.9	-31.1
5.588	4.517	-111.2	-53	-24.9	175.5	-13.6
Interaction 2.2						
1.554	5.037	-47.7	-18	-12.8	49.4	-29.1
2.175	5.016	-48.5	-18.5	-13.2	51.1	-29.1
3.794	4.972	-49.3	-18.8	-14.2	52	-30.3
5.588	4.939	-52.6	-21.2	-15.2	58.5	-30.4
Interaction 2.3						
1.554	3.255	-6.9	-4.6	-17.8	18.8	-10.5
2.175	3.197	-8.2	-5.4	-19.9	25.6	-7.9
3.794	3.174	-8.9	-6	-21.5	32.5	-3.9
5.588	3.11	-13.1	-8.5	-24.8	48.6	2.2
Interaction 2.4						
1.554	4.888	-8.7	-4	-14.1	16.9	-10
2.175	4.884	-10.1	-4.6	-15.2	20.4	-9.5
3.794	4.88	-13.8	-6.5	-17.7	30.5	-7.5
5.588	4.885	-16	-8	-18.8	36.1	-6.6
Interaction 2.5						
1.554	5.074	-4.6	-1.9	-9.9	7.8	-8.7
2.175	4.999	-5	-2.2	-10.7	9.2	-8.8
3.794	4.811	-5.8	-2.6	-12.2	11.4	-9.2
5.588	4.711	-6.9	-3.5	-14.1	15.5	-8.9

From Table 5.11, it is seen that Interaction 2.1 rapidly destabilises as pressure increases, with its total stabilising energy contribution dropping from -53.8 kJ mol^{-1} at 1.554 GPa to -13.6 kJ mol^{-1} at 5.588 GPa. Interactions 2.2 and 2.5 becomes marginally more stabilising over the

pressure range observed. Over the course of the pressure range, the overall contribution of Interaction 2.3 shifts from a stabilising contribution of -10.5 kJ mol^{-1} to a destabilising contribution of +2.2 kJ mol^{-1}, while Interaction 2.4 also becomes weaker as pressure increases (but remains a stabilising interaction at the highest pressure of 5.588 GPa).

There is nothing remarkable about the repulsive molecule-molecule interactions seen in Form II, with the strongest such force contributing +3.6 kJ mol^{-1} at the highest pressure of 5.588 GPa.

5.5.3 Form III

PIXEL calculations were carried out on structures refined at eight pressure points: 1.159(6) GPa, 1.645(6) GPa, 2.093(8) GPa, 2.839(7) GPa, 3.148(7) GPa, 3.903(8) GPa, 4.797(8) GPa and 5.338(8) GPa. All structures were refined from data collected during the experiment using IPA as the PTM. The most significant intermolecular interactions observed at the lowest pressure data set (1.159 GPa), were traced with increasing pressure to observe changes in the forces acting upon the molecules in the crystal lattice. The five strongest interaction, herein labelled Interactions 3.1 – 3.5, are summarised below.

Table 5.11 - The five strongest interactions, as calculated at 1.159 GPa

Interaction	**Symmetry Relation**
3.1	1-x,1-y,1-z
3.2	0.5+x,0.5+y,z
3.3	1-x,-y,1-z
3.4	1.5-x,-0.5+y,0.5-z
3.5	1.5-x,0.5-y,1-z

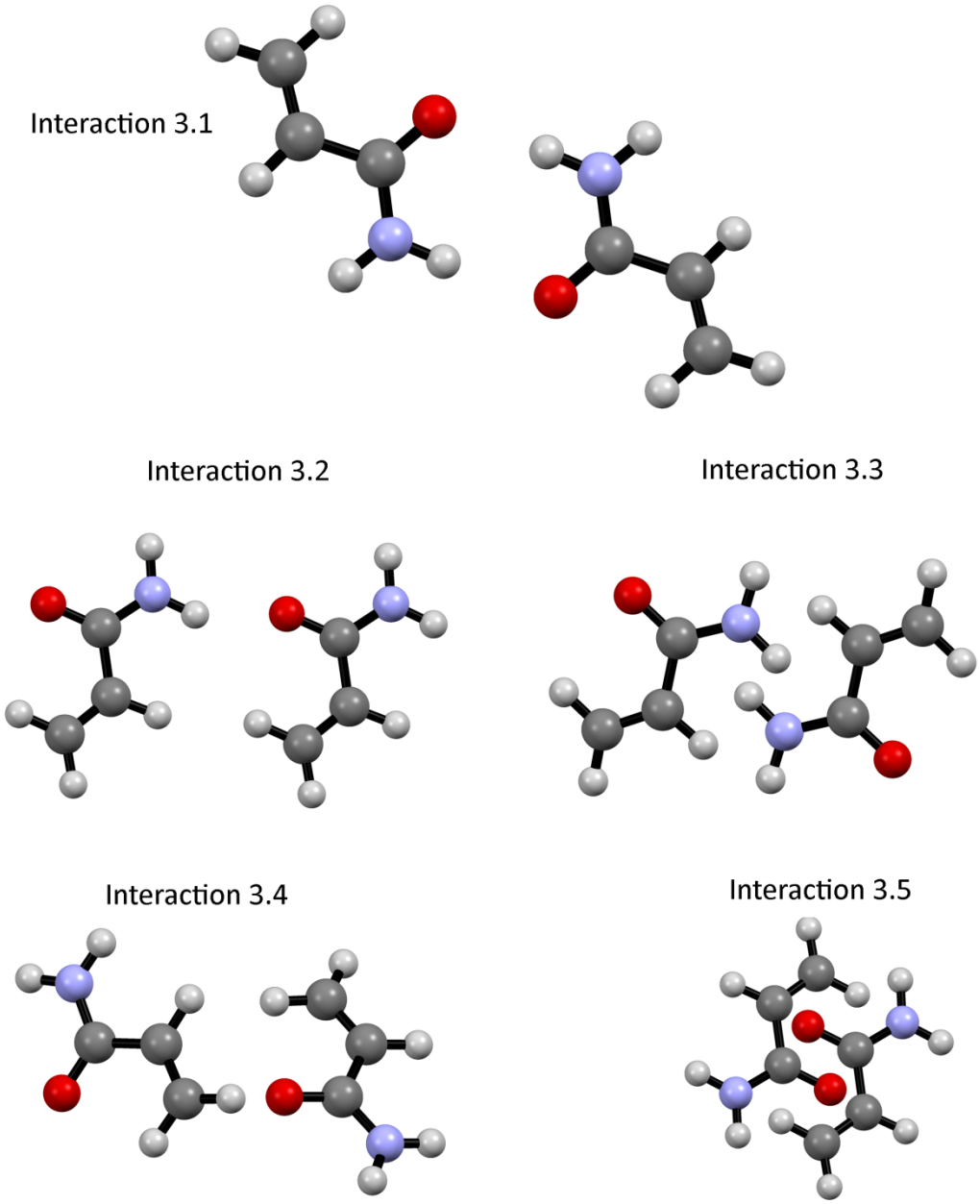

Figure 5.34 - The pairs of molecules forming Interactions 3.1 – 3.5. Interaction 3.1 is comparable to Interactions 1.1 and 2.1, whilst Interaction 3.2 is comparable to Interactions 1.2 and 2.2. Interaction 3.3 is dominated by hydrogen bonding between the N-H components of the two amide groups, as opposed to the carbonyl-carbonyl interaction seen in Interactions 1.3 and 2.3. Interaction 3.4 is largely attributable to the proximity of the carbon atoms but is not comparable to any interactions studied in Forms I or II. Interaction 3.5 is comparable to Interactions 1.3 and 2.3, being dominated by the anti-parallel carbonyl-carbonyl interaction.

Table 5.12 - Changes in Interactions 3.1 – 3.5 with pressure

Pressure (GPa)	**C_m-C_m Distance** (Å)	**E_c** (kJ mol-1)	**E_p** (kJ mol-1)	**E_d** (kJ mol-1)	**E_r** (kJ mol-1)	**E_{tot}** (kJ mol-1)
Interaction 3.1						
1.159	5.163	-60.7	-16.5	-13.6	32.7	-58.1
1.645	5.182	-59	-15.4	-12.9	28.8	-58.5
2.093	5.102	-69.7	-20.7	-15.5	46	-60
2.839	4.988	-86.1	-28.4	-18.3	75.3	-57.6
3.148	4.927	-97.8	-35.2	-19.9	93.9	-59.1
3.903	4.922	-98.5	-35.7	-20.3	98.4	-56.1
4.797	4.926	-97.3	-35.4	-20.2	96.5	-56.3
5.338	4.913	-100.4	-37.8	-20.6	102	-56.8
Interaction 3.2						
1.159	5.073	-36.5	-13.1	-13.8	32.4	-30.9
1.645	5.046	-37.9	-14.2	-14.6	35.9	-30.7
2.093	5.025	-39.3	-15	-14.7	38.5	-30.5
2.839	4.994	-38.2	-14.6	-15.3	40	-28
3.148	4.982	-41.3	-15.5	-15.5	44.5	-27.8
3.903	4.957	-45.4	-17.7	-16.4	53.3	-26.3
4.797	4.93	-47.6	-18.9	-17.1	60.2	-23.4
5.338	4.917	-48.7	-19.9	-17.7	62.8	-23.5
Interaction 3.3						
1.159	4.977	-6.6	-2.8	-12.1	7.5	-14.1
1.645	4.961	-6.3	-3.3	-12.7	7.8	-14.5
2.093	4.995	-4.2	-2.7	-11.8	6.4	-12.3
2.839	4.966	-4.2	-3.1	-12.9	7.4	-12.7
3.148	4.893	-4	-3.5	-14.3	9.1	-12.8
3.903	4.862	-5.8	-3.1	-13.7	9.2	-13.4
4.797	4.854	-7	-2.9	-13.8	9.8	-13.8
5.338	4.86	-7.5	-3	-14.4	10.8	-14
Interaction 3.4						
1.159	5.545	-4.9	-3.3	-13.6	13.9	-7.9

1.645	5.462	-6.2	-4.1	-14.9	18.1	-7.2
2.093	5.426	-7.9	-5.1	-16.2	22.4	-6.8
2.839	5.415	-8.8	-5.8	-17.2	26	-5.8
3.148	5.456	-8.3	-5.6	-16.8	24.4	-6.3
3.903	5.42	-8.3	-5.7	-17.8	25.7	-6.2
4.797	5.355	-12	-7.5	-19.9	34.7	-4.7
5.338	5.323	-13.2	-8.1	-20.2	38.1	-3.4
Interaction 3.5						
1.159	3.186	-18.2	-9.4	-22.1	43.9	-5.9
1.645	3.194	-18.9	-9.5	-21.9	42.7	-7.7
2.093	3.169	-17.6	-9.2	-22.6	39.7	-9.7
2.839	3.145	-17.6	-8.6	-22.1	38.6	-9.7
3.148	3.068	-24.1	-11.7	-25.2	54.3	-6.7
3.903	2.958	-37.3	-16.6	-30.4	97.6	13.4
4.797	2.962	-35.3	-16	-30.2	95.2	13.6
5.338	2.981	-29.1	-14.4	-29.1	77.8	5.2

Interaction 3.1 is comparable to Interaction 2.1 in that it is dominated by the hydrogen bonding of the amide dimer. However, unlike the observations of Interaction 2.1, Interaction 3.1 does not rapidly destabilise as pressure is increased. This is accounted for by two factors: the stabilising impact of the E_c term increases by more in Interaction 3.1 than in Interaction 2.1; and the destabilising impact of the E_r term increases by less in Interaction 3.1 than in Interaction 2.1. Interaction 3.5, dominated by the antiparallel carbonyl-carbonyl dimer interaction, destabilises over the observed pressure range (as had been seen in the related Interaction 2.3).

The changes observed in Interactions 3.1, 3.2, 3.3 and 3.4 with increasing pressure are not of any particular interest. However, Interaction 3.5 (which has a total stabilising energy contribution of -5.9 kJ mol^{-1} at the lowest pressure point of 1.159 GPa) changes significantly over the pressure range observed. Between 1.159 GPa and 2.839 GPa, the total stabilising energy contribution of Interaction 3.5 increases by approximately 50%, to -9.7 kJ mol^{-1}, before it rapidly destabilises. The PIXEL calculations at 3.903 GPa and 4.797 GPa reveal this intermolecular interaction to be the single most destabilising interaction acting upon the

molecules of the crystal lattice (with E_{tot} values of +13.4 kJ mol^{-1} and +13.6 kJ mol^{-1}, respectively), before stabilising slightly to an overall destabilising contribution of +5.2 kJ mol^{-1} at the highest pressure point of 5.338 GPa. Although this looks unusual, it has been verified that each step of the PIXEL process was carried out correctly, and that there has been no human error leading to this observation. It must be noted that although PIXEL calculations are not intended for working with high pressure systems, they have been used in multiple high pressure studies apparently without any such issues as described in Section 2.7 of this thesis.

Breaking this interaction down into its component parts, the most significant difference is in the repulsion term. The repulsion term is most important at short separation difference, reflected in the C_m-C_m distances of interaction 3.5. Compared to Interactions 3.1 – 3.4, and indeed most of the interactions studied in Forms I and II, the distance between the centres of mass of the molecules is notably smaller. As this distance drops below 3 Å (at 3.903 GPa), the repulsion term of the molecule-molecule interaction rises dramatically as the carbon backbones are forced together. The increase in the coulombic component can be accounted for by the proximity of the carbonyl groups, as seen in Figure 5.35.

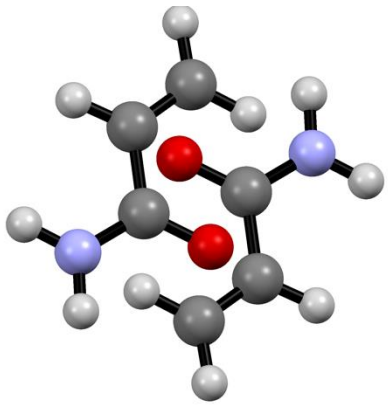

Figure 5.35 - The alignment of the carbon backbones and the carbonyl groups of the two molecules forming Interaction 3.5.

Figures 5.36 and 5.37 show the changes in total energy, repulsion energy and coulombic energy contributions with pressure towards the molecule-molecule interactions dominated by the amide dimer interaction and the carbonyl-carbonyl interaction, respectively, of each of the three forms.

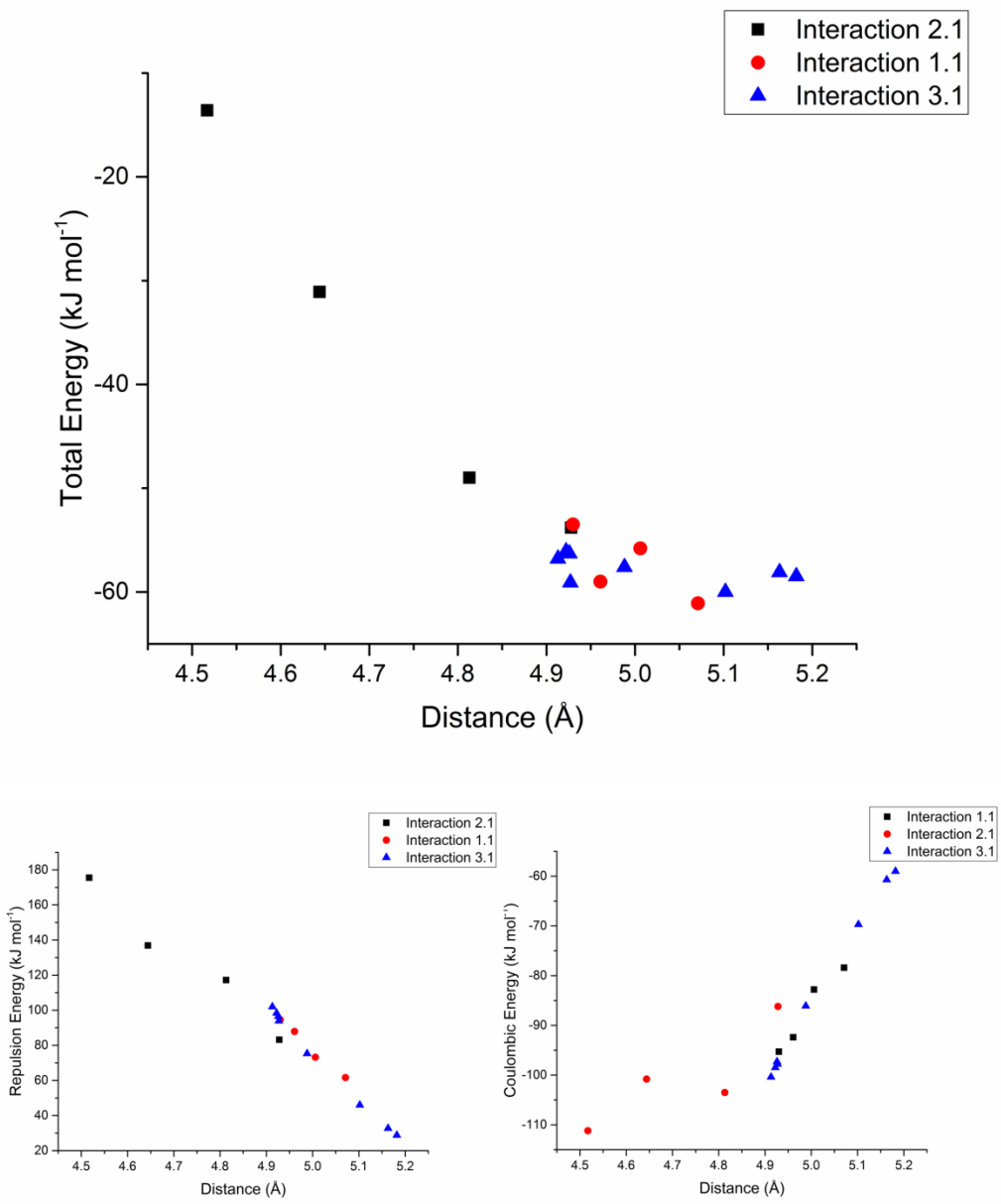

Figure 5.36 - The variation in the amide dimer interactions seen in Forms I, II and III.

It can be seen from Figure 5.36 that the amide dimer interaction in Form II is much less stabilising than in Form III as pressure is increased (and C_m-C_m distance decreased). The molecules involved in this interaction in Form II are much closer together than in Form III, resulting in a significantly higher repulsion term.

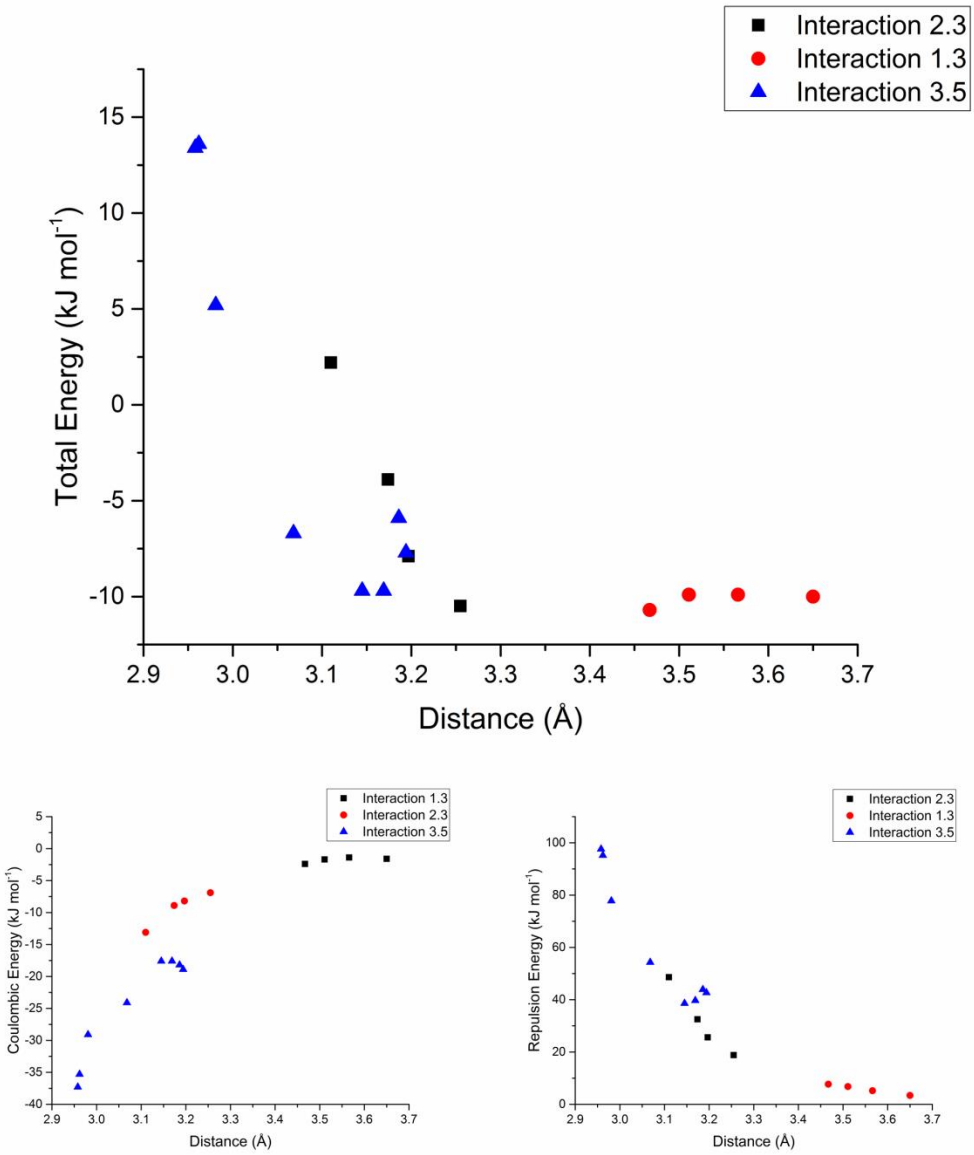

Figure 5.37 - Changes in the carbonyl-carbonyl interaction observed in Forms I, II and III.

It can be seen that the carbonyl-carbonyl interaction of Form III becomes destabilising as the sample is subject to high pressure. This is also the case for Form II, although to a lesser extent since the molecules are further apart and so the repulsion term is not as dominant.

5.6 Conclusions

In this chapter, it has been demonstrated that acrylamide undergoes three different phase transitions under high pressure, depending upon the environment the sample is in. Two of the three high pressure phases (Forms II and III) have been structurally solved, with their unit cell parameters studied as a function of pressure. It is proposed that the degree to which acrylamide can solubilise in the PTM is a fundamental factor in determining which high pressure form is obtained. It is suggested that Form III, the high pressure form obtained via compression in a 4:1 (v/v) methanol:ethanol mixture, is the more stable of the two high pressure forms successfully solved and that the solubility of the sample in alcohols permits the sample to overcome the energy barrier required to cross the phase transition. When compressed in an environment in which it is insoluble, a 1:1 (v/v) pentane:iso-pentane mixture, the sample cannot overcome the energy barrier to permit transition to Form III, and so an alternate transition to Form II is observed.

Attempts to solve the structure of Form IV have so far been unsuccessful; further work is required.

5.7 References

Gavezzotti, A. (2003). Calculation of Intermolecular Interaction Energies by Direct Numerical Integration over Electron Densities. 2. An Improved Polarization Model and the Evaluation of Dispersion and Repulsion Energies. *Journal of Physical Chemistry B*, *107*(10), 2344–2353. http://doi.org/Doi 10.1021/Jp022288f

Oswald, I. D. H., & Urquhart, A. J. (2011). Polymorphism and polymerisation of acrylic and methacrylic acid at high pressure. *CrystEngComm*, *13*(14), 4503. http://doi.org/10.1039/c1ce05295k

Yang, Q., Song, C., Chen, Q., Zhang, P., & Wang, P. (2008). Synthesis and aqueous solution properties of hydrophobically modified anionic acrylamide copolymers. *Journal of Polymer Science Part B: Polymer Physics*, *46*(22), 2465–2474. http://doi.org/10.1002/polb.21577

Zhou, Q.-L., Zhang, Z.-H., Jing, Z.-L., IUCr, M., K. B., M., M., … E., K. P. (2007). Acrylamide. *Acta Crystallographica Section E Structure Reports Online*, *63*(6), o3039–o3039. http://doi.org/10.1107/S1600536807024816

Chapter 6 – Pressure-induced polymorphism of caprolactam: a neutron diffraction study

6.1 Introduction

Caprolactam, $C_6H_{11}NO$, is the cyclic amide precursor to Nylon-6. A solid at room temperature, it comes in the form of white powder or opaque pellets. Nylon-6, typically synthesised via ring-opening of caprolactam in an inert nitrogen environment at temperatures in excess of 500 K, finds applications ranging from toothbrush bristles and sutures to strings for musical instruments and clothing. Having previously studied acrylamide, as well as another ring structure (the cyclic di-ester glycolide) under high pressure, it was decided that the study of a cyclic amide would be an appropriate next step. Since the typical polymerisation route for caprolactam required temperatures in excess of 500K and an inert atmosphere, it was suggested that if solid state polymerisation were to be achieved through the application of pressure that this may represent not only a greener synthesis route but also a significantly more cost-effective way of manufacturing Nylon-6.

Previous research on caprolactam has shown it to crystallise in space group *C*2/*c*, with the unit cell parameters given in Table 6.1 (Winkler, Dunitz, & IUCr, 1975).

Table 6.1 - Unit cell parameters of caprolactam.

Unit Cell Parameter	**Value**
a (Å)	19.28(2)
b (Å)	7.780(10)
c (Å)	9.570(10)
α (°)	90.00
β (°)	112.39(10)
γ (°)	90.00
Unit Cell Volume (Å^3)	1327.267
Space Group	*C*2/*c*
Z	8
Z’	1
R-factor (%)	4.8

Winkler and Dunitz (1975) reported the crystal structure of caprolactam under ambient conditions. This crystal structure is shown in Figure 6.1, below. The dominant feature of the packing arrangement is an amide dimer interaction between two of the adjacent caprolactam molecules. The distance between the nitrogen atom of one molecule and the oxygen atom of its neighbour is 2.895 Å, with the N-H--O angle measuring 172.23°.

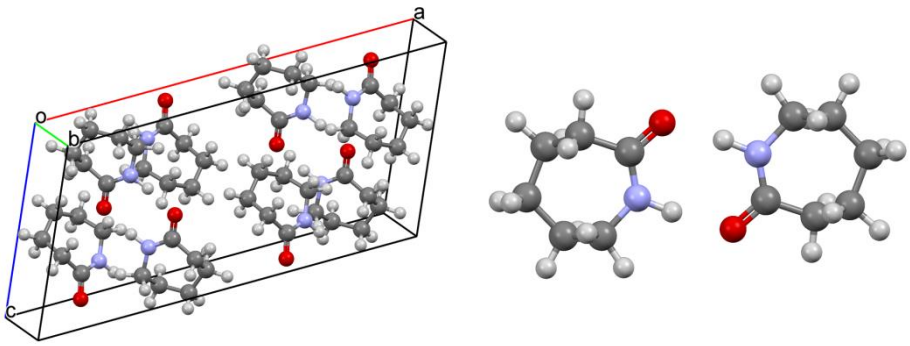

Figure 6.1 - The unit cell of caprolactam (left) and two of the molecules within the unit cell forming an amide dimer interaction (right).

6.2 Experimental

6.2.1 Lab-based experiments

A solvent screen was set up in which caprolactam (Sigma-Aldrich UK) was recrystallised via slow solvent evaporation from acetone, acetonitrile, ethyl acetate, ethanol, methanol, and 1-butanol. The crystals obtained were screened using Raman spectroscopy and those suitable for SXRD analysis were also analysed using this technique. All Raman spectra showed the same pattern, indicating that no novel polymorphs had been obtained by recrystallization from the different solvents. The only samples which produced crystals of sufficient quality for analysis via SXRD were the samples recrystallised from ethyl acetate and 1-butanol. Analysis of crystals obtained from each of these recrystallised samples showed the crystals to match the known form of caprolactam (Table 6.1).

A crystal of caprolactam, produced via slow solvent evaporation of ethyl acetate, was loaded into a DAC following the normal procedures. SXRD and Raman data were taken at pressures of 0.64 GPa and 1.26 GPa. SXRD data obtained at both pressure points showed the sample to be in the known crystal form, herein designated Form I. A third data collection, at 2.2 GPa showed that the sample quickly lost its crystallinity and that the intense spots associated with single crystal diffraction were no longer present.

Ambient pressure analysis of a crystal obtained via slow evaporation of 1-butanol showed the crystal structure to again match that of the known phase. This crystal was then loaded into a DAC and analysed at 1.20 GPa, with the data obtained showing a phase transition had occurred. Data collected at 1.70 GPa showed this second polymorph to still be present.

Based on the curious results observed from the experiments conducted at the home laboratory, which suggested differences in high pressure behaviour between two crystals of caprolactam from two different solvents, a proposal was submitted to conduct further experiments on the system on the PEARL beamline at ISIS neutron spallation source.

6.2.2 Neutron diffraction experiments

Caprolactam was recrystallised via slow solvent evaporation of ethyl acetate and ethanol. Deuterated ethanol was used due to the unavailability of 1-butanol in its deuterated form. Since there is no labile proton which could exchange with the sample, hydrogenous ethyl acetate was used. Samples were gently ground and loaded into a Paris-Edinburgh press as in chapter 4 using a lead pellet as the pressure marker and drops of a 1:1 (v/v) mixture of pentane and iso-pentane as a PTM. The cell was loaded into the PEARL beamline, with neutron diffraction data being as the load was incrementally increased up to maximum pressures of 3.25 GPa and 5.69 GPa for the samples recrystallised from ethyl acetate and ethanol, respectively. Data were also collected upon decompression in each case. The disparity in maximum

pressure was a result of the limited time and pressure step size. Figure 1.2 shows the response of pressure to the increasing mechanical load in both loadings. The filled shapes show the points at which extended data sets were collected with a view to permitting Rietveld refinement of the data, with the data collected at the points illustrated by hollow shapes intended to be Pawley-fitted. In both cases, the response of pressure to the applied load is relatively linear. The load was increased in increments of 2-3 tonnes during the first experiment (with the sample recrystallised from ethyl acetate). The maximum load (39 tonnes) was achieved after approximately 48 hours, before decompression to ambient conditions over approximately 4 hours. After the second loading (with the sample recrystallised from ethanol), the load was increased in increments of 5 tonnes. The maximum load (60 tonnes) was achieved after approximately 28 hours before subsequent decompression to ambient conditions over the course of approximately 2 hours.

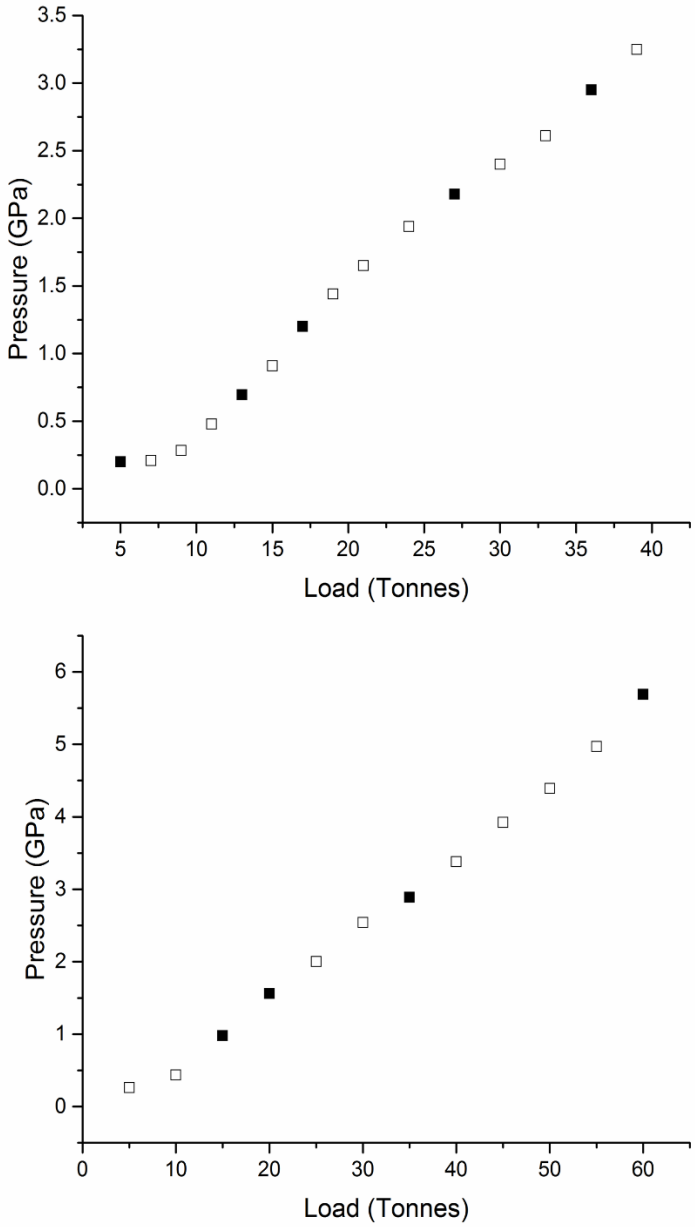

Figure 6.2 - The response of pressure to the applied load in the neutron diffraction experiments. Top: loading 1, in which the caprolactam sample had been obtained through recrystallisation from ethyl acetate. Bottom: loading 2, in which the caprolactam sample had been obtained through recrystallization from ethanol.

6.3 Results and Discussion

6.3.1 DAC Experiments

SXRD data of caprolactam were collected in two separate DAC experiments. It was observed that the data collected on a crystal of caprolactam, recrystallised from ethyl acetate, at 1.26 GPa showed the sample to still be in the known polymorph, herein designated Form I. Interestingly, SXRD data collected on a single crystal of caprolactam, recrystallised from 1-butanol, at 1.20 GPa showed the sample to have undergone a phase transition. The structure of the new phase, herein designated Form II, was successfully solved. The unit cells of each of the Forms are shown in Figure 6.3, with the unit cell parameters of both Forms shown in Table 6.2. Form III will be discussed in detail in section 6.3.2.

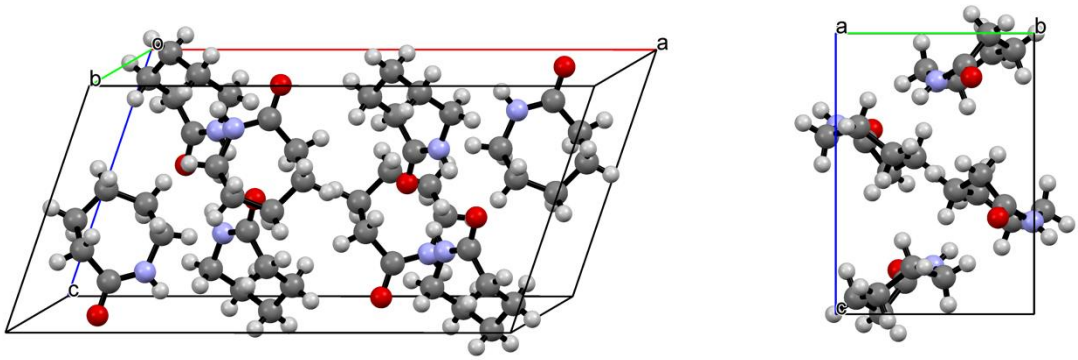

Figure 6.3 - The unit cells of Form I (left) and Form II (right) of caprolactam.

There are no significant differences in molecular conformation between Forms I and II, with the molecules in both polymorphs adopting a chair conformation as shown in Figure 6.4.

Table 6.2 - Crystallographic table of Forms I and II

	Form I	Form II
Crystal data		
Chemical formula	$C_6H_{11}NO$	$C_6H_{11}NO$
M_r	113.16	113.16
Crystal system, space group	Monoclinic, *C*2/*c*	Monoclinic, $P2_1/c$
Temperature (K)	293	293
a, *b*, *c* (Å)	18.3051 (16), 7.4100 (3), 9.3418 (4)	8.4819 (8), 6.8714 (10), 9.7503 (10)
β (°)	111.926 (4)	94.204 (8)
V (Å^3)	1175.47 (13)	566.74 (11)
Z	8	4
Radiation type	Mo *K*α	Mo *K*α
μ (mm^{-1})	0.09	0.09
Crystal size (mm)	0.10 × 0.10 × 0.05	0.20 × 0.10 × 0.05
Data collection		
Diffractometer	Bruker Kappa Apex2	Bruker Kappa Apex2
Absorption correction	Multi-scan *SADABS* (Siemens, 1996)	Multi-scan *SADABS* (Siemens, 1996)
T_{min}, T_{max}	0.93, 1.00	0.87, 1.00
No. of measured, independent and observed [$I > 2.0\sigma(I)$] reflections	2703, 458, 404	2645, 481, 347
R_{int}	0.025	0.052
θ_{max} (°)	23.3	23.3
$(\sin\theta/\lambda)_{max}$ (Å^{-1})	0.555	0.556
Refinement		
$R[F^2 > 2\sigma(F^2)]$, $wR(F^2)$, *S*	0.029, 0.069, 1.00	0.044, 0.124, 0.68
No. of reflections	455	471
No. of parameters	73	73
No. of restraints	65	65
H-atom treatment	H-atom parameters constrained	H-atom parameters not refined
$\Delta\rangle_{max}$, $\Delta\rangle_{min}$ (e Å^{-3})	0.08, -0.09	0.21, -0.19

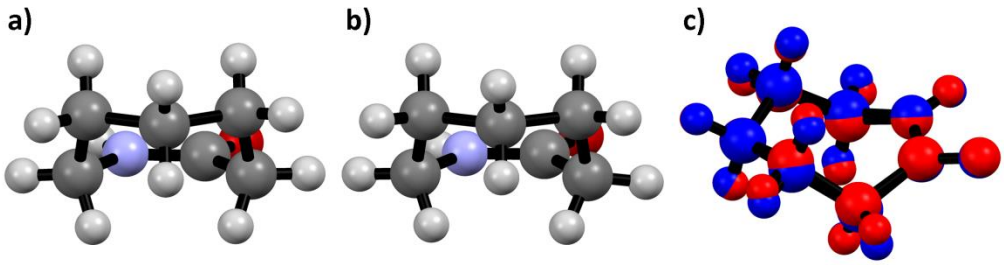

Figure 6.4 – The chair conformation adopted by the molecules in a) Form I and b) Form II. The overlapped molecular conformations, c), of Form I (red) and Form II (blue) show no significant differences.

Whilst there is no significant difference between Forms I and II in terms of the molecular conformation, the packing arrangement does vary markedly. The amide dimer arrangement, a prominent feature of Form I, is absent in Form II. Instead, Form II consists of catemeric chains of the amide group, similar to those of carbamazepine form V (Arlin et al., 2011). Figure 6.5 shows this anti-parallel arrangement of the amide functional groups in neighbouring molecules in Form I, next to the arrangement seen in Form II, where N-H portion of the amide group forms a H-bond with the C=O portion of one neighbouring molecule, while the C=O portion of the amide group forms another H-bond with the N-H portion of a second neighbouring molecule.

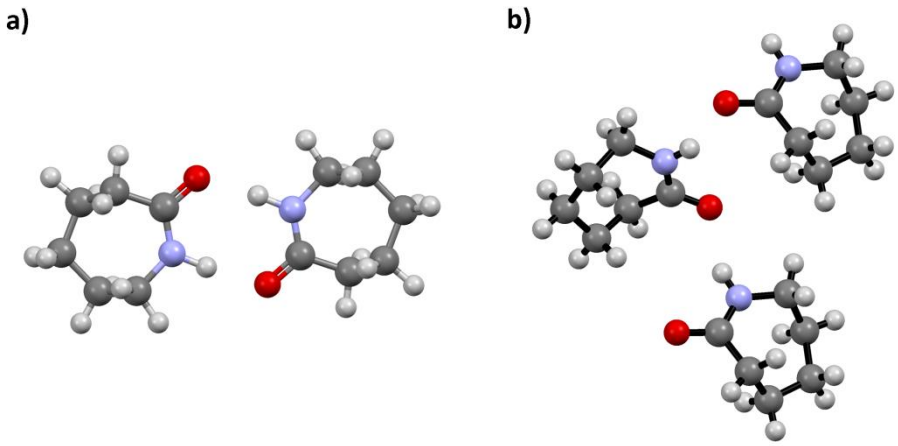

Figure 6.5 - The amide dimer interaction in Form I (a), and the arrangement of the amide groups in neighbouring molecules of Form II (b).

6.3.2 Neutron diffraction studies

A high pressure phase transition was observed in each of the two loadings. In the first loading (with the sample recrystallised from ethyl acetate), the diffraction pattern did not match the high pressure phase previously observed in the DAC experiment (Form II). The high pressure diffraction pattern observed in the second loading (with the sample recrystallised from ethanol) matched the simulated diffraction pattern of the previously observed Form II. The diffraction patterns of the three polymorphs are shown in Figure 6.6.

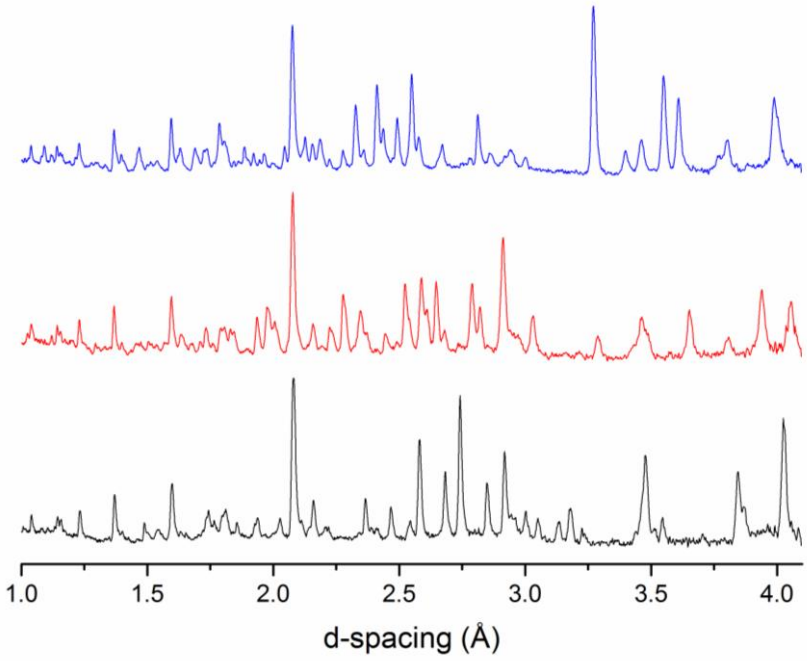

Figure 6.6 - The diffraction patterns of Form I (black; collected at 0.201 GPa), Form II (red; collected at 1.563 GPa) and Form III (blue; collected at 2.18 GPa).

6.2.3.1 Loading 1 – Neutron diffraction study of caprolactam recrystallised from ethyl acetate

In the previous work carried out on the lab diffractometer with a sample of caprolactam recrystallised from ethyl acetate, there were no signs of a phase change at high pressure. This contrasts with the observations made during the neutron

diffraction study, in which the pattern was appearing to show signs of this high pressure form at 0.696(17) GPa with complete conversion by 0.91(3) GPa. This high pressure phase observed did not match Form II, previously observed when a single crystal of caprolactam (recrystallised from 1-butanol) had been compressed in the DAC. Diffraction patterns of the caprolactam sample, collected upon compression up to 2.88 GPa, are shown in Figure 6.7.

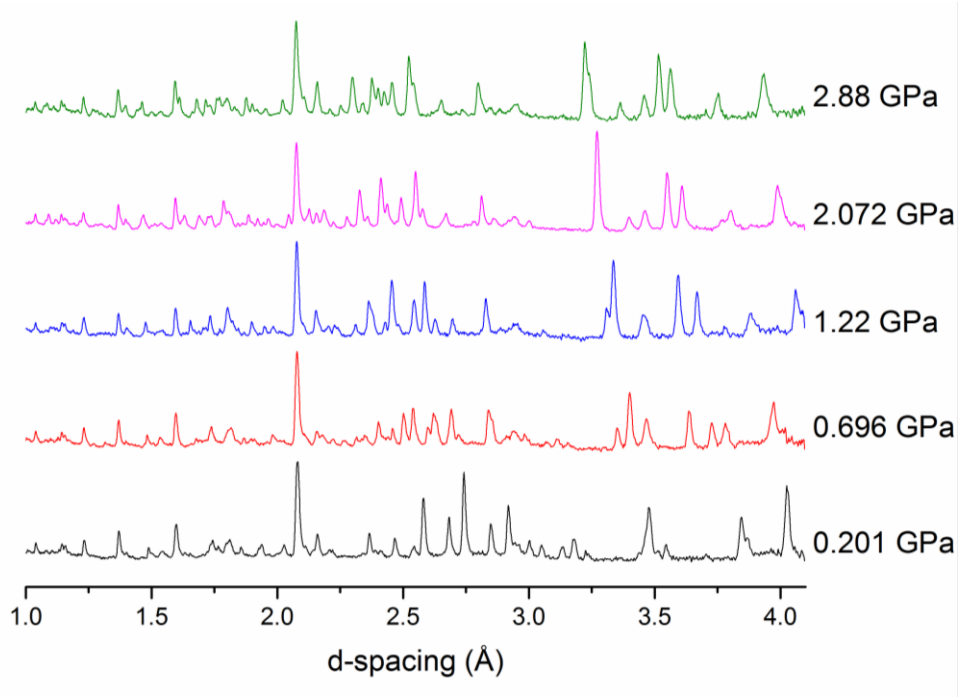

Figure 6.7 - Neutron diffraction patterns of the caprolactam sample recrystallised from ethyl acetate upon compression.

Attempts to solve the structure of the high pressure phase, herein designated as Form III, were unsuccessful during the lifetime of the PhD. However recent experiments continued within the group have been able to isolate the new phase. Due to the late discovery of this phase discussion around the phase will be limited. To observe this phase a saturated solution of caprolactam in ethyl acetate was loaded into the DAC and pressure applied to induce crystallisation. Crystallisation did not occur and so heat was applied (~150 °C or 323 K) to induce nucleation. Multiple crystals formed that were sufficient for X-ray diffraction. These were identified as Form II at a pressure of 3.45 GPa. The cell was decompressed to ~0.7 GPa (where

Form III was known) and a diffraction dataset taken; this was observed to be Form II, with the pressure measuring 0.55 GPa after data collection. Overall the cell was left at this pressure for two days having been decompressed from 3.45 GPa. During this period, a single crystal of Form III grew (Figure 6.8) and was identified. The unit cell parameters from this structure solution were used to perform Pawley fits of the neutron diffraction data, with the results summarised in Table 6.3 and plotted in Figure 6.9.

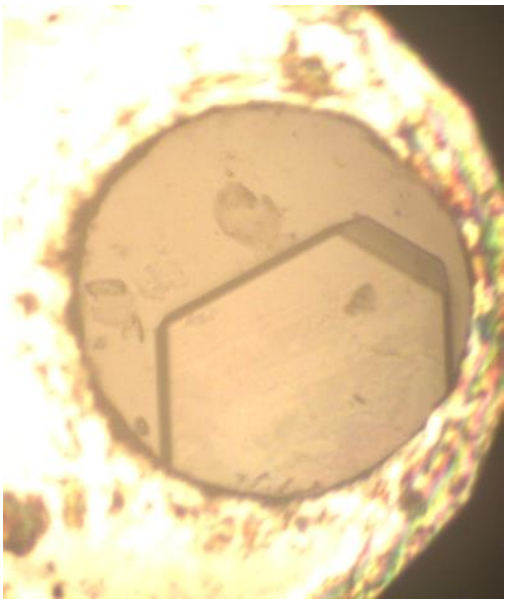

Figure 6.8 - The single crystal of caprolactam Form III, which formed at 0.7 GPa after decompression of a Form III sample from 3.45 GPa.

Table 6.3 - Refined unit cell parameters of caprolactam (recrystallised from ethyl acetate) upon increasing pressure and recovery to ambient conditions.

Pawley / Rietveld	Load (tonnes)	Pressure (GPa)	Form	Space Group	a-axis (Å)	b-axis (Å)	c-axis (Å)	β (°)	Unit Cell Volume (Å^3)	R_wp
Rietveld	5	0.201(11)	I	C2/c	19.251(2)	7.7647(7)	9.5567(10)	112.304(7)	1321.6(2)	3.421
Pawley	7	0.210(17)	I	C2/c	19.256(3)	7.7628(13)	9.5536(15)	112.335(9)	1320.9(4)	4.092
Pawley	9	0.283(7)	I	C2/c	19.1743(12)	7.7397(9)	9.5317(7)	112.255(4)	1309.2(2)	1.736
Pawley	11	0.479(9)	I	C2/c	18.9787(13)	7.6663(12)	9.4885(9)	112.119(5)	1278.9(3)	1.932
Rietveld	13	0.696(17)	I	C2/c	18.713(5)	7.5894(13)	9.416(2)	111.694(15)	1242.6(5)	5.125
Pawley	15	0.94(2)	III	$P2_1/c$	9.6066(9)	5.9184(7)	10.9366(6)	107.461(6)	593.15(10)	2.456
Pawley	17	1.22(2)	III	$P2_1/c$	9.5687(10)	5.8547(8)	10.8506(6)	107.137(6)	580.88(11)	2.435
Pawley	19	2.95(8)	III	$P2_1/c$	9.5488(10)	5.8230(7)	10.8084(6)	106.964(6)	574.83(10)	2.788
Pawley	21	1.53(7)	III	$P2_1/c$	9.5361(11)	5.8056(8)	10.7796(8)	106.856(8)	571.15(11)	3.06
Pawley	24	1.74(2)	III	$P2_1/c$	9.5098(12)	5.7701(9)	10.7196(13)	106.630(10)	563.61(13)	3.436
Pawley	27	2.072(13)	III	$P2_1/c$	9.4726(9)	5.7279(6)	10.6565(14)	106.401(13)	554.67(12)	2.216
Pawley	30	2.329(16)	III	$P2_1/c$	9.4417(11)	5.6996(7)	10.6014(14)	106.101(9)	548.12(12)	2.733
Pawley	33	2.588(18)	III	$P2_1/c$	9.4206(14)	5.6661(11)	10.5559(10)	105.910(9)	541.87(14)	3.275
Pawley	36	2.88(2)	III	$P2_1/c$	9.3935(10)	5.6364(7)	10.5089(6)	105.728(6)	535.57(10)	2.56
Pawley	39	3.13(3)	III	$P2_1/c$	9.3628(13)	5.6207(10)	10.4697(7)	105.550(8)	530.81(12)	3.231
Pawley	2	0.65(5)	III	$P2_1/c$	9.584(7)	6.045(7)	11.020(8)	107.70(5)	608.3(9)	4.994
Pawley	2	0.65(5)	II	C2/c	8.618(5)	6.902(5)	9.813(6)	94.49(9)	582.0(6)	4.994
Pawley	0	0.24(3)	I	C2/c	19.260(6)	7.768(3)	9.552(3)	112.34(18)	1321.8(8)	9.565

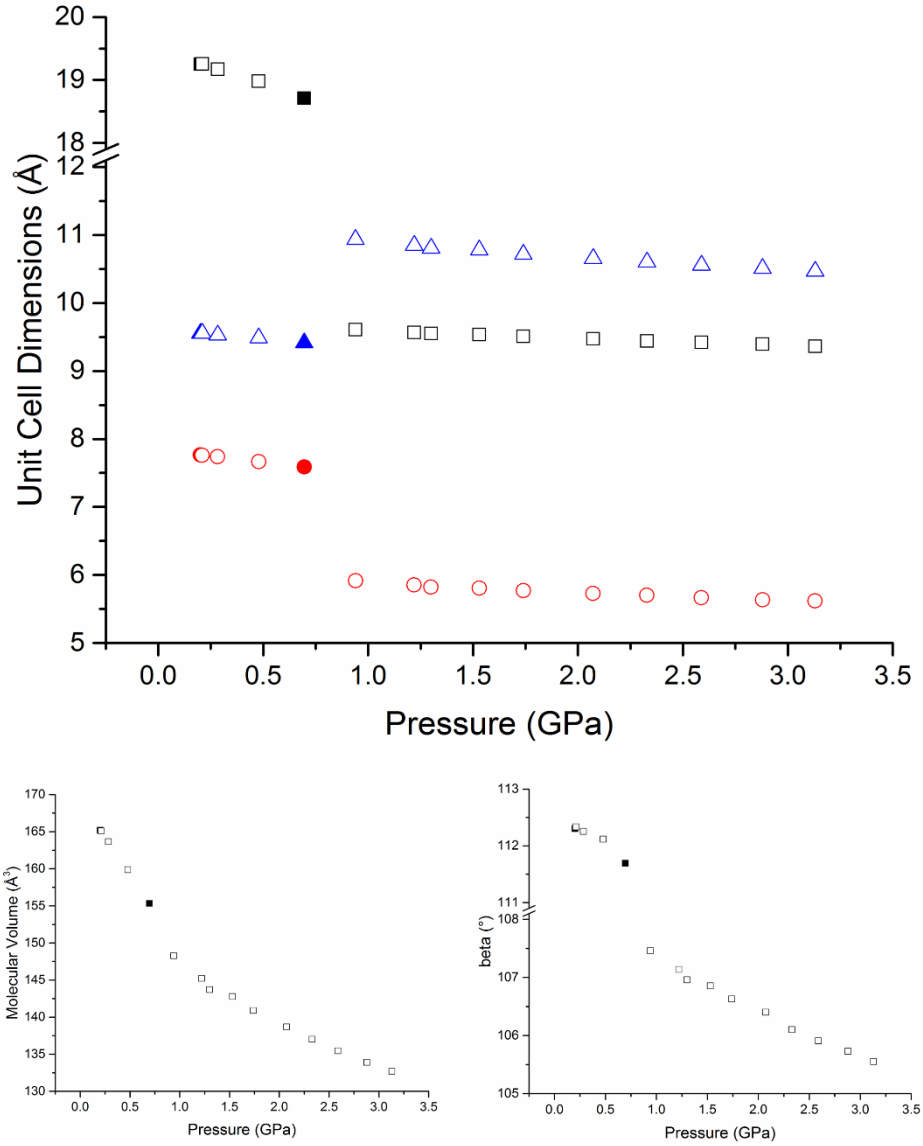

Figure 6.9 - Refined unit cell parameters of form I of caprolactam (recrystallised from ethyl acetate) upon compression. In the plot showing unit cell dimensions, the a-axis, b-axis and c-axis are represented by black squares, red circles and blue triangles, respectively. Filled shapes show data which were Rietveld-fitted; hollow shapes show data which were Pawley-fitted.

Figure 6.9 shows the compression of Form I up to 0.696 GPa, at which point caprolactam undergoes a phase transition to Form III. A steady compression of all three axes is shown either side of the transition, with distinct steps clearly seen in each axis, as well as the beta angle, as the sample undergoes the phase transition. There is a moderate step in the molecular volume across the phase transition, illustrating the higher density of Form III.

The neutron data collected at 0.201 GPa and 0.696 GPa were Rietveld-fitted with the known structure of Form I, whilst data collected between these two pressure points were Pawley-fitted with this model. These fits are shown in Figure 6.10, clearly showing a mixed phase of Forms I and III to be present at 0.696 GPa.

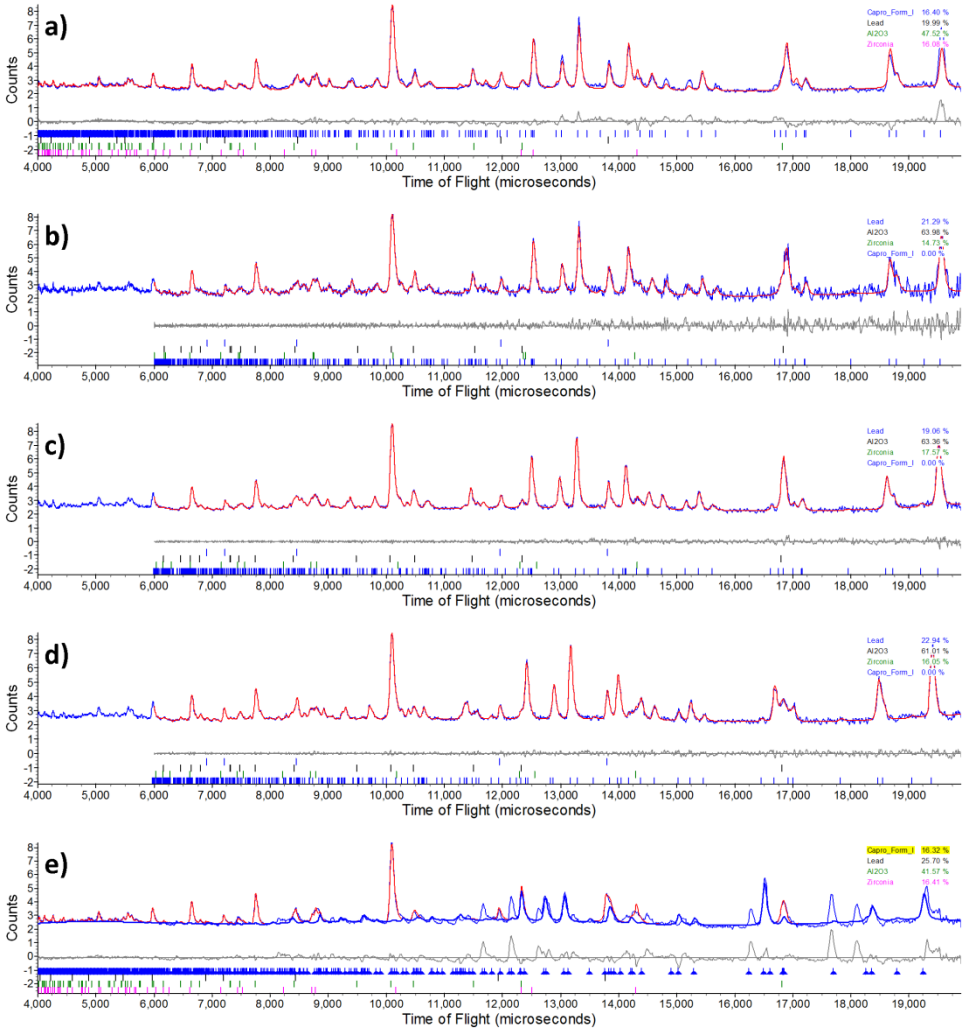

Figure 6.10 - Rietveld fit of the data collected at a) 0.201 GPa and e) 0.696 GPa, and Pawley fits of the data collected at b) 0.210 GPa, c) 0.283 GPa, and d) 0.479 GPa. The Rietveld fit shown in e) shows a mixed phase to be present, containing Form I and an unknown form.

Further compression to 3.13 GPa showed no significant change in the observed diffraction pattern (with the diffraction pattern observed in the second-highest pressure point shown in Figure 6.7), with the recently-obtained unit cell parameters of Form III being used to perform Pawley fits on the data collected up to the highest

pressure of 3.13 GPa. Rapid decompression to 0.65 GPa and 0.24 GPa showed marked changes in the diffraction pattern (Figure 6.11). Pawley fits of the data at 2.88 GPa (the second-highest pressure point upon compression), and the two pressure points upon decompression (0.65 GPa and 0.24 GPa) are shown in Figure 6.12. It should be noted that the data point at which the pressure refined to 0.24 GPa was in fact collected after the complete removal of the mechanical load. The fact that the pressure refined to 0.24 GPa can be attributed in part to the speed at which the load was removed, and in part the small quantity of data collected at this pressure. Combined, this meant the sample was not given sufficient time to equilibrate to give an accurate pressure reading.

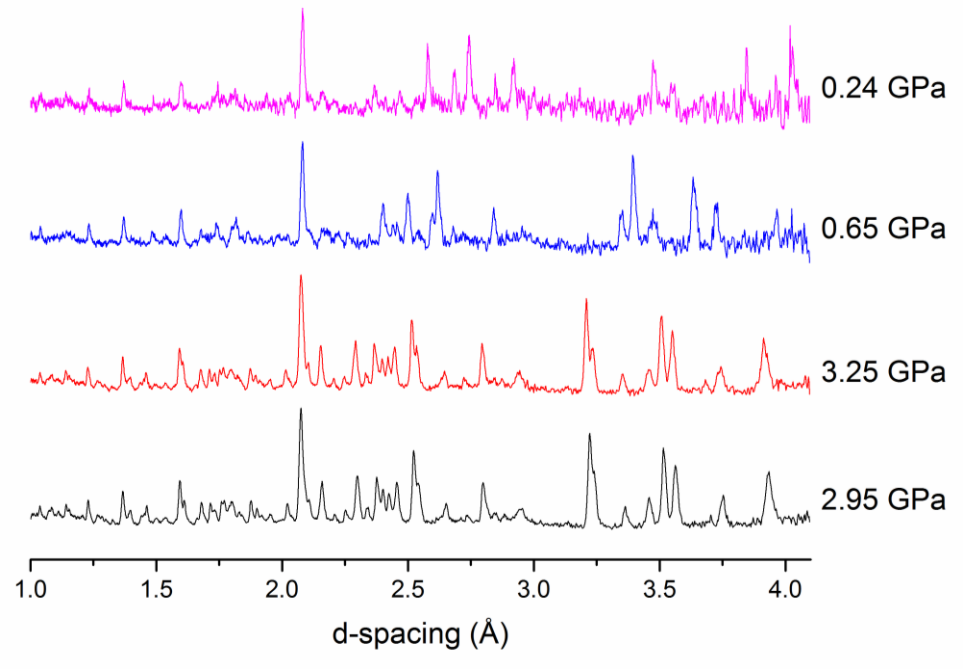

Figure 6.11 - Neutron diffraction patterns of the data collected at the two highest pressures (2.95 GPa and 3.25 GPa), and the two pressure points upon decompression (0.65 GPa and 0.24 GPa).

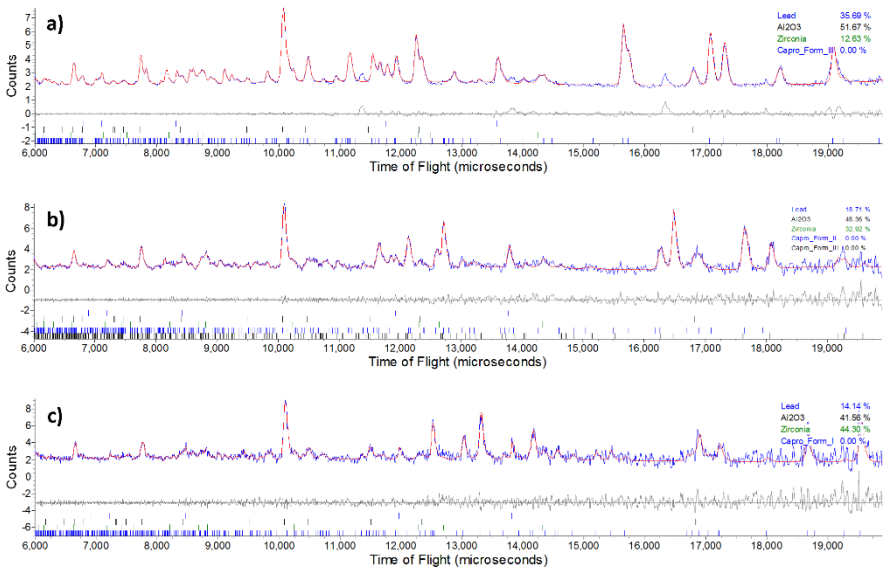

Figure 6.12 - Pawley fits of the data collected at: a)2.88 GPa, b) 0.65 GPa upon decompression, and c) 0.24 GPa upon decompression.

The Pawley fits in Figure 6.11 show the sample to be in Form III at 2.88 GPa. Decompression to 0.24 GPa gives a mixed phase, containing both Forms II and III, before the ambient Form I is observed when the load is completely removed (albeit with the pressure refining to 0.24 GPa).

6.2.3.2 Loading 2 – Neutron diffraction study of caprolactam recrystallised from ethanol

As with the experiment conducted on the lab diffractometer caprolactam was observed to undergo a phase transition at high pressure to the previously determined Form II between 0.981 and 1.563 GPa. Figure 6.14 shows the neutron diffraction patterns collected upon increasing pressure up to a maximum of 5.69 GPa, with no further significant changes in the diffraction pattern beyond the phase transition at 1.563 GPa.

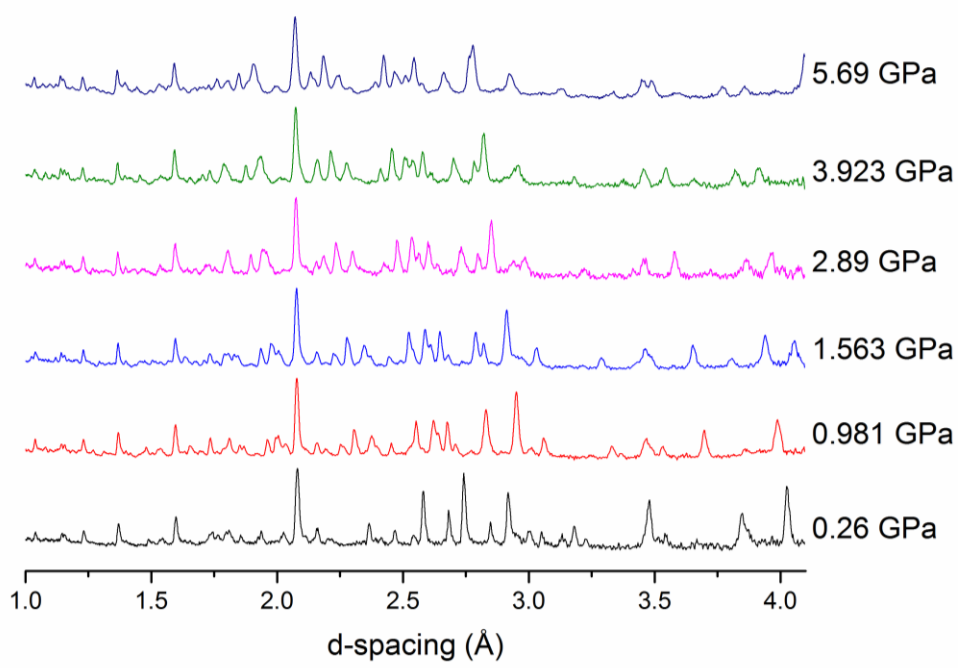

Figure 6.13 – Neutron diffraction patterns of the caprolactam sample recrystallised from ethanol with increasing pressure.

All data were Pawley fitted, and where sufficient data had been collected, Rietveld fits were performed. The refined unit cell parameters are summarised in Table 6.4 and plotted in Figure 6.14.

Table 6.4 - Refined unit cell parameters of caprolactam (recrystallised from ethanol) upon compression and decompression. The unit cell parameters from the DAC experiment, which were used as a starting point to solve the neutron data, are also shown in blue.

Pawley / Rietveld	Load (tonnes)	Pressure (GPa)	Form	Space Group	a-axis (Å)	b-axis (Å)	c-axis (Å)	β (°)	Unit Cell Volume (Å^3)	R_wp
Pawley	5	0.26(3)	I	C_2/c	18.901(3)	7.7065(15)	9.525(2)	111.743(16)	1288.8(4)	5.251
Pawley	10	0.436(12)	I	C_2/c	19.0531(12)	7.6934(9)	9.5069(7)	112.166(4)	1290.6(2)	1.976
Rietveld	15	0.981(16)	II	$P2_1/c$	8.5501(8)	6.9073(6)	9.8460(8)	94.196(11)	579.93(9)	3.29
N/A	DAC	1.2	II	$P2_1/c$	8.4819(4)	6.8714(10)	9.7503(10)	94.204(8)	566.74(11)	6.167
Rietveld	20	1.563(15)	II	$P2_1/c$	8.4341(7)	6.8435(6)	9.7059(7)	94.269(9)	558.66(8)	3.223
Pawley	25	2.001(15)	II	$P2_1/c$	8.3813(16)	6.7978(8)	9.6285(7)	94.281(12)	547.05(13)	2.456
Pawley	30	2.54(2)	II	$P2_1/c$	8.317(2)	6.7607(11)	9.5503(8)	94.363(16)	535.42(18)	2.785
Rietveld	35	2.89(3)	II	$P2_1/c$	8.2447(9)	6.7431(9)	9.4883(9)	94.321(12)	526.00(10)	3.908
Pawley	40	3.381(18)	II	$P2_1/c$	8.1912(15)	6.7262(9)	9.4337(9)	94.371(14)	518.25(13)	2.45
Pawley	45	3.923(17)	II	$P2_1/c$	8.1435(15)	6.7034(9)	9.3730(13)	94.338(14)	510.20(14)	2.252
Pawley	50	4.39(2)	II	$P2_1/c$	8.097(2)	6.6832(13)	9.3284(15)	94.26(2)	503.40(18)	3.108
Pawley	55	4.97(5)	II	$P2_1/c$	8.0580(17)	6.6547(11)	9.2829(13)	94.269(19)	496.40(15)	2.614
Rietveld	60	5.69(3)	II	$P2_1/c$	8.0164(8)	6.6211(8)	9.2288(10)	94.208(12)	488.51(10)	3.023
Pawley	30	4.99(3)	II	$P2_1/c$	8.0524(16)	6.6547(10)	9.2789(10)	94.225(19)	495.88(14)	2.947
Pawley	15	3.63(2)	II	$P2_1/c$	8.169(2)	6.7201(14)	9.391(2)	94.37(2)	514.1(2)	3.299
Pawley	5	1.44(5)	II	$P2_1/c$	8.390(5)	6.759(4)	9.739(3)	94.53(4)	550.5(5)	5.115
Pawley	2	0.63(5)	II	$P2_1/c$	8.305(5)	6.7308(9)	9.735(3)	94.80(3)	542.2(3)	3.43
Pawley	2	0.63(5)	I	C_2/c	19.008(5)	7.729(4)	9.377(4)	112.27(2)	1274.9(9)	3.43
Pawley	0	0.21(5)	I	C_2/c	19.243(4)	7.767(2)	9.544(2)	112.279(15)	1319.9(6)	8.153

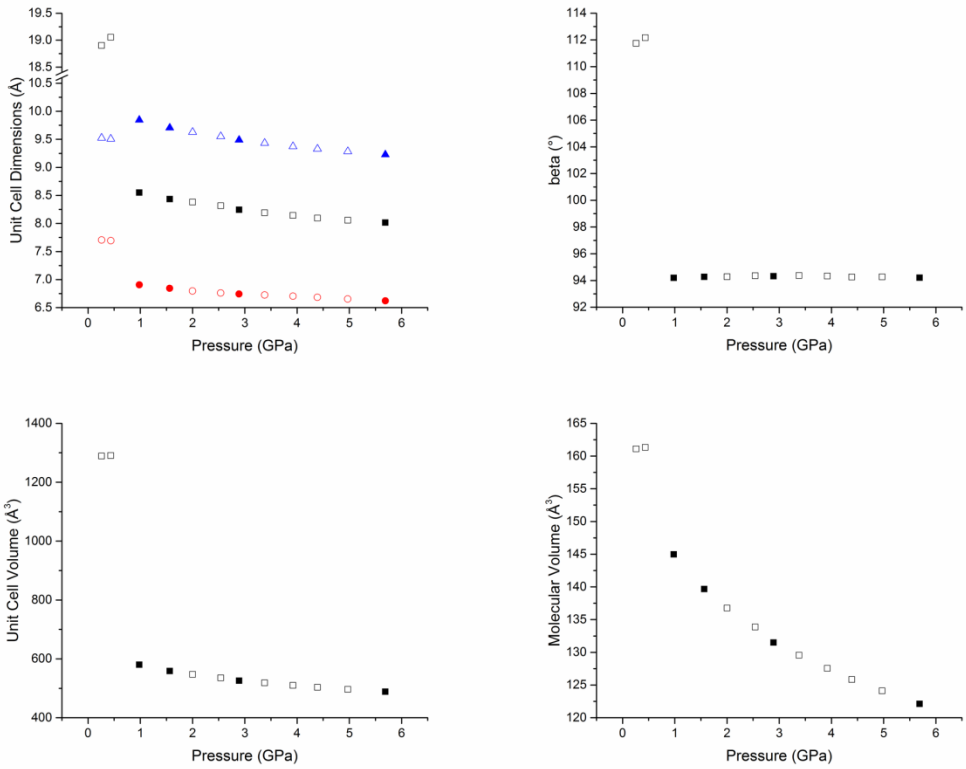

Figure 6.14 - Refined unit cell parameters of caprolactam (recrystallised from ethanol) upon compression. Upon increasing the pressure from 0.436 GPa to 0.981 GPa, the sample transformed from Form I to Form II. In the plot showing unit cell dimensions, the a-axis, b-axis and c-axis are represented by black squares, red circles and blue triangles, respectively. Filled shapes show data which were Rietveld-fitted; hollow shapes show data which were Pawley-fitted.

Rietveld fits of the data collected at 0.981 GPa, 1.563 GPa, 2.89 GPa and 5.69 GPa (as well as Pawley fits, including of the data collected at 3.923 GPa) all show the caprolactam sample to be Form II (Figure 6.15).

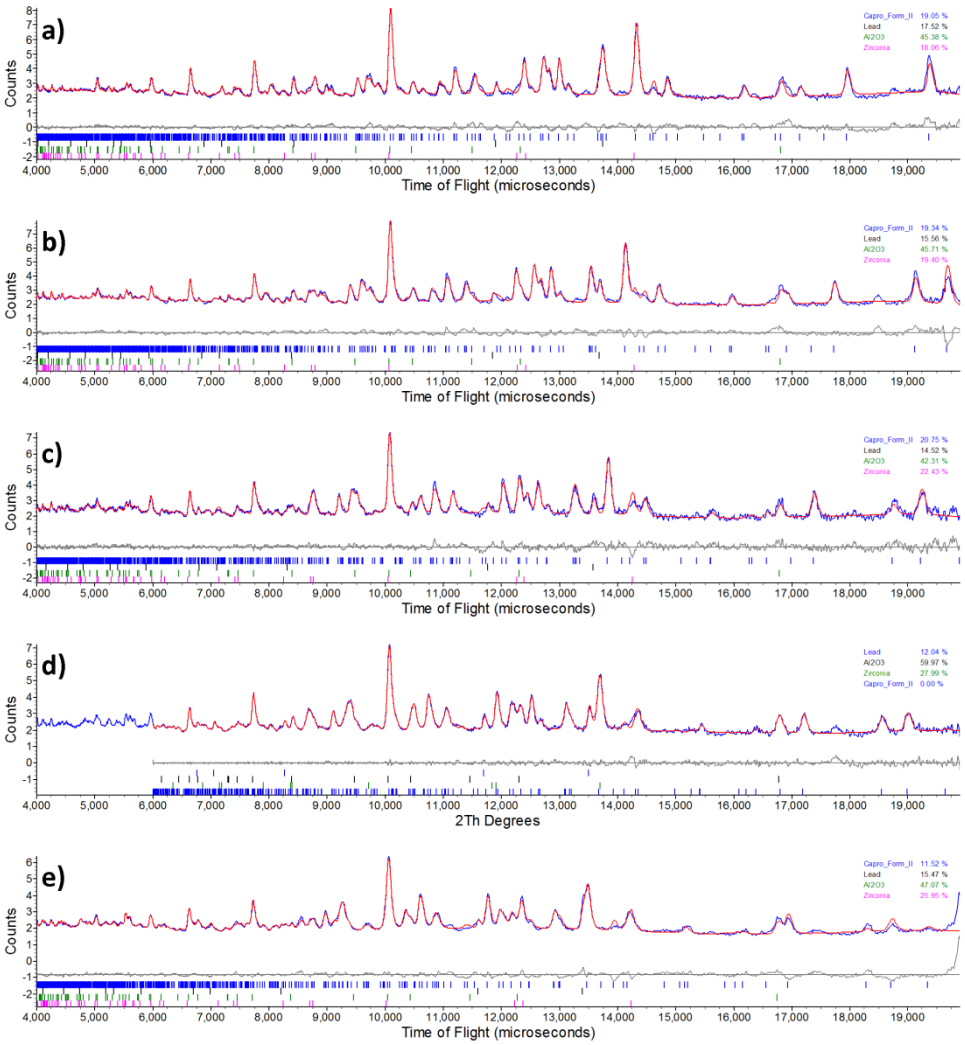

Figure 6.15 - Fits of the neutron diffraction data collected upon compression at a) 0.981 GPa, b) 1.563 GPa, c) 2.89 GPa, d) 3.923 GPa and e) 5.69 GPa. Rietveld fits are shown in a), b, c) and e); a Pawley fit is shown in d). All pressure points show the sample to be in Form II.

Subsequent decompression of the sample shows Form II to be stable as far as 1.44 GPa (Figure 6.16). The next data collected, at 0.63 GPa showed the presence of both Forms I and II. The Pawley refinement shows the molecular volume in Form I to be 159.36 Å^3 compared to 135.55 Å^3 in Form II, illustrating that at this pressure, the density of Form II is approximately 17.6% higher than that of Form I.

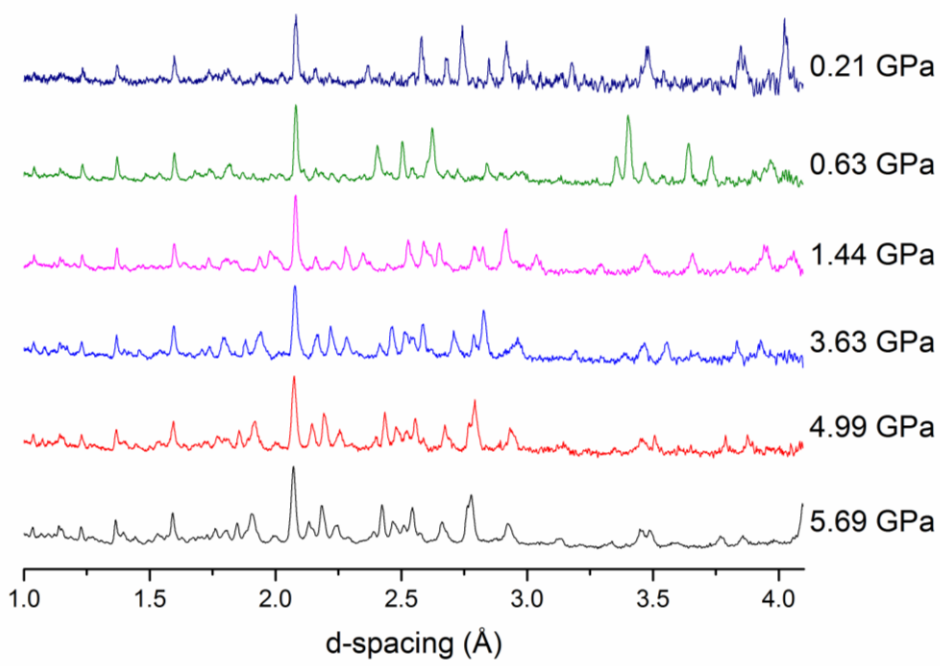

Figure 6.16 - Neutron diffraction data collected upon decompression of the caprolactam sample recrystallised from ethanol.

Figure 6.17 shows Rietveld and Pawley fits of the data collected upon decompression. Plots 6.16 a) through 6.16 d) show the sample to be in Form II, before plot e) shows a mixed phase of Forms I and II. The final plot, f), shows a clean sample of Form I as the load is completely removed from the sample. Note again that, as with the first loading, the pressure refined to be approximately 0.2 GPa.

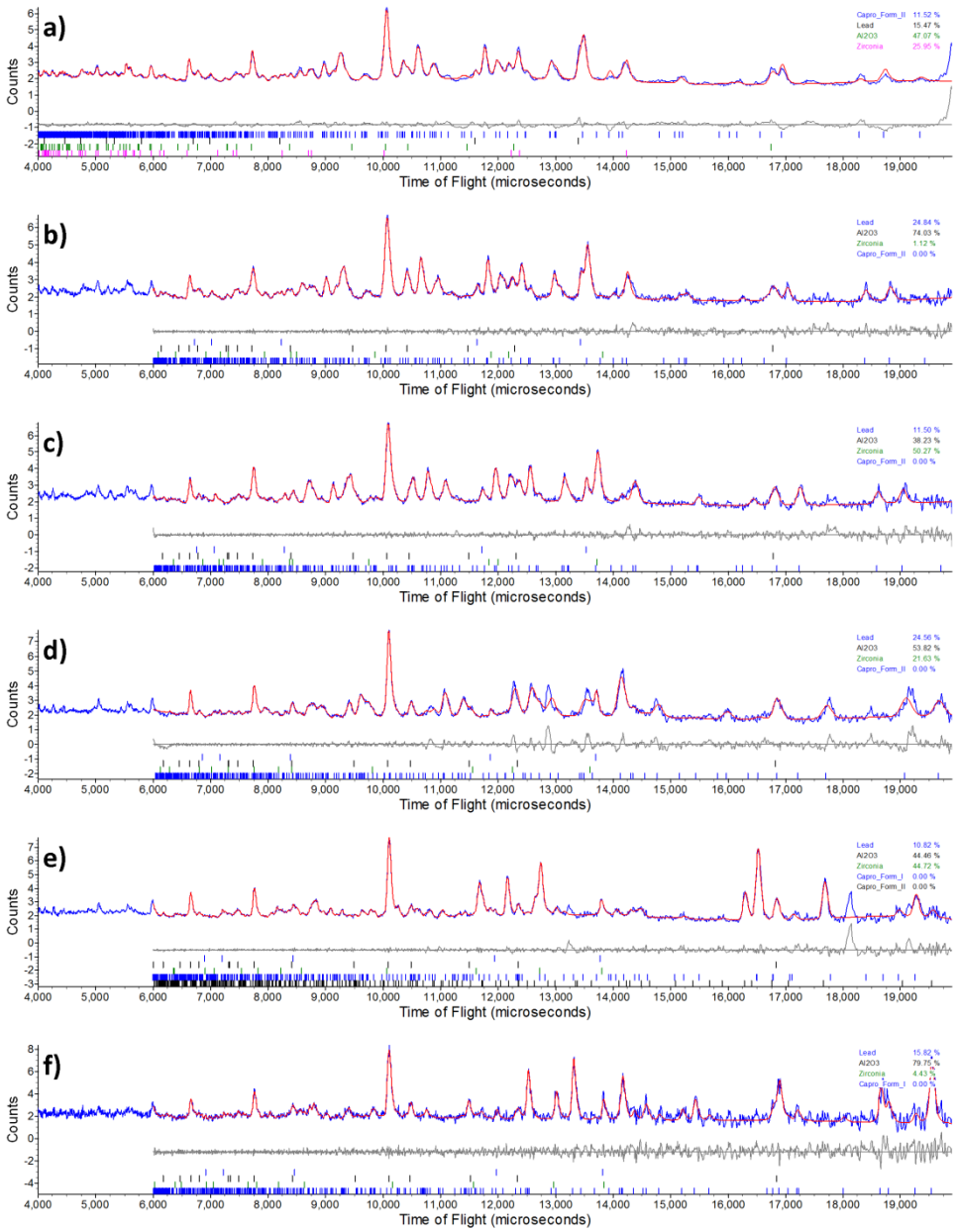

Figure 6.17 - Rietveld fit of the data collected at a) 5.69 GPa, and Pawley fits of the data collected at b) 4.99 GPa, c) 3.63 GPa, d) 1.44 GPa, e) 0.63 GPa and f) 0.21 GPa. Fits a) through d) show Form II, whilst fits e) and f) show a mixed phase (containing Forms I and II) and Form II, respectively.

6.3.3 PIXEL Calculations

PIXEL calculations were carried out on Form I (at 1.26 GPa), and on the refined structure of Form II (both from the SXRD data at 1.20 GPa and the four pressure points at which Rietveld refinements were conducted on the neutron diffraction data.

The six strongest molecule-molecule interactions in Form I are shown in Figure 6.18, with the energies of each listed in Table 6.5.

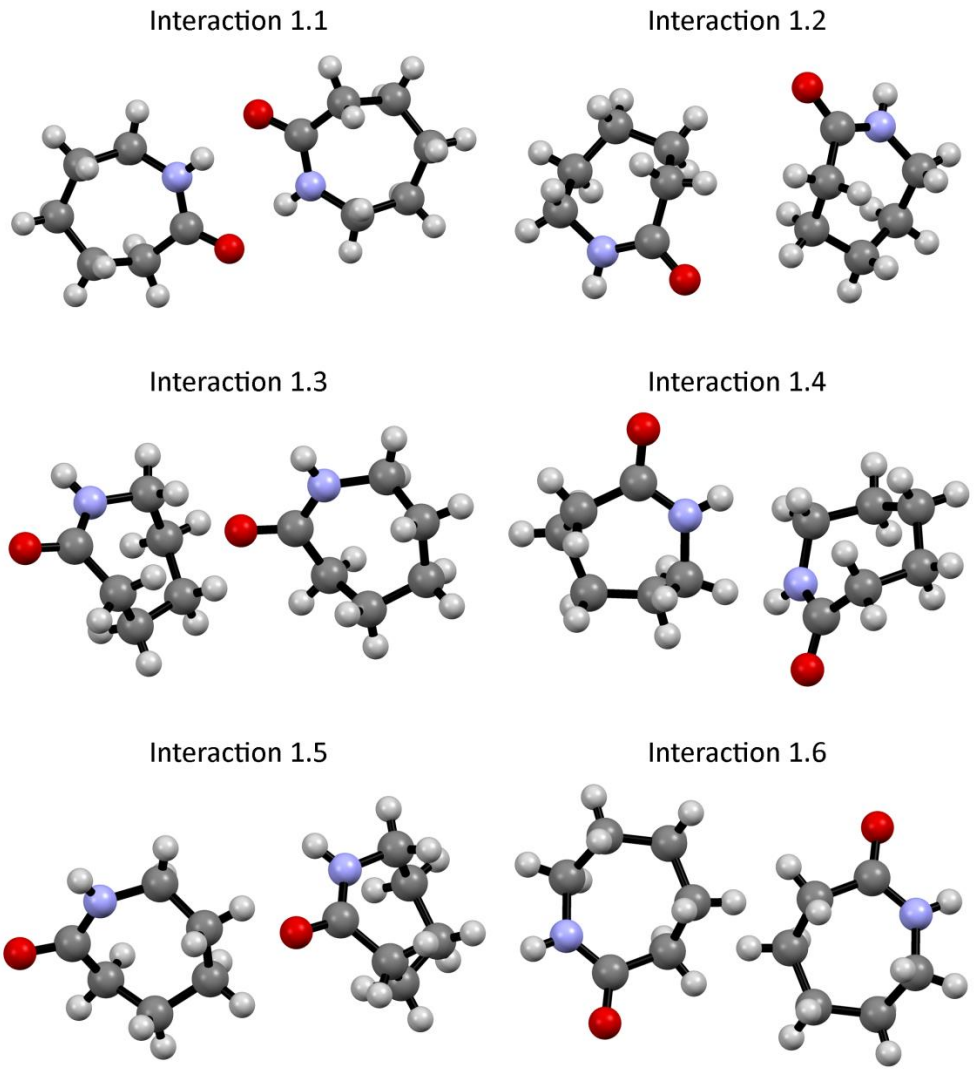

Figure 6.18 - The molecules involved in Interactions 1.1 - 1.6.

Table 6.5 - The six strongest molecule-molecule interactions in Form I of caprolactam, as identified at 1.26 GPa

Interaction	Symmetry Relation	E_c (kJ / mol)	E_p (kJ / mol)	E_d (kJ / mol)	E_r (kJ / mol)	E_{tot} (kJ / mol)
1.1	0.5-x, 1.5-y, -z	-96.2	-33.3	-22.5	94.2	-57.8
1.2	1-x, y, 0.5-z	-10.3	-5.3	-16.6	15	-17.3
1.3	x, 1-y, 0.5+z	-16.4	-8.3	-14.8	24.1	-15.4
1.4	0.5-x, -0.5+y, 0.5-z	-4.9	-3.4	-17.4	12	-13.8
1.5	x, 2-y, 0.5+z	-1.2	-2	-11.4	6.4	-8.2
1.6	1-x, 1-y, 1-z	-5.4	-2.9	-17.5	18	-7.8

As one would expect, the PIXEL calculations show the amide dimer interaction to be the most stabilising interaction present in the crystal structure of Form I. The total lattice energy at 1.26 GPa was -32.2 kJ mol^{-1}.

Form II

PIXEL calculations were conducted on the refined structures obtained from the neutron diffraction data. The strongest six interactions at the lowest pressure, 0.981 GPa, were tracked as pressure was increased to the maximum pressure at which data were collected, 5.69 GPa. The molecules involved in each of these six interactions are related by the symmetry operations listed in Table 6.6, with the pairs of molecule for each of these six interactions shown in Figure 6.19. Table 6.7 summarises the changes in these interactions upon increasing pressure to 5.69 GPa.

Table 6.6 - The six most significant molecule-molecule interactions in Form II caprolactam, as calculated at 0.981 GPa.

Interaction	Symmetry Relation
2.1	2-x,-0.5+y,0.5-z
2.2	2-x,-y,1-z
2.3	2-x,1-y,1-z
2.4	1-x,-y,1-z
2.5	x,0.5-y,0.5+z
2.6	1-x,-0.5+y,0.5-z

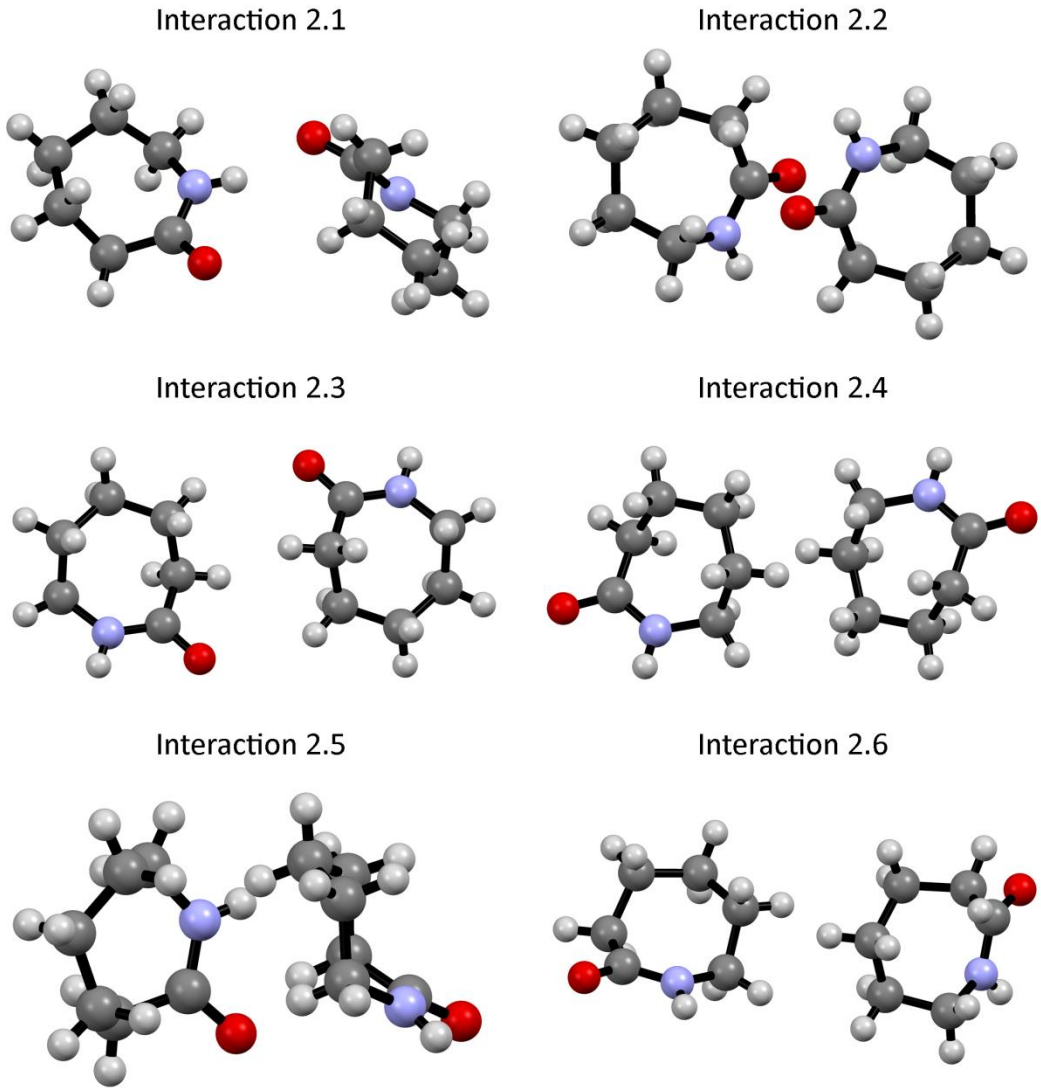

Figure 6.19 - The molecules involved in Interactions 2.1 - 2.6.

Table 6.7 - The six strongest interactions in the Form II of caprolactam.

Pressure (GPa)	**C_m-C_m Distance (Å)**	**E_c (kJ / mol)**	**E_p (kJ / mol)**	**E_d (kJ / mol)**	**E_r (kJ / mol)**	**E_{tot} (kJ / mol)**
Interaction 2.1						
0.981	5.735	-31.6	-10.5	-13	26.6	-28.5
1.563	5.686	-30.6	-9.9	-12.9	24	-29.4
2.89	5.582	-36	-13.6	-15.2	35.6	-29.2
5.69	5.405	-49.5	-21.9	-19.1	67	-23.6
Interaction 2.2						
0.981	4.607	-19.7	-6.6	-26.9	29	-24.3
1.563	4.518	-27.2	-10.4	-30.8	44.3	-24.1
2.89	4.439	-29.6	-12.1	-35	57.6	-19.1
5.69	4.237	-49.6	-22.4	-48.2	124.2	4
Interaction 2.3						
0.981	6.002	-11.3	-6.2	-17.8	22	-13.3
1.563	5.928	-11.6	-6.2	-18.5	21.6	-14.7
2.89	5.768	-18.7	-10.8	-24.3	43.8	-10
5.69	5.611	-24.4	-13.2	-29.1	53.7	-12.9
Interaction 2.4						
0.981	6.156	-3.7	-2.7	-21.8	20.3	-7.9
1.563	6.061	-5.4	-3.5	-25.2	27.4	-6.7
2.89	5.953	-7.9	-5.1	-27.7	36.4	-4.2
5.69	5.846	-12.2	-7.2	-32.2	52.1	0.5
Interaction 2.5						
0.981	5.038	0.3	-3.3	-18.9	14.3	-7.6
1.563	4.971	-0.1	-4	-21.4	18	-7.5
2.89	4.85	-4.2	-6.2	-25.9	29.9	-6.5
5.69	4.726	-8.5	-8.7	-31	44.6	-3.6
Interaction 2.6						
0.981	6.588	-3.5	-2.4	-16.9	16.2	-6.6
1.563	6.523	-3.7	-2.7	-17.9	17.9	-6.4
2.89	6.403	-6.6	-3.8	-20.7	26.3	-4.8
5.69	6.324	-12.5	-7.3	-25.6	46.8	1.5

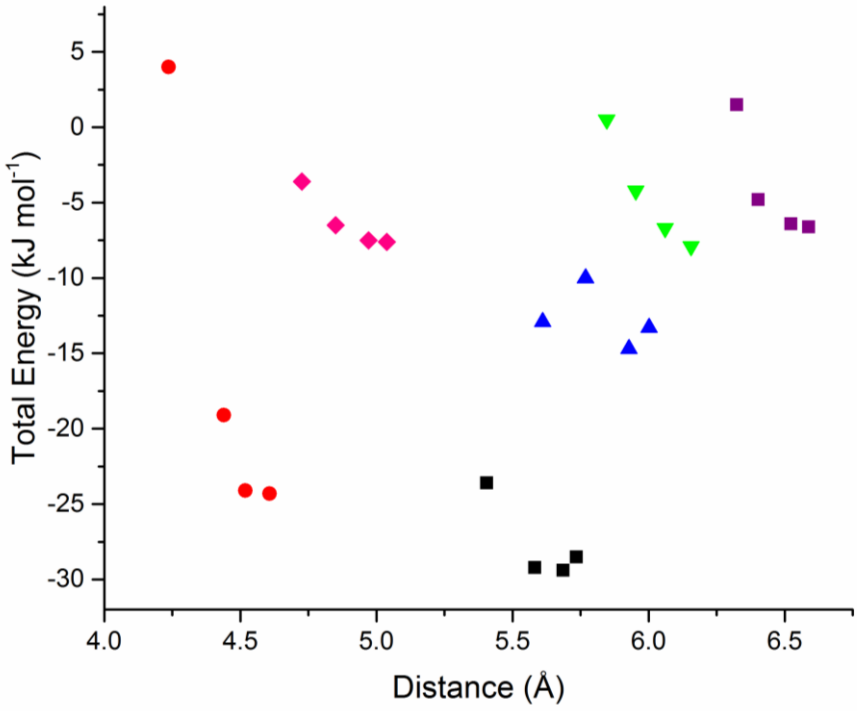

Figure 6.20 - Changes in the total energies of Interactions 2.1 (black squares), 2.2 (red circles), 2.3 (blue triangles), 2.4 (green triangles), 2.5 (pink diamonds) and 2.6 (purple squares) as pressure is increased and C_m-C_m distance decreases.

As pressure is increased and the unit cell is compressed, the stabilising contributions of all six of the studied interactions decreases. The decrease in the stabilising contributions of Interactions 2.1, 2.4, 2.5 and 2.6 are relatively smooth across the pressure range studied. E_{tot} of Interaction 2.3 fluctuates across the observed pressure range, resulting in a minimal net change between the lowest pressure and highest pressure points. The most significant change is in the contribution of Interaction 2.2. At 0.981 GPa, Interaction 2.1 has a total contribution of -24.3 kJ mol^{-1} before rapidly destabilising as pressure is increased to 5.69 GPa, at which point this interaction has a net destabilising contribution, with E_{tot} +4.0 kJ mol^{-1}. The extreme change in this interaction, which can be assumed to be largely attributable to the anti-parallel carbonyl-carbonyl interaction between the neighbouring molecules, can be explained by the close proximity of the molecules and of the carbonyl groups in particular.

Form III

Due to the structure of Form III being solved recently by work within the group beyond the end of this PhD, PIXEL calculations of Form III have not yet been conducted.

6.3.4 Equations of state and unit cell comparison

The unit cell volumes upon compression of Forms II and III were fitted to 3rd order Birch-Murnaghan equations of state (Table 6.8). The fitted equations of state show Form II to have a smaller calculated V_0, and hence higher density. It is therefore proposed that Form II is the more stable of the two high pressure phases, and that the sample converts from Form III to Form II upon decompression as this is the energetically preferred packing arrangement. This is further evidenced by the mixed phase obtained upon decompression of Form III, where it is seen that Forms II and III have unit cell volumes of 582.0 Å^3 and 608.3 Å^3, respectively.

Table 6.8 - Third order Birch-Murnaghan equations of state of caprolactam Forms II and III.

Polymorph	**V_0 (Å^3)**	**K_0**	**K'**	**K''**
Form II	639.2(4)	5,86(19)	11.3(5)	-11.1
Form III	653.1(6)	6.34(19)	9.1(5)	-5.2

6.4 Summary of Observations and Conclusions

The neutron diffraction study has shown that compression of two samples of caprolactam (both in the same polymorph, Form I, but recrystallised from two different solvents, ethyl acetate and ethanol) gives rise to two behaviours.

When compressed, a sample recrystallised from alcohol (ethanol or 1-butanol) undergoes a phase transition to Form II, which has been fully structurally solved.

Upon decompression, the phase transition is seen to be reversible, with Form I being obtained upon decompression to ambient conditions.

When compressed, a sample recrystallised from ethyl acetate undergoes a phase transition to Form III. Upon decompression, Form III briefly converts to Form II, before Form I is obtained upon recovery to ambient conditions.

During the decompression of this sample, a further phase transition to Form III is observed. Attempts to solve the structure of Form III have so far been unsuccessful. Contrastingly, compression of a sample recrystallised from ethyl acetate results in a phase transition directly to Form III. In both cases, Form I is recovered upon complete decompression to ambient conditions.

As far as we are aware, this is the first time that such a phenomenon has been observed, and the reasons for the different high pressure forms being observed are not definitely known. One possibility is that residual solvent molecules within the crystals may somehow impact the high pressure form adopted upon compression of the sample.

Further work is required in order to gain more insight into the reasons for two seemingly identical samples behaving very differently.

6.5 References

Arlin, J.-B., Price, L. S., Price, S. L., Florence, A. J., Price, S. L., Dunitz, J. D., … Day, G. M. (2011). A strategy for producing predicted polymorphs: catemeric carbamazepine form V. *Chemical Communications*, *47*(25), 7074. http://doi.org/10.1039/c1cc11634g

Winkler, F. K., Dunitz, J. D., & IUCr. (1975). Medium-ring compounds. XIX. Caprolactam: structure refinement. *Acta Crystallographica Section B Structural Crystallography and Crystal Chemistry*, *31*(1), 268–269. http://doi.org/10.1107/S0567740875002440

Chapter 7 – Summary of Findings

7.1 Summary

As discussed in Chapter 1 of this thesis, the thorough screening for polymorphs is of utmost importance in the pharmaceutical industry. With many important physico-chemical properties of drug substances (and excipients) – including solubility, dissolution rate and stability – depending on their solid-state forms, as well as the intellectual property implications, it is well worth manufacturers going to great lengths to ensure an exhaustive knowledge of the possible forms.

The research in this thesis highlights three specific aspects of screening for polymorphism using high pressure: the role of particle size on the pressure at which a polymorph transition is observed; the role of the pressure-transmitting medium on the high-pressure behaviour of a substance; and the role of the solvent of recrystallization on the high-pressure behaviour of a substance. The observations made during this research show that implementing a rigorous screening process using high pressure can result in the observation of polymorphs not seen through typically-used ambient pressure polymorph screening techniques and could be particularly important in areas such as the pharmaceutical industry.

In Chapter 3, it was observed that the transition to a high-pressure form of glycolide occurred at lower pressures in samples which had been ground prior to being subjected to high pressure. For ground samples of glycolide, this transition was observed as low as 0.12 GPa compared to unground samples for which the transition was observed at 0.58 GPa. Given that the tabletting process can commonly apply pressures of 0.20 GPa (Takeuchi, Nagira, Yamamoto, & Kawashima, 2004), it can be seen that failure to use pressure as a screening tool may result in important polymorphs remaining undiscovered during the initial screening process.

The ability to use neutron diffraction to perform high pressure studies on hydrogenous samples was demonstrated in Chapter 4 to have greatly improved thanks to the development of the Zirconium-Toughened Alumina (ZTA) anvils. The quality of data was shown to be similar to that of data collected using tungsten carbide anvils (the ZTA anvils' predecessors) on deuterated samples.

Chapter 5 explores the impact of the pressure-transmitting medium on the high-pressure behaviour of acrylamide, with three different high-pressure forms being observed from compression of the material in three different media. The different behaviour observed can be explained by the relative solubility of the material in the PTM, with media in which the material is soluble aiding solvent-mediated phase transitions. In a medium in which the material is insoluble, a high-pressure phase transition is observed with the resulting polymorph being less stable than that observed through the solvent-mediated phase transition. Thus, it has been demonstrated that the potential exists to tailor the stability of the high-pressure polymorph through careful selection of the medium in which the sample is compressed. For pharmaceutical compounds, this may permit one to alter the stability in order to optimised solubility or dissolution rate of the drug molecule.

In Chapter 6, the role of residual solvent molecules from the recrystallization process on the high-pressure behaviour of caprolactam is observed, adding a further level of complexity to the conclusions drawn from the research in Chapter 5. Two samples of caprolactam, both the same polymorph but produced via recrystallization from two different solvents, were subjected to high pressures with each of the samples undergoing phase transitions to different high-pressure forms. It is postulated that this may be due to residual interstitial solvent molecules within the crystal lattice facilitating a solvent-mediated polymorph transition, like those seen in Chapter 5. As with the potential implications of the observations from Chapter 5, this demonstrates that the solvent from which a sample is recrystallised may allow the stability of a high-pressure polymorph to be tailored to suit the desired application.

On the whole, the research presented in this thesis shows that the use of high pressure can be a powerful tool when screening for polymorphs of small organic materials. Such a screening process should include a number of experiments in which effects of factors such as particle size, pressure-transmitting medium and solvent of recrystallisation are assessed. The impact of these factors should be studied in isolation, as well as in combination with each other.

Further work is required in order to establish whether the observations made in Chapter 6 are, as hypothesised, due to residual solvent present within the crystal lattice. Mass spectrometry may be employed to detect trace levels of any solvent present in these crystals. In the case of each of the materials studied, there is also the scope to employ initiator species in an attempt to induce polymerisation from the high-pressure forms produced. This may permit the production of novel polymeric materials and, as with their properties somewhat tailored towards particular applications. In addition to this, the structures of the third form of glycolide and Form IV of acrylamide remain unknown.

For pharmaceutical companies, this represents an important avenue of research which should be further explored during the development of new products in order to avoid the costly consequences of instances such as those of the Ritonavir case discussed in Chapter 1, as well as the modification of important properties in order to optimise drug efficacy.

7.2 References

Takeuchi, H., Nagira, S., Yamamoto, H., & Kawashima, Y. (2004). Die wall pressure measurement for evaluation of compaction property of pharmaceutical materials. *International Journal of Pharmaceutics*, *274*, 131–138. http://doi.org/10.1016/j.ijpharm.2004.01.008